Report Prepared by:

Alberto A. Sagüés
S.C. Kranc
A.K.M. Al-Mansur
Sherry Hierholzer

FACTORS CONTROLLING CORROSION OF STEEL-REINFORCED CONCRETE SUBSTRUCTURE IN SEAWATER

Final Report to Florida D.O.T.
WPI No. 0510537, State Job No. 99700-7530-119

Alberto A. Sagüés, P.I.
Department of Civil Engineering and Mechanics

College of Engineering
University of South Florida
Tampa, Florida 33620-5350
December, 1994

Technical Report Documentation Page

1. Report No.	2. Government Accession No.	3. Recipient's Catalog No.
FL/DOT/RC/0537-3523		

4. Title and Subtitle

FACTORS CONTROLLING CORROSION OF STEEL-REINFORCED CONCRETE SUBSTRUCTURE IN SEAWATER

5. Report Date: December, 1994

6. Performing Organization Code

8. Performing Organization Report No.

7. Author's

Alberto A. Sagues, S.C. Kranc, A.K.M. Al-Mansur, S. Hierholzer

9. Performing Organization Name and Address

Department of Civil Engineering and Mechanics
University of South Florida
Tampa, FL 33620

10. Work Unit No. (TRAIS)

11. Contract or Grant No.: WPI 0510537

13. Type of Report and Period Covered

Final Report
September 1990 - December 1993

12. Sponsoring Agency Name and Address

Florida Department of Transportation
Materials Office
P.O. Box 1029
Gainesville, FL 32602

14. Sponsoring Agency Code

15. Supplementory Notes

Prepared in cooperation with the Federal Highway Administration

16. Abstract

Laboratory experiments and computer model calculations were performed to assess the effect of critical design variables and concrete properties on the distribution of corrosion in reinforced concrete marine bridge substructures. Instrumented laboratory test columns were exposed for a period of three years in conditions simulating field service. One set of columns was made with concrete containing fly ash, concrete with fly ash plus silica fume, and concrete with either silane or siloxane surface treatments. This set was prepared for evaluation of the effects of concrete composition and surface treatments on corrosion distribution. From concrete resistivity measurements, the concrete with fly ash plus silica fume showed evidence of having the lowest permeability at early test ages (first two years), but the differences between both types of concrete tended to be less near the end of the test. Both surface treatments tended to reduce the intake of water but did not cause excessive water retention. Another set of columns was made with concrete without pozzolanic additions, and used to evaluate the effect of partial and saturating moisture application in the region above the waterline. Corrosion macrocell measurements indicated that cathodic activity (and macrocell action) increased with partial moisture application but reached a limiting amount upon saturation. The behavior was linked to diffusional transport limitation of the oxygen reduction reaction. The computer calculations produced a comprehensive model to predict corrosion current distribution. The predicted corrosion was greatest at the top of the active steel zone in the reinforcement assembly. The calculations indicated than the diffusivity of oxygen in the concrete was relatively more important than concrete resistivity in determining the overall extent of corrosion. Applications of the findings to design of future structures are proposed.

17. Key Words	18. Distribution Statement
Reinforcing Steel, Corrosion, Rebar, Concrete, Computation	No restrictions. This document is available to the public through the National Technical Information Service, Springfield, VA 22161

19. Security Classif.(of this report)	20. Security Classif. (of this page)	21. No. of Pages	22. Price
Unclassified	Unclassified	115	

Form DOT F 1700.7 (8-72)

METRIC CONVERSION FACTORS

		CONVERT	TO	MULTIPLY BY
1.	LENGTH	inch	mm	25.4
		foot	mm	304.8
		yard	meter	0.9144
		meter	foot	3.281
		meter	inch	39.37
2.	FORCE	pound (lb)	newton (N)	4.448
		kip (1000 lb)	kilo newton (kN)	4.448
		newton (N)	pound (lb)	0.225
		kilo newton (kN)	kip k	0.225
3.	FORCE/ LENGTH	kip/ft	kN/m	14.59
		kN/m	lb/ft	68.52
		kN/m	kip/ft	0.0685
4.	STRESS	pound/in^2 (psi)	N/mm^2 (MPa)	0.0069
		kips/in^2 (ksi)	N/mm^2 (MPa)	6.895
		newton/mm^2	ksi	0.145
5.	MOMENTS	ft-kip	kN-m	1.356
		in-kip	kN-m	0.113
		kN-m	ft-kip	0.7375

CREDITS/DISCLAIMER

This report was prepared in cooperation with the State of Florida Department of Transportation (FDOT) and the U.S. Department of Transportation. The Corrosion Section of the Materials Office, Florida Department of Transportation, Gainesville, Florida provided valuable assistance in the preparation of concrete laboratory specimens and analysis of concrete samples. The opinions, findings and conclusions expressed in this publication are those of the authors and not necessarily those of the State of Florida Department of Transportation or the U.S. Department of Transportation.

TABLE OF CONTENTS

EXECUTIVE SUMMARY

Reinforcement corrosion severely limits the service life of concrete exposed to seawater. To achieve extended design service life, it is important to quantitatively assess the relative importance of design parameters such as concrete composition, concrete properties, structural dimensions and concrete surface treatments. To that effect, this three-part investigation examined selected factors that control the corrosion of reinforcing steel in the substructure of marine bridges.

The first part of the investigation had the objective of examining the effect of concrete composition and surface treatment on the development of corrosion. This objective was addressed experimentally by constructing instrumented reinforced concrete columns and placing them in a laboratory salt water tank simulating submerged, splash, and atmospheric exposure regions. The concrete compositions used reflect current and near-future Florida DOT design: F specimens (Type II cement with 20% Fly Ash replacement) , and F+S specimens (20% Fly Ash and 5% Microsilica). The concrete surface treatments used were Silane and Siloxane, applied to the above-water portion of the test columns. Testing took place over a 3-year period. The columns developed concrete resistivity patterns representative of those encountered in the field. The resistivity results indicated that both concrete surface treatments prevented water ingress but did not cause water to be retained to the extent that unwanted enhancement of corrosion macrocell action would have taken place. The resistivity results for the zones below water and corrosion macrocell current measurements indicated that the F concrete was initially significantly more permeable than the F+S concrete, but the differences between both types of concrete tended to become much less pronounced as time progressed. The effect, which resulted in comparable behavior for both mixes after about two years of exposure, was ascribed to the maturing of the pozzolanic reaction during that period in the F specimens. It was concluded that future assessment of the relative merits of mixtures with and without microsilica give special attention to long term field experience.

Corrosion macrocell patterns in the test columns had began to reach maturity by the end of the project, and continued testing is planned for the future.

The second part of the investigation had the objective of establishing the extent of corrosion macrocell action and its variation with concrete moisture in marine substructure service. This objective was addressed also using laboratory columns partially submerged in salt water. The column geometry allowed for detailed separation of the reinforcing steel into individual elements. Only one concrete, with Type I cement, was used. The evolution of corrosion was followed for a period of 3 years as a function of time and of the degree of moisturizing of the above-water portion of the columns. The cathodic current in the upper portion of the columns was increased upon partial moisturizing, as a result of the reduction of ohmic potential drops in the corrosion macrocell system. However, as the region above water was moisturized to saturation, the cathodic current did not increase proportionally but reached a limiting value consisting with concentration polarization of the cathodic reaction. The value of the limiting current density in saturated concrete corresponded to an effective diffusion coefficient for oxygen in concrete of 6 10^{-6} cm^2/sec, in agreement with values independently reported in the literature.

The objective of the third part of the investigation was to develop a comprehensive model for the prediction of corrosion distribution in reinforced concrete piling as a function of concrete properties and system geometry. A computational model was developed for a generic substructure column using finite difference calculations. The distributions of electric potential and oxygen concentration were calculated for the corrosion propagation stage. The concrete resistivity and oxygen diffusivity distribution profiles of the column were used as inputs. The model provided quantitative prediction of the resulting corrosion rate along the reinforcement cage. The concentration of oxygen inside the column was found to vary from a value near equilibrium with the exterior at the top, to almost zero below water. Oxygen transport to the steel below water was almost exclusively through the concrete cover and not

downward through the center of the column. The corrosion current density was greatest at the top of the active zone of the column. Corrosion below water proceeded at a smaller rate even though the steel potential was significantly less noble than in the region of highest corrosion. The overall level of corrosion increased with increasing oxygen diffusivity and reduced concrete resistivity. However, the relative changes in oxygen diffusivity had the greatest impact on corrosion activity.

The different approaches of the investigation confirmed the importance of corrosion macrocells in the development of corrosion in macrocell columns. Oxygen transport was a critical factor in determining corrosion severity. Design that promotes moist concrete conditions (as in submerged substructure footers) is recommended as a corrosion prevention/control approach. Concrete resistivity is another critical variable. Monitoring of concrete resistivity is recommended not only as a gage of possible corrosion severity, but also in moist specimens as an additional indicator of overall concrete quality.

1. INTRODUCTION

The substructure of reinforced concrete bridges over marine waters in Florida is subject to damage due to corrosion of the reinforcing steel. The steel reinforcing bars (rebars) are initially protected by the alkaline nature of the surrounding concrete. However, chloride ions from the seawater accumulate on the surface of the concrete and slowly migrate through the concrete cover to the underlying steel. When the chloride ion concentration at the rebar depth exceeds a critical threshold value, the protective passive layer on the steel surface breaks down and active corrosion of the steel begins. The corrosion products occupy a volume that can be several times larger than that of the initial steel, thus causing cracks of the concrete cover with consequent structural damage.

The time period from construction until the beginning of active rebar corrosion is called the initiation stage of the corrosion process. The following period from beginning of active corrosion until appearance of external manifestation of structural damage (cracking, rust, spalling) is called the propagation stage. This investigation was aimed primarily at determining the relative importance of design and service factors on the extent of corrosion experienced during the propagation stage in marine substructures of Florida bridges. The factors selected for examination concerned parameters that can be affected by the outcome of decisions presently being made by the Florida Department of Transportation (FDOT) on concrete mix design and structural dimensioning. These parameters include the extent of pozzolanic additions (fly ash and microsilica) to the concrete mix, concrete surface treatments, the physical dimensions of the substructure, and the extent of concrete wetting that can result in service. These parameters are expected to affect the electrical resistivity and oxygen diffusivity of the concrete. Prior to this investigation, there was qualitative agreement that corrosion was less severe when concrete resistivity was greater, and that corrosion macrocells played a significant role on the extent and distribution of corrosion of rebar in concrete. However, relatively little was known about the value of

these parameters and their relative importance in Florida substructures. There was also no quantitative treatment to serve as a tool to investigate the effect of changes in the relevant variables on the overall corrosion extent and distribution. The investigation described here addressed those matters by establishing the objectives indicated below.

1.1 OBJECTIVES

(1) Examine the effect of selected concrete compositions and surface treatments on the development of corrosion in marine substructure.

(2) Establish the extent of corrosion macrocell action and its variation with concrete moisture in marine substructure service.

(3) Develop a comprehensive model for the prediction of corrosion distribution in reinforced concrete piling as a function of concrete properties and system geometry.

2. APPROACH

The first objective, the effect of concrete composition and surface treatment, was addressed experimentally by constructing reinforced concrete columns and placing them in a salt water tank with the lower portion of each column submerged. Periodic salt-water wetting of the portion of each column just above water replicated the splash-evaporation regime encountered in the field. The reinforcement in each column was split electrically to allow measurement of macrocell currents and overall corrosion activity as a function of time. The baseline column contained concrete made with Type II cement and 20% fly ash replacement. Variations included the addition of 5% microsilica, and the use of silane or siloxane surface treatments on the portion of the columns above water. Testing took place for for nearly 3 years.

The second objective, the determination of macrocell action and effect of moisture, was also addressed using laboratory columns partially submerged in salt water. The geometry of these columns allowed for more detailed separation of the reinforcing steel into individual elements. The only concrete formulation used was Type I cement with no pozzolanic additions. The evolution of corrosion in these systems was evaluated as a function of time, and the upper portion of selected columns was subject to fresh-water wetting to cause pronounced variations in the concrete resistivity profile. This testing also took place for nearly 3 years.

The third objective, modelling, was accomplished by the development of a computational model of a generic substructure column using finite difference calculations that divided the column into a large number of computational nodes. The distributions of electrical potential and oxygen concentration were calculated for the steady state case during the propagation stage. The concrete resistivity and oxygen diffusivity distribution profiles of the column were used as input. The model provided quantitative predictions of the resulting corrosion rate along the reinforcement cage, and the effect of the concrete variables on that distribution.

Each objective has been organized below into a section of its own (Sections 3 - 5 correspond to Parts I - III). Each of these three sections (or Parts) includes the procedure/approach, results/discussion, references, tables and figures that pertain to that part of the investigation.

3. PART I: EXPERIMENTAL INVESTIGATION OF THE EFFECT OF CONCRETE COMPOSITION AND SURFACE TREATMENT.

3.1 PROCEDURE

3.1.1 Concrete Columns.

The test specimens were reinforced concrete columns 244 cm (96 in) high, with a square cross-section 12.7 cm (5 in) on the side. The columns contained two No. 4 (1.27 cm diameter) rebars placed lengthwise at corners of the cross section oppisite one another. The concrete cover (minimum distance between the surface of each rebar and the external surface of the concrete) was 2.5 cm (1 in). Each rebar was cut into four separate segments that were 57 cm (22.5 in) long, in order to create four levels of testing. Each segment was provided with an individual electrical connection to a switch box on the outside of the column (see Figure I.1). The segments of each rebar were kept normally electrically connected to each other by closing the switches in the box. Four solid reference electrodes (activated Titanium) were positioned in the centerline of the column by the midpoint of each rebar-segment level. The electrodes were connected by wires to an external contact box and calibrated periodically against a saturated Calomel electrode (SCE).

Before concrete placement, the surface of the rebar segments was conditioned with a pre-rusting treatment to simulate the conditions often encountered in actual concrete structures when exposed to construction yard environments. The treatment consisted of mist spraying the segments once daily for seven days, using a 3.5% NaCl water solution. The final surface appearance was a dulled "rust-orange" color.

Because the steel was mechanically segmented, two continuous No. 4 fiberglass bars were placed along the columns to act as additional structural strengtheners to prevent damage during positioning of the columns in the test tank. These bars provided additional strengthening without affecting the electrical properties of the system.

3.1.2 Concrete and Surface Treatments.

Two concrete compositions, labeled F and F+S were used. Both compositions had a water/cementitious ratio of 0.45 which was higher than that used in normal FDOT construction and was intended to accelerate the testing procedure.

Both concrete compositions had a total cementitious content of 302 Kg/m^3 (512 pounds per cubic yard (pcy)). The low value of cementitious content was also intended to accelerate the testing procedure. Both compositions used Type II portland cement. Composition F contained fly ash (Type F, meeting FDOT acceptance specifications) in an amount equal to 20% of the total cementitious weight. Composition F+S contained fly ash in an amount equal to 20% of the total cementitious weight and microsilica in an amount equal to 5% of the total cementitious weight. The air content of the concrete was 5.5%. The fine aggregate (silica sand) had a fineness modulus of 2.27 and a specific gravity of 2.63. The coarse aggregate (limestone) had a specific gravity of 2.45. The coarse aggregate had a maximum size of 1 cm (3/8 in) which was half the size normally used in FDOT construction. The coarse aggregate was intended to accommodate for the small concrete cover used in the laboratory columns. Except as indicated, both concrete mixtures approached the FDOT Structure Design Guidelines (Chapter 7) for Florida Concrete Design and Construction Criteria.

The columns were divided into four groups of 3 columns each. Each group corresponded to a material/surface treatment combination as shown in Table I.1.

All columns were cured in their horizontal wooden forms beneath a plastic cover for 20 days. The columns remained in the forms, with the plastic removed, for another 8 days in the laboratory environment (60% relative humidity). The columns were then removed from their forms and allowed to dry in the laboratory for a period of 6 to 10 days. The columns were then placed vertically in the test tank. The rebar

segments were interconnected, by closing the switches, shortly after placement in the tank (about one month after casting). Salt-water splashing (see below) began simultaneous with the closing of the switches. Day zero of the time-test sequence was defined by that event.

Two types of surface treatments were used. One was an alkyl alkoxy silane and the other was an alkyl alkoxy siloxane (called silane and siloxane respectively hereafter). The silane treatment was produced by Huls of America, and is known by its product name as Chem-Trete BSM 40. The siloxane product was made by Prosoco, Inc. and its product name is Consolideck SX.

Before application of the surface treatments, the columns were cleaned with a steel wire brush and rinsed with distilled water. Then the treatments were applied to the entire exposed portion of the column (from 2 in (5 cm) above the waterline to the top of the column). Both treatments were applied after the columns had undergone 68 days of regular exposure. The wait replicated field practice whereby concrete curing is allowed to advance enough to appropriately receive the surface treatment. The treatments were applied with a paint brush.

Each of the columns to be treated with the siloxane treatment received two successive applications, approximating the manufacturer's recommended practice. The first application was a saturating treatment and the second coat was applied approximately 10 minutes after the material from the first treatment was absorbed by the concrete. The total siloxane coverage was 6.4 m^2/liter, comparable to the nominal manufacturer's specification of 7.4 m^2 /liter for vertical surfaces. The columns receiving the silane treatment had one application only, also approximating recommended manufacturer's practice. The coverage rate was 4.6 m^2/liter (recommended value was 4.3 m^2/liter).

3.1.3 Testing Environment.

All columns were placed vertically into a fiberglass tank containing 5% NaCl water solution. The lower 63 cm (25 in) of each specimen was submerged. This placed the lower rebar level (level No. 4) completely under the waterline, while the remaining levels were completely above water. The surface of the concrete extending from the waterline to 63 cm (25 in) above it (level No. 3), was splashed with the salt-water solution, by means of a hose and pump, five times a week (Monday to Friday). Each surface experienced about one minute of direct wetting from the water jet during each wetting event. This portion of each column was called the splash-evaporation zone, simulating the region of the same name present in actual field service.

In addition to the saltwater application, one column from each group (columns 6, 9, and 12) other than the F+S group was mist sprayed with distilled water over the entire unsubmerged portion also five times a week. This fresh-water wetting took place 5 hours after the salt-water application. Approximately 300 cm^3 of distilled water was used every time for each sprayed column. This procedure began on test day No. 230. The purpose of the procedure was to examine the effectiveness of the silane and siloxane surface treatments as moisture barriers. From day 500 to day 920 fresh-water wetting of column 12 (siloxane) was discontinued. From day 920 on, fresh-water wetting of column 12 was renewed and wetting of column 3 (microsilica) was initiated.

The laboratory was at a nearly constant temperature of 21° C and typical relative humidity of 60%±10%. Starting on day No. 666, a plastic canopy was placed around the top 127 centimeters (50 in) of all the columns to moderate the extent of drying of the concrete in that region.

3.1.4 Corrosion monitoring

The potential of the rebars within each column was periodically measured with respect to the internal reference electrodes embedded at each of the four levels. The potential measurements were performed with the switches in the normally closed condition, to reflect the actual steady state polarization condition present at each level of the rebar. The embedded electrodes were periodically calibrated with respect to an external saturated calomel electrode (SCE) in contact with the water. The calibration was performed with all switches in the column momentarily open. The switches were momentarily open to minimize errors from ohmic potential drops that would otherwise be caused by macrocell currents. While this procedure could not eliminate all ohmic drop errors in the calibration, the method was considered to be more dependable than calibration against an external reference electrode in contact with the concrete surface. The latter procedure is subject to considerable deviation depending on the condition of the concrete surface [I.1].

The amount of macrocell current flowing between the rebar segments placed at two different levels was measured by momentarily opening the inter-level switch and inserting a low resistance meter (1 ohm or less) into the circuit. All switches in the column other than the one being sampled remained closed.

The resistance of the concrete was measured between the pair of side-by-side rebar elements at each of the four levels of each column. These measurements were taken with a Model 400 Nilsson Soil Resistance Meter. During the resistance measurements, the switches were opened at all levels. Disregarding end effects, the average concrete resistivity ρ at each column level can be roughly approximated by

$$\rho = C_c * R \qquad (I.1)$$

where C_c = 60 cm is the cell constant for column segments above the waterline, and C_c = 90 cm is the value for the segments below the waterline. The cell constants

were evaluated by means of U. C. plexiglas test-cell models that contained segments of rebar submerged in a liquid of known resistivity. A Nilsson Model 400 meter was used for measuring the resistance of the model cells. The below-water condition was simulated by lining the sides of the model cell with aluminum foil. That simulation was based on treating the salt water surrounding the concrete as a medium of negligible resistivity compared to that of the concrete (see Part III). For verification, finite element computations of the cell constants were made using an Algor software package. The computed cell constants closely matched the results from the physical models.

A limited number of polarization resistance and electrochemical impedance measurements were performed on independent rebar elements of selected columns. The steady-state DC polarization condition of the element being measured was maintained during the polarization test to reflect the actual element operating condition [I.2].

3.2 RESULTS AND DISCUSSION

3.2.1 Concrete resistance.

The resistance of the concrete between elevation and parallel rebar elements varied with time in all column groups. Figures I.2 to I.13 show the evolution of the interelement resistance of each column through the nearly 3-year test period reported here. Conversion to nominal concrete resistivity values can be made using the appropriate cell constant and Eq. (I.1). The conversion does not apply for level 3 because resistivity was highly non-uniform at that level, and because the adjacent low resistance at level 4 provided an additional low resistance current path.

The initial concrete resistances at column level 4 (submerged portion) were approximately 230Ω (about 20,000 Ω-cm) for the column group 1 (F+S concrete,

Table I.1). The initial resistance was nearly 80 Ω (about 7,000 Ω-cm) for groups 2 to 4 (F concrete). Because of the faster microsilica reaction, the concrete with microsilica and fly ash should develop lower porosity at early ages compared to the concrete with fly ash alone [I.3-I.5]. For the same reason, the pore solution pH of the F+S concrete at early ages should be lower than that of the F concrete. A lower pore solution pH is also expected to result in higher resistivity of the pore solution [I.6]. Consequently, the observed difference between the early concrete resistivities of types F+S and F are in agreement with the expected smaller pore volume and the higher pore solution resistivity of the F+S concrete. Considering that the concrete was near water saturation, the absolute resistivity values can be used to obtain a rough indication of the corresponding Coulomb result that would have been obtained with a rapid chloride permeability test at the same age. Using the correlation reported in Reference [I.5], the approximate Coulomb values would have been 800 C for the F+S concrete and 3,000 C for the F concrete. Those values were in the range of values expected for the concrete mix designs used [I.5].

The resistance of the submerged portion of the columns increased with time reflecting the curing process. The resistance was initially smaller in the F concrete specimens than in the F+S specimens (following the behavior discussed above). However, the F specimens experienced larger proportional resistance increases with time than the F+S specimens, so that both types reached comparable resistance values near the end of the test period. As expected, these trends suggest that in this permanently wet concrete, the pozzolanic reaction of the fly ash eventually developed to an appreciable extent (although the reaction of the fly ash was slower than the reaction of the microsilica). The effect of the microsilica, which strongly differentiated the resistivity behavior at early ages, was no longer predominant after the system evolved beyond 2 years. Because the resistance measured at level 4 was considerably influenced by the resistivity of the concrete between the bars and the surrounding salt water, the measurements might reflect the effect of chloride intrusion (as well as some extent of concrete leaching with salt water invasion of concrete

pores near the surface) in that region. These are possible causes for the slight downturn in the resistance at level 4 observed in some of the specimens near the end of the test period. Disregarding these and other complicating factors, the concrete resistivity values of both types of concrete (after 3 years of submersion) were in the 30,000 to 40,000 Ω-cm range, corresponding to an estimated Coulomb value of about 300 C. That value approaches the range of values reported for similar concrete mixtures under comparable conditions.

The resistance at the upper levels above water increased with time reflecting a combination of continuing curing and loss of water by evaporation. The increasing trend was monotonic during the first year, and showed fluctuations afterwards reflecting changes in humidity of the surrounding air (all columns) plus the effect of fresh water surface wetting (columns 6 and 9 since day 230, column 12 during days 230-500 and since day 920, and column 3 since day 920).

The resistivity of the upper concrete in the columns of group 2 (Base, F concrete) that were not subject to surface wetting approached 600 KΩ-cm after 3 years. This observation reflected extensive drying of the concrete although a canopy for increasing water retention was placed at day 666. Resistivity values this high are not uncommon in concrete exposed for long times to average relative humidities on the order of 60% to 70%, as present in the laboratory. The resistivity of the upper concrete in the columns of groups 3 (Silane) and 4 (Siloxane) that were not exposed to surface wetting followed essentially the same trend as those in Group 2. Thus, the surface treatments did not alter the drying/curing trends of the concrete under those conditions. The resistivity of the upper concrete in the columns of group 1 (F+S concrete) that were not exposed to surface wetting also increased with time. However, the increase was proportionally less than for the type F concrete columns so that the concrete resistivity values were eventually similar for both types of concrete. This behavior is in line with that of the submerged region, suggesting that the differences between both types of concrete became less marked as the fly ash undergoes sufficient reaction.

Surface wetting of the concrete of the Base group (Column 6) resulted in a resistivity of the upper level concrete that was two to three times lower than in the unwetted surface columns in the same group. However, concurrent surface wetting in the Silane (Column 9) and Siloxane (Column 12) groups during the period 230 to 500 days resulted in no discernible effect. These results suggest that both surface treatments succeeded in preventing significant ingress of water when it was periodically sprinkled on the surface of the concrete. As shown above, the treatments did not cause water to be retained in the concrete. Both observations indicate desirable results of the treatments, since in an actual field application preventing sea-water entry in the splash-evaporation zone would also hinder chloride ion ingress, and facilitating concrete drying could reduce the extent of corrosion macrocell activity [I.2, I.7, I.8]. Because the resistivity of nearly dry concrete is highly sensitive to relative humidity changes, the resistivity data showed increasingly higher fluctuations as the test progressed. Therefore, little information could be derived from the resistivity monitoring during the last year of the test. The possible effects of wetting column No. 3 (F+ S group) could not be determined.

3.2.2 Steel Potential and Macrocell Current.

Figure I.14 illustrates the typical potential vs time trends observed for the various elements within the test columns. Most columns displayed qualitatively similar behavior. The potential changes with time were generally larger at element 4, in the portion of the column below water. Figure I.15 illustrates the typical trends observed in the test columns for the absolute magnitude of macrocell current flowing between the various levels. In the long term, the amount of current flowing at switch 3 between rebar levels 3 and 4 (just above and below the water line, respectively) greatly exceeded the amount of current flowing through switches 1 and 2 (in the drier portion of the columns). This indicated that with the test conditions used in these experiments, most of the long-term macrocell action was confined between the lowest two column elements. Therefore, the analysis below will focus on those two elements. Part II (Section 4) of this report deals with another test system where macrocell action affecting multiple elements was achieved.

Figures I.16 through I.19 show the electrode potential of the steel in the submerged portion of each column group as a function of exposure time. Figures I.20 through I.23 show the macrocell current measured at switch 3 (between the submerged portion and the rest of the column) for each column group as a function of time.

Shortly after starting the test, all steel elements developed very negative potentials (as low as -1.1 V SCE in the Microsilica group and -1 V SCE in the Base group). In the Microsilica group the potentials rose to values of about -250 mV to 0 mV SCE over periods from 100 to 400 days. This was followed by a decrease to potentials of -300 mV to -500 mV SCE afterwards. Disregarding the first few weeks of testing, the period of potential rise was associated with the presence of generally decreasing macrocell currents in which the portion below water behaved as a net anode. With the exception of element A in column 3, the macrocell currents decayed from values of 50 μA to 150 μA to nearly zero during the potential increase regime. The later return to more negative potentials was associated with corresponding increases in the macrocell current of the elements experiencing the potential transition. The potential in element A of column 3 decayed earlier than any other element, and the corresponding current started to increase before it had a chance to approach zero.

The Base, Silane, and Siloxane groups experienced potential and current trends comparable to those of the Microsilica group, except that the initial potential rise to more noble values took place at a rate that was 2 to 3 times faster than that of the Microsilica group.

The potential-current trends of the steel in all the test columns may be interpreted in the idealized manner summarized in Figure I.24. The analysis assumes (for simplification) that the portion of the reinforcing steel above water was the site of only cathodic reactions, while the steel below water was experiencing primarily anodic

behavior. Because the steel was placed in the concrete in a strongly pre-rusted condition with some residual salt contamination, the steel showed highly negative initial potentials. This is characteristic of steel in the active condition. The steel below water was likely to quickly consume its immediately surrounding oxygen by means of cathodic oxygen reduction reactions. Since the oxygen supply through fully submerged concrete is slow (see Part II), the steel was then expected to have developed potentials approaching those of the Fe/Fe^{++} equilibrium. Some deviation from that equilibrium in the positive direction would be provided by an electronic macrocell current to the steel portion above water, where oxygen flow across the partially dry concrete cover should be more efficient. The electronic macrocell current had the initial value I_{M1}. The current decreased with time as the surface of the steel below water began to passivate under the action of the alkaline concrete pore solution environment. This initial period of decreasing macrocell currents is defined in Figure I.24 as the passivation period. (Macrocell currents during the very first few days of exposure might in some cases have followed more complicated patterns not addressed here). After a time, t_p , the macrocell current reached very small values and the steel potential exceeded a value, E_{pp} , which is typically associated with the condition of steel passivity (as for example in the criterion set by ASTM C-876).

The analysis in Figure I.24 assumes that (concurrent with the initial passivation process) chloride ions from the surrounding saltwater had been penetrating the concrete cover. As a result, the chloride ion concentration at the surface of the reinforcing steel steadily increased. After a time t_i , the concentration exceeded, at some spot on the steel surface, the amount needed to cause breakdown of the passive layer. The steel surface on the affected spot became locally active, releasing iron ions into the surrounding environment and freeing electrons into the steel body. That event was manifested by a sharp reduction in the steel potential, often followed by a gentler potential decline as a larger fraction of the steel surface became active because of increasing chloride contamination and other factors [I.9]. Many of the

electrons released by the anodic reactions were consumed in the region above water by oxygen reduction reactions. This resulted in the development of a sizable macrocell current that started also at time t_i . A smaller fraction of the electrons might have been consumed below water, depending on the extent of oxygen transport that the wet concrete would have allowed (see Sections II and III). As most of the steel surface subject to chloride ingress became active, the system approached a steady state regime characterized by a steel potential E_A and a macrocell current I_{M2} .

The potential and macrocell current data showed few indications of active behavior in the segments above the waterline during the test period reported here. In most cases, as exemplified in Figure I.14, after the initial passivation stage the potential of the segments above water remained in the regime usually associated with passive steel in concrete exposed to air. Figures I.25 and I.26 illustrate typical potential-current behavior for the rebar elements immediately above and below the waterline. The figures were prepared by plotting the value of the net current of any given rebar element, as a function of the potential of the same element, for every test date. The resulting composite diagram shows the overall E-log i record of each element over 3 years of testing.

For the element below water (level 4), the main cluster of points (around -500 mV and 100 μA) corresponds to the active steel behavior encountered during the earliest and latest stages of evolution. Points at higher potentials and lower currents correspond to the transition stages at intermediate times. For the element above water, the main data cluster also corresponds generally to the active stage of the element below water. The current densities are of the same magnitude as those of the level 4, but correspond to net cathodic instead of net anodic currents. The overall data for the cathodic behavior could be approximated by a straight line with slope between 100 mV and 200 mV per decade. This corresponds to the Tafel slope of the oxygen reduction reaction [I.2]. The anodic potential-current data could be approximated by a similar slope only at small current values, but the slope becomes

much larger at high currents. This was to be expected if the reaction below water was predominantly the anodic oxidation reaction, limited by both the extent of the cathodic reaction above water and the ohmic drop in the concrete between the steel that was above and below the water.

Only two instances of long-term potentials clearly approaching the active regime (more negative than -300 mV SCE) were recorded for rebar segments at level 3 of any column during the test period. These were in columns 10, side A, and column 11, side A (both in group 4, siloxane). Near the end of the three-year test period, external evidence of corrosion above water was observable in the form of a rust spot near the bottom of level 3 on side A of column 10, a rust spot near the bottom of level 3 on side A of column 4 (group 2, base), and a fine crack with no rust near the center elevation of level 3 on side B, also in column 4.

Attempts to evaluate the relative extent of corrosion taking place at elements 4 and 3 were made by means of polarization resistance (PR) and EIS measurements. These types of measurements detect corrosion only indirectly through the combined effects of both anodic and cathodic activity, and are subject to many sources of error [I.10]. Results of EIS tests and polarization resistance measurements performed during the second year of exposure are provided in Ref.[I.11]. The EIS measurements revealed that the electrochemical response in the columns (both in EIS and PR tests) was severely complicated by the column geometry and interfacial charge storage effects. Keeping those limitations in mind, the results of the PR measurements performed at that time suggested that the level of electrochemical activity was comparable for all four column groups, and comparable for rebar levels 3 and 4 (immediately above and below the waterline respectively). This was in agreement with the indications of the potential/current measurements: that the zone above the water was in most cases not experiencing active corrosion and it was the site of predominantly cathodic reaction.

The evidence discussed above suggests that, during the 3-year test interval, the zone below water reached an active surface condition quite early (roughly at day 300 for the group with F+S concrete and at day 150 for the groups with F concrete). A rough estimate can be made of the absolute value of the time that would have been required for the steel to reach active behavior if simple diffusion mechanisms were taking place. The resistivity estimates suggested effective chloride diffusion coefficients of about 0.15 in^2 /y [0.97 cm^2 /y] and 0.45 in^2 /y [2.9 cm^2 /y] for the Microsilica and Base groups respectively [I.5]. (It should be emphisized that correlations between chloride diffusivity and electric conductivity of the concrete are only approximate and still subject to controversy [I.13]). For the zone below water, assuming that the concrete had about 20% average porosity (taking into account the high water to cement ratio and porous limestone aggregate) saturated with 5% NaCl water, the region near the surface of the concrete could be expected to acquire a chloride content approaching 10 pcy [8 Kg/m^3]. A chloride concentration threshold for active corrosion initiation of 1.2 pcy (0.7 Kg/m^3) may be assumed on first approximation [I.5, I.12]. Nominal application of Fickian diffusion assumptions [I.5, I.12] and consideration of corner effects [I.5, I.14] project times to active corrosion initiation of about 500 and 170 days for the F+S and F concrete groups respectively. The actual times for the observation of active conditions were comparable to those projected from the simplified conditions just assumed.

It must be kept in mind that the above analysis used rough approximations. Therefore, it is not suitable for a precise evaluation of times to activation of the steel surface. Chloride transport processes, other than simple diffusion, cannot be disregarded. Possible acceleration of the corrosion initiation period could result from additional transport mechanisms for the chloride ions to the rebar surface (convective processes such as capillary absorption of saltwater shortly following immersion of the columns, microcracks in the concrete, chloride-flow bypasses through large aggregate particles, and faster-than-expected chloride transport while the concrete was undergoing early curing). The slow passivation of the steel (and possible small values

of the pore solution pH) might also result in an effective lowering of the chloride concentration threshold during the early life of the system. Consequently, a reduction could take place in the time needed for buildup of the necessary chloride content for depassivation. The data from element A in column 3 (early onset of the chloride-induced stage of corrosion before the initial passivation stage had finished) may correspond to an example of such behavior.

The evidence to date indicates that severe corrosion had developed in only a few of the above-water segments (all in columns with concrete F) by the end of the 3-year test period. This finding (subject to confirmation by future monitoring of the column set) suggests that the chloride concentration threshold for initiation of active corrosion had not been reached in most of the type F concrete groups or in any of the F+S column groups that were above water after 3 years of the salting procedure. This circumstance could have resulted from various possible factors. These include a higher chloride threshold for the steel in the concrete above water, a slower transport of chloride through the dryer concrete, or a combination of the above. In addition, relatively low chloride concentrations on the concrete above water can result because the salt accumulation mechanism may require some time to develop [I.15, I.16]. In the case of the Silane and Siloxane groups, the coatings might have been effective in reducing chloride accumulation. Exposure and testing of the column groups, including determination of chloride concentration profiles, will continue in the future to test those possibilities as mature corrosion patterns develop.

An alternative explanation for the apparently small incidence of corrosion above water is that the portion of steel below water was acting as a sacrificial anode. If only segment No.3 (steel area ~220 cm^2 (0.23 ft^2)) was susceptible to corrosion, the typical electronic macrocell current (~100 μA) sinking into that element in most columns corresponded then to a protective current density of 0.45$\mu A/cm^2$ (0.43 mA/ft^2). That amount of protective current approaches values commonly used in impressed current systems to considerably retard the effect of corrosion [I.17].

The results supported the expectation that the concrete with the higher amount of pozzolanic replacement, including both fly ash and microsilica, would have the lowest early permeability and consequently would retard the initiation of corrosion under the accelerated conditions used. On the other hand, the observed longer time for steel passivation in the F+S concrete underscored the importance of keeping in mind the possibly greater susceptibility for corrosion of the steel if the use of pozzolanic additions results in a significant lowering of the pore solution pH.

In the mode of corrosion operating by the end of the test period (most corrosion below water), the extent of macrocell current flowing in the F+S concrete group was not significantly different from that in any of the other column groups. As suggested by the resistivity results, this is not surprising since (after about two years) both types of concrete had comparable resistivity values, indicative of similar ohmic macrocell limiting effects (see Part III) and comparable permeability. As indicated before, the differences between both types of concrete were expected to become less as more of the fly ash reacted, a process that appeared to have taken place to a large extent by the end of the second year. In actual field conditions, with larger concrete covers over the rebar, the behavior of both types of concrete might be comparable also from the point of view of chloride ion penetration since most of the transport would take place after the fly ash reactions reached a mature stage.

The surface coatings succeeded in reducing water entry (and did not increase retention) in the upper portion of the columns. Those are desirable trends. However, within the time frame of the experiment, there was no discernible effect on the extent of macrocell current or in the tendency for corrosion development. Prolonged monitoring and coring of the columns for chloride profile evaluation will be necessary to reveal any possible effects.

3.3 PART I REFERENCES

I.1. Bennet, J., and Mitchell, T., "Reference Electrodes for Use with Reinforced Concrete Structures" , Paper No. 191, Corrosion/92, National Assoc. of Corrosion Engineers, Houston, 1992.

I.2. Sagüés, A., Electrochemical Impedance of Corrosion Macrocells on Reinforcing Steel in Concrete, Paper No. 132, Corrosion/90, Nat. Assoc. of Corr. Engs., Houston, 1990.

I.3. Hussain, E. and Rasheeduzzafar, J., Materials in Civil Engineering, Vol. 5, p. 155, 1993.

I.4. ACI Commitee 226, "Silica Fume in Concrete", ACI Materials Journal, Vol. 84, p.158, 1987.

I.5 Berke, N.S. and Hicks, M.C., "Estimating the Life Cycle of Reinforced Concrete Decks and Marine Piles Using Laboratory Diffusion and Corrosion Data", p. 207 in "Corrosion Forms and Control for Infrastructure", ASTM STP 1137, Victor Chacker, Ed., American Society for Testing and Materials, Philadelphia, 1992.

I.6 Goñi, S., Moragues, A. and Andrade, M.C., "Influence of the Conductivity and the Ionic Strength of Synthetic Solutions Which Simulate the Aqueous Phase of Concrete in the Corrosion Process", Materiales de Construccion, Vol. 39, p. 19, 1989.

I.7 Andrade, C., Maribona, I., Feliu, S., Gonzalez, J., and Feliu Jr., S., Corrosion Science, Vol. 33, p. 237, 1992.

I.8. Gonzalez, J., Lopez, W. and Rodriguez, P., Corrosion, Vol. 49, p. 1004.

I.9 Aguilar, A., Sagüés, A. and Powers, R., Corrosion Measurements of Reinforcing Steel in Partially Submerged Concrete Slabs, p. 66 in Corrosion Rates of Steel in Concrete, N. Berke, V. Chaker and D. Whiting, Eds., STP 1065, ASTM, Philadelphia, 1990.

I.10 Sagüés, A. "Corrosion Measurement Techniques for Steel in Concrete", Paper No. 353, 22 pp., Corrosion/93, National Assoc. of Corrosion Engineers, Houston, 1993.

I.11 Hierholzer, S., "The Effects of Silica Fume and Silicone Concrete Surface Treatments on Controlling Corrosion in Reinforced Concrete Bridge Pilings", M.S. Thesis, University of South Florida, Tampa, November, 1992.

I.12 Sagüés, A., "Corrosion of Epoxy-Coated Rebar in Florida Bridges", Final Report to Florida D.O.T., WPI No. 0510603, University of South Florida, Tampa, May, 1994.

I.13 Pfeifer, D., McDonald, D.B. and Krauss, P., PCI Journal, p.38, January-February, 1994.

I.14 Sagüés, A., Research in Progress, 1994.

I.15 K.Uji, Y.Matsuoka and T.Maruya, "Formulation of and Equation for Surface Chloride Content of Concrete Due to Permeation of Chloride", in Corrosion of Reinforcement in Concrete, C.Page, K.Treadaway and P. Bamforth, Eds., p.258, Elsevier, New York, 1990.

I.16 Bamforth, P.B., "Concrete Classifications For R.C. Structures Exposed to Marine and Other Salt-Laden Environments", 11 pp., Paper presented at "Structural Faults and Repair", Edinburgh, June 29-July 1, 1993.

I.17 J.Bennett, J. Bartholomew and T. Turk, "Cathodic Protection Criteria Related Studies Under SHRP Contract", Paper No. 323, Corrosion/93, NACE International, Houston, Texas, 1993.

TABLE I.1
COLUMN GROUPS

COLUMN GROUP	COLUMN No.	CONCRETE	SURFACE TREATMENT
1 (MICROSILICA)	1-3	F+S	NONE
2 (BASE)	4-6	F	NONE
3 (SILANE)	7-9	F	SILANE
4 (SILOXANE)	10-12	F	SILOXANE

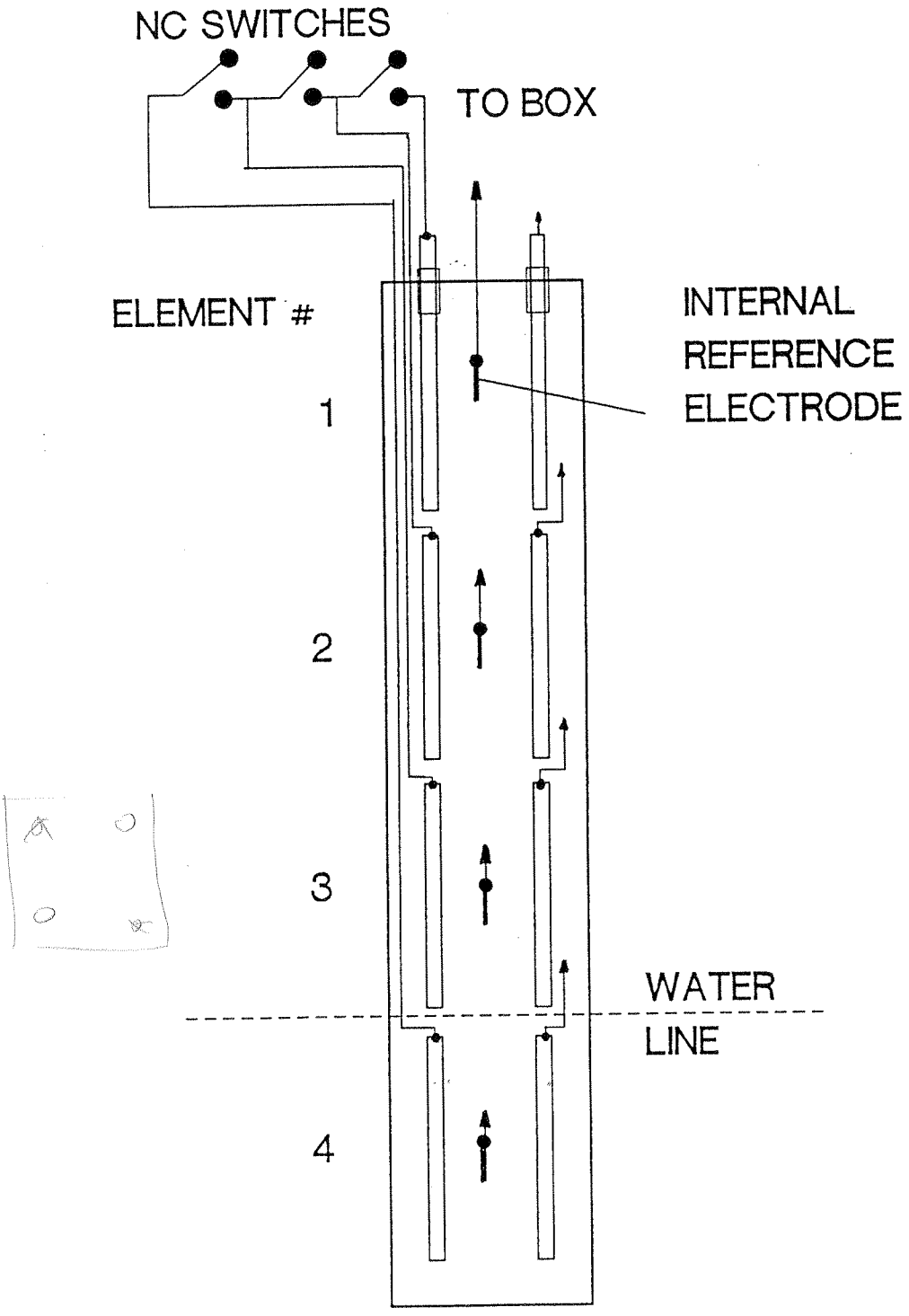

Figure I.1 Column Wiring Schematics.

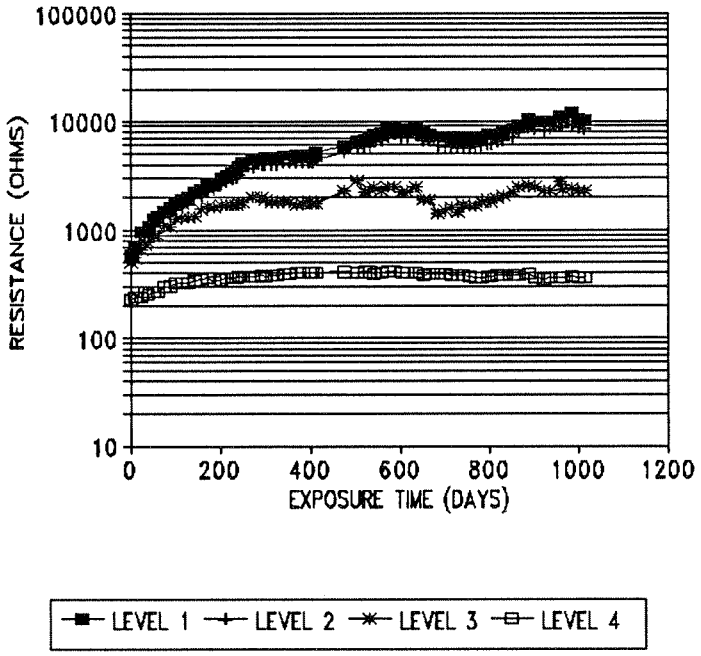

Figure I.2: Concrete resistance vs. time for col. 1.

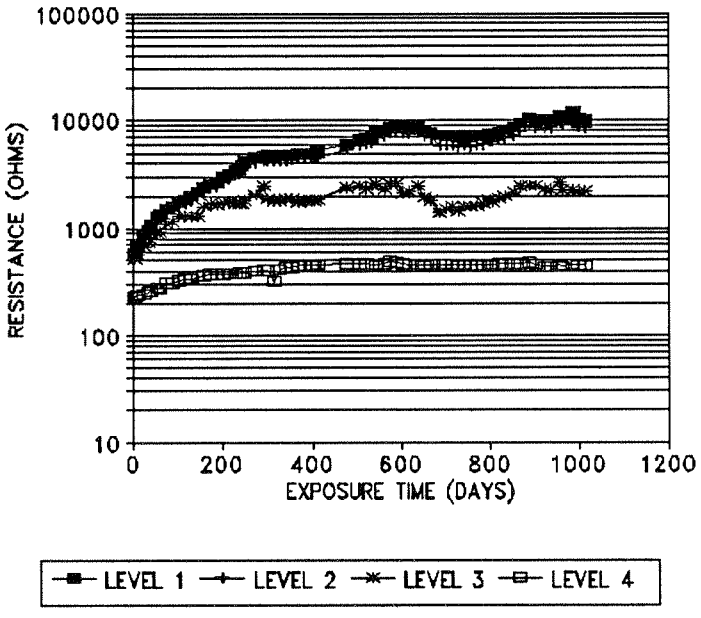

Figure I.3: Concrete resistance vs. time for col. 2.

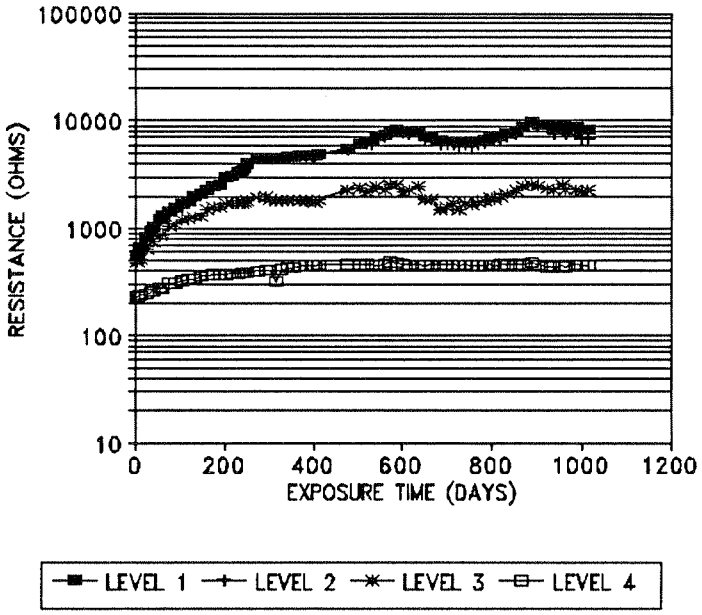

Figure I.4: Concrete resistance vs. time for col. 3.

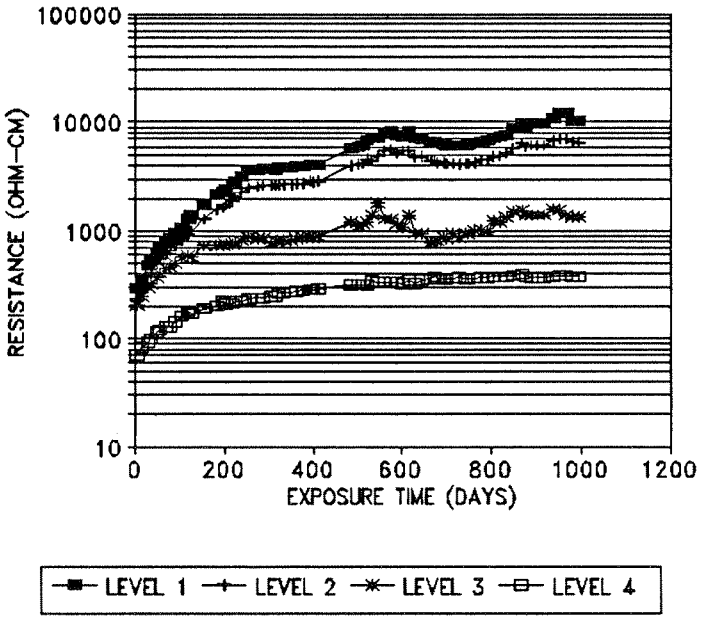

Figure I.5: Concrete resistance vs. time for col. 4.

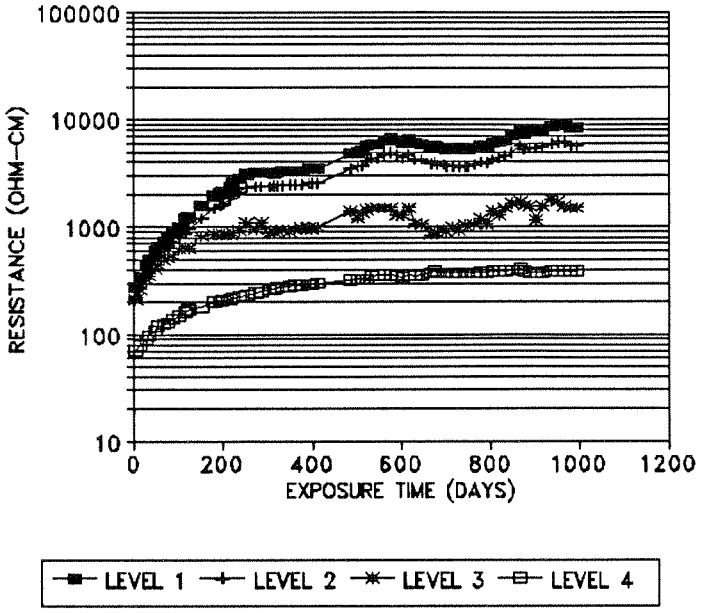

Figure I.6: Concrete resistance vs. time for col. 5.

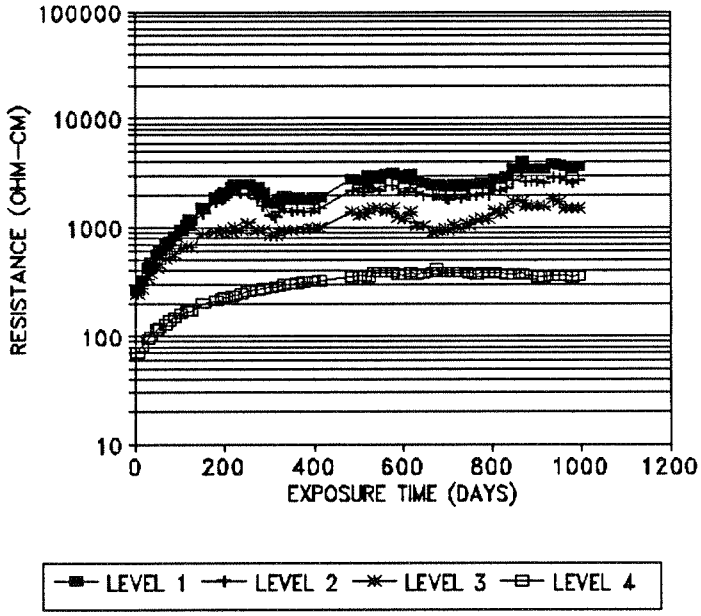

Figure I.7: Concrete resistance vs. time for col. 6.

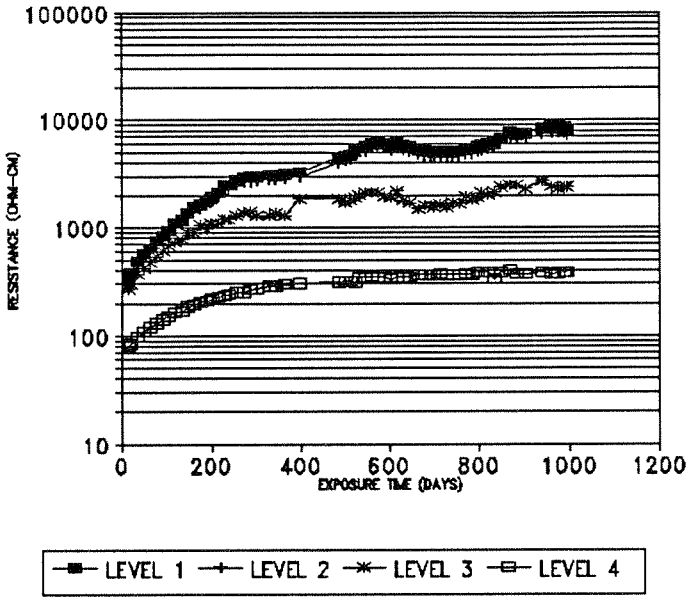

Figure I.8: Concrete resistance vs. time for col. 7.

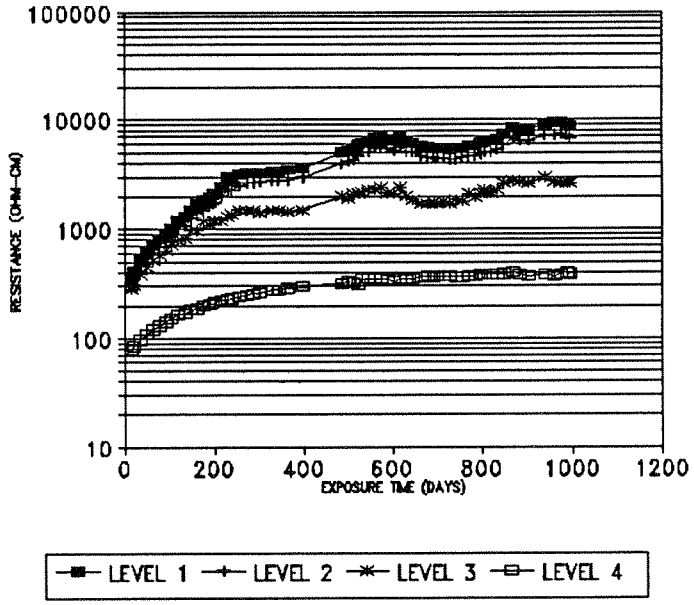

Figure I.9: Concrete resistance vs. time for col. 8.

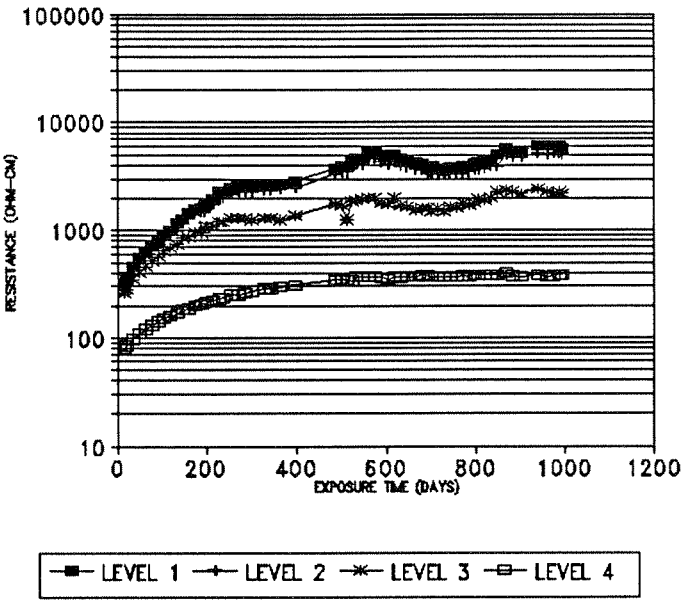

Figure I.10: Concrete resistance vs. time for col. 9.

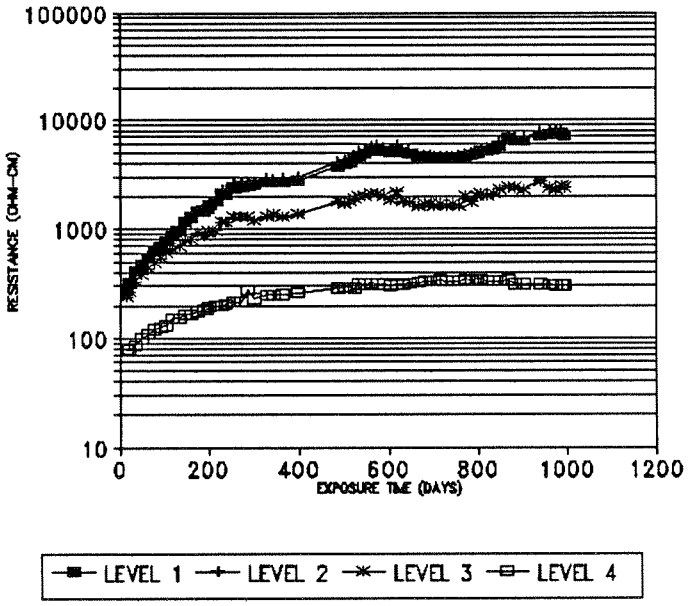

Figure I.11: Concrete resistance vs. time for col. 10.

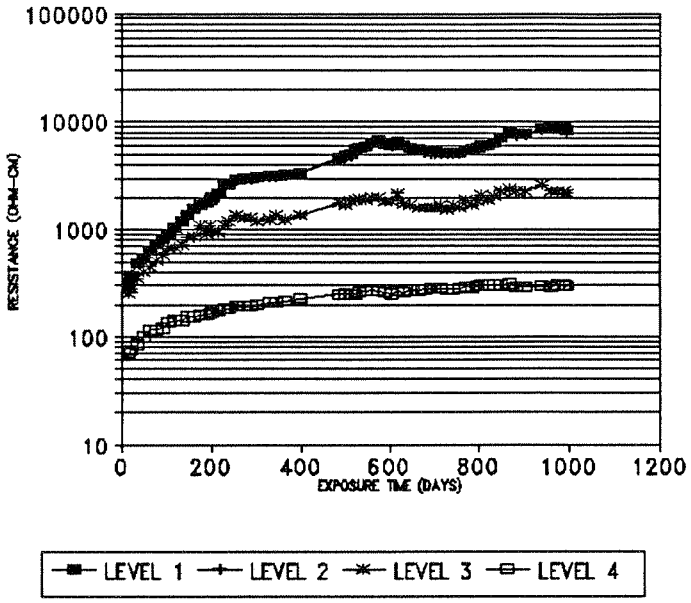

Figure I.12: Concrete resistance vs. time for col. 11.

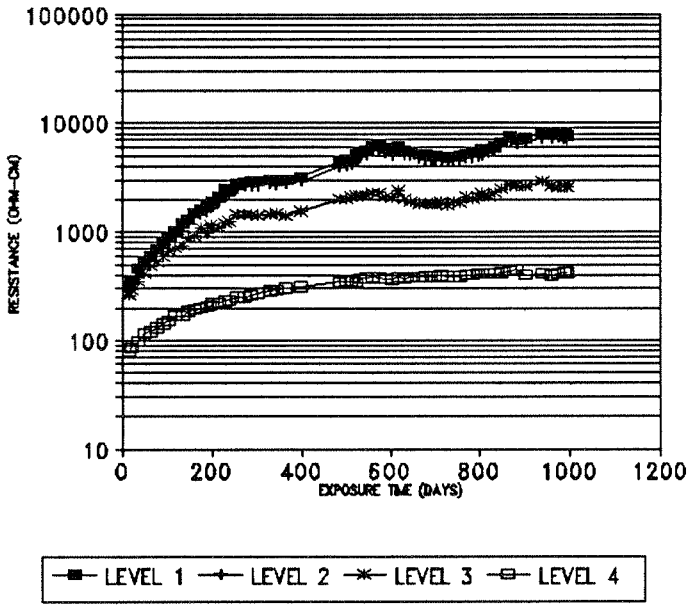

Figure I.13: Concrete resistance vs. time for col. 12.

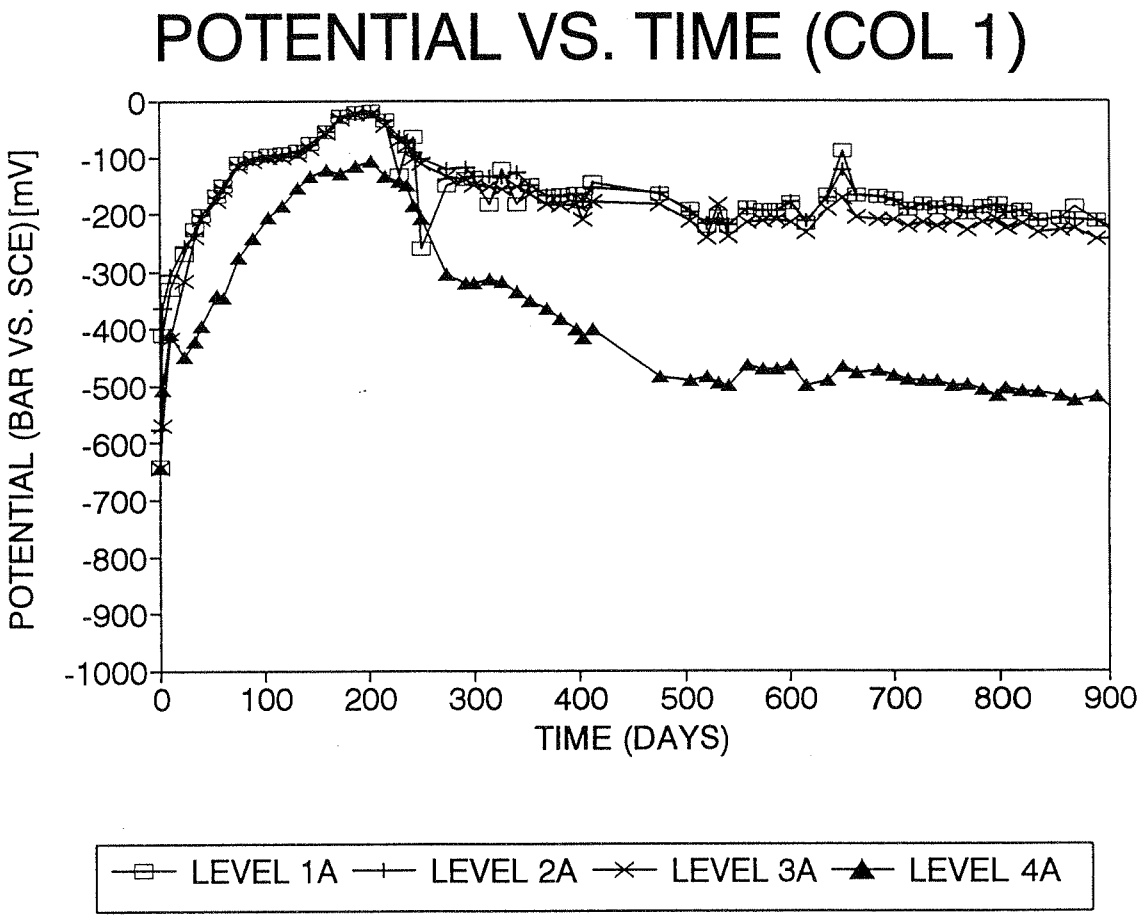

Figure I.14 Potential vs. Time Trends for Rebar On Side A of Column No. 1 (S +F Concrete).

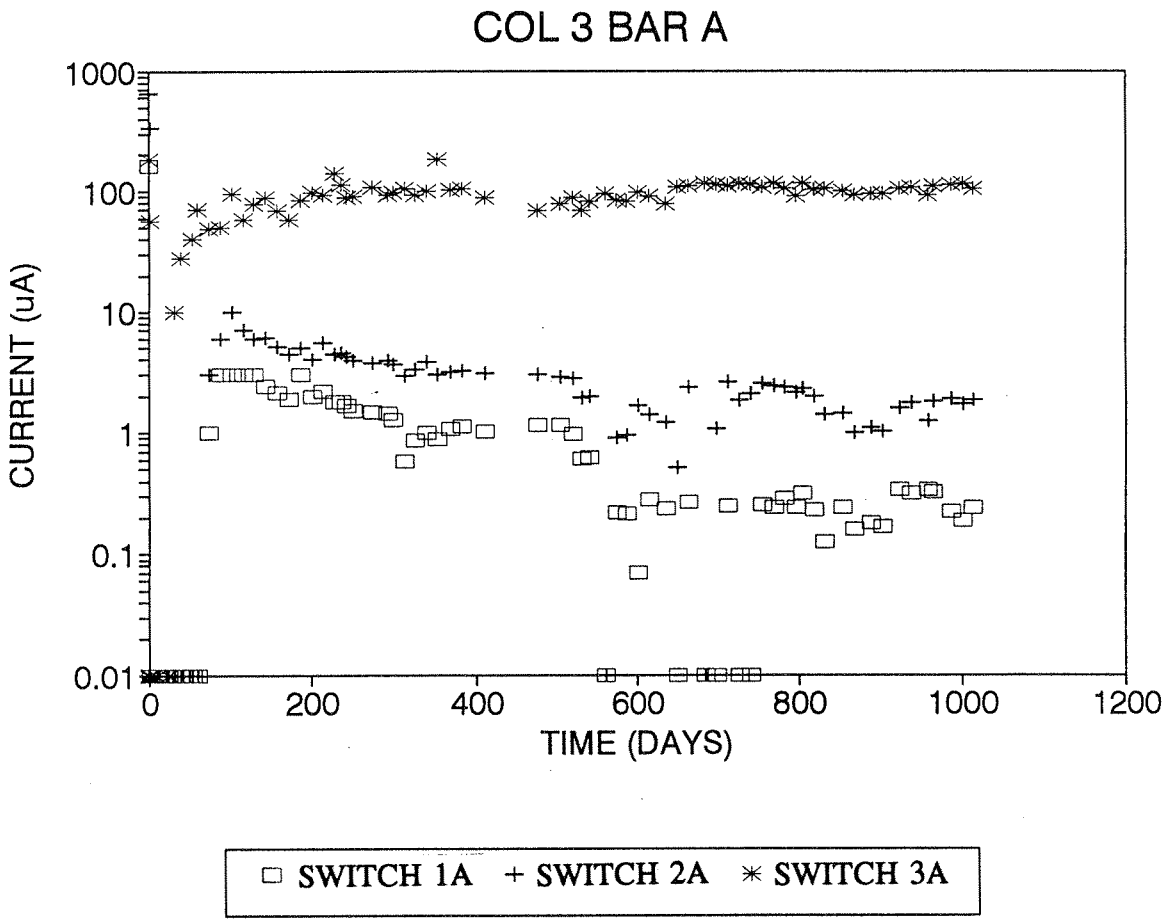

Figure I.15 Example of Magnitudes of the Macrocell Currents Flowing Through Switches (Switch No. 1 is the Highest) as a Function of Time. (Side A, Column No. 3, S + F concrete)

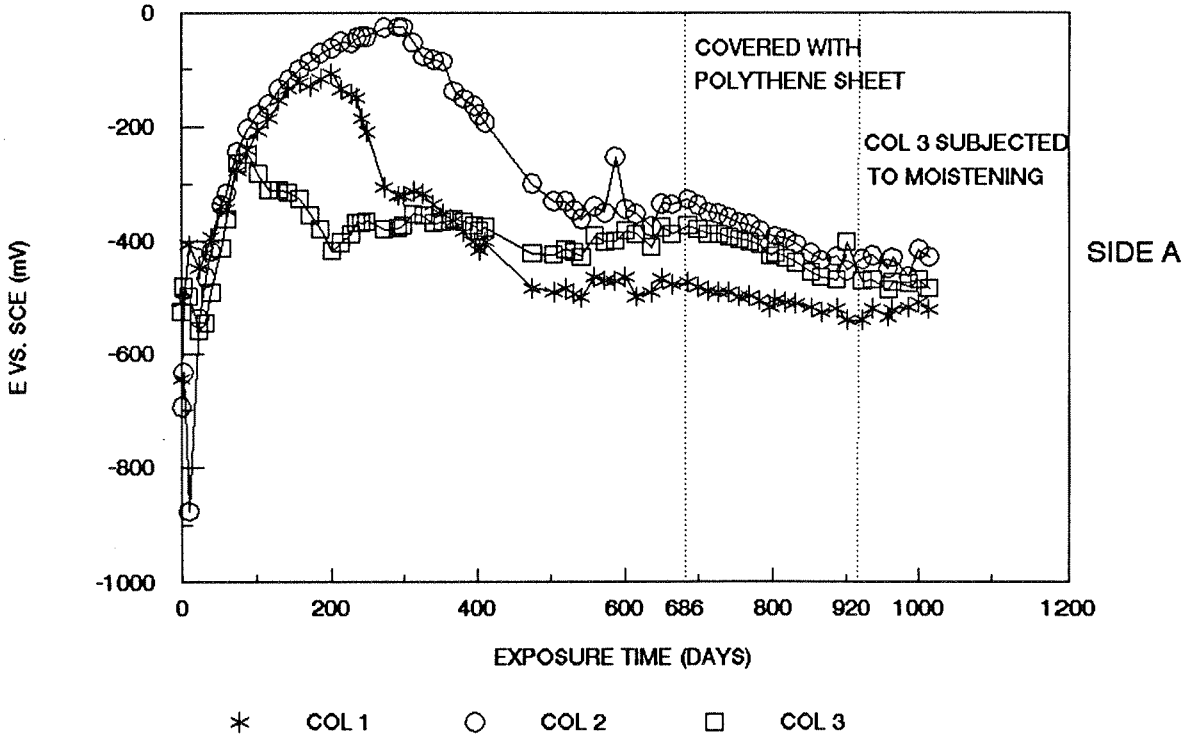

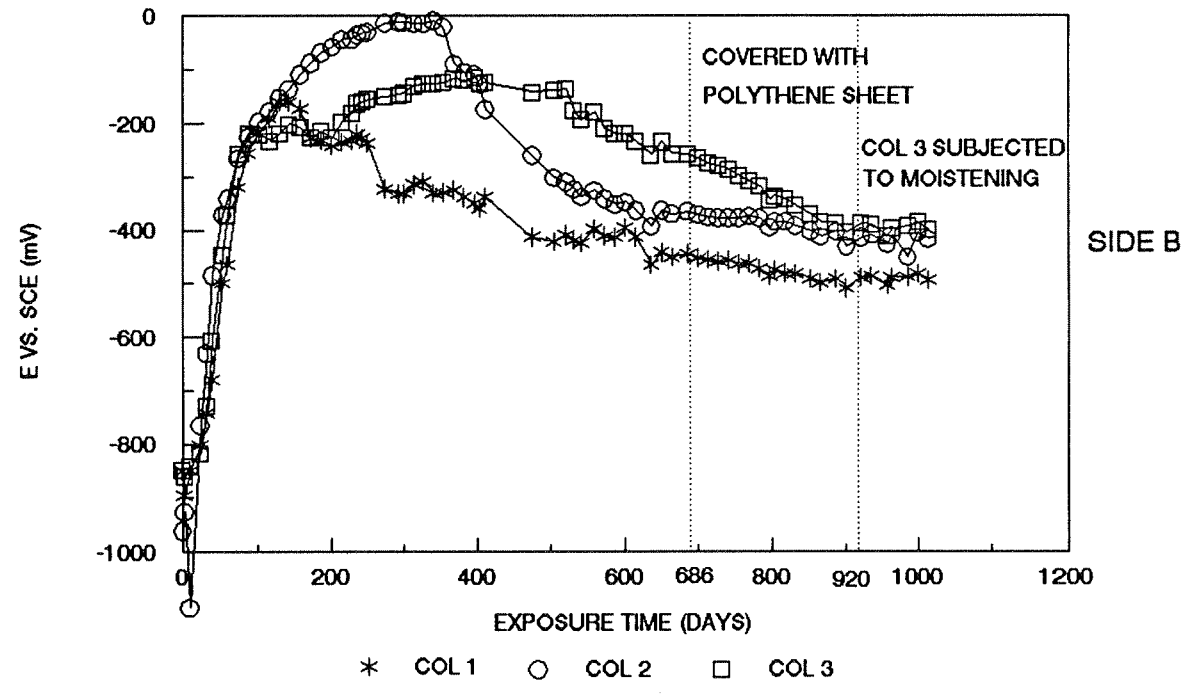

Figure I.16 Open Circuit Potential vs. Time at Level 4 in Group 1.

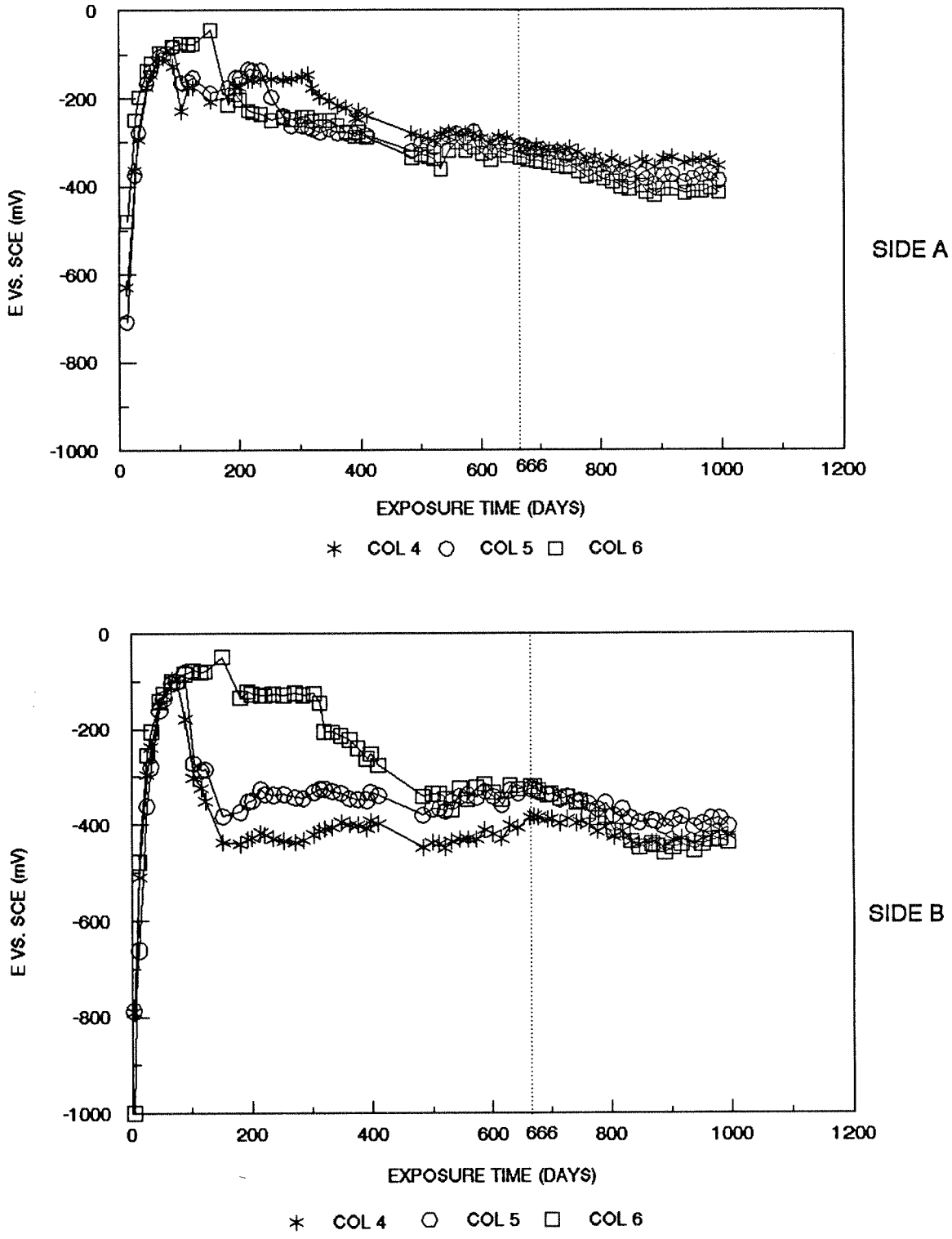

Figure I.17 Open Circuit Potential vs. Time at Level 4 in Group 2.

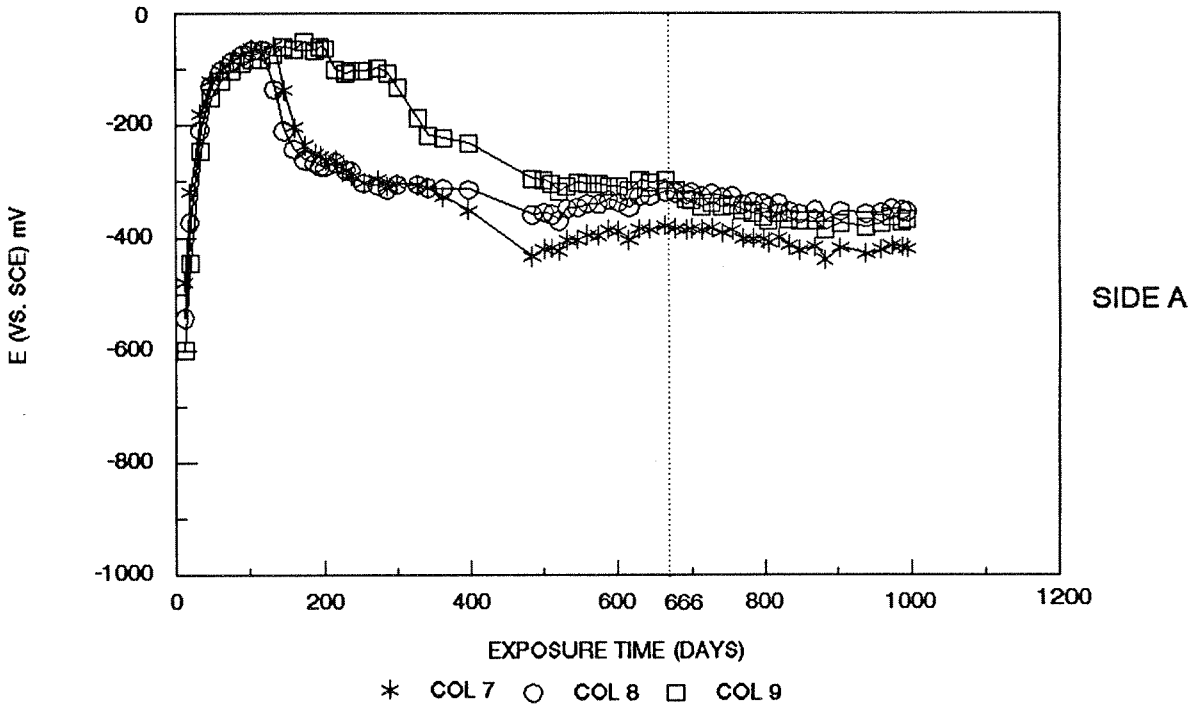

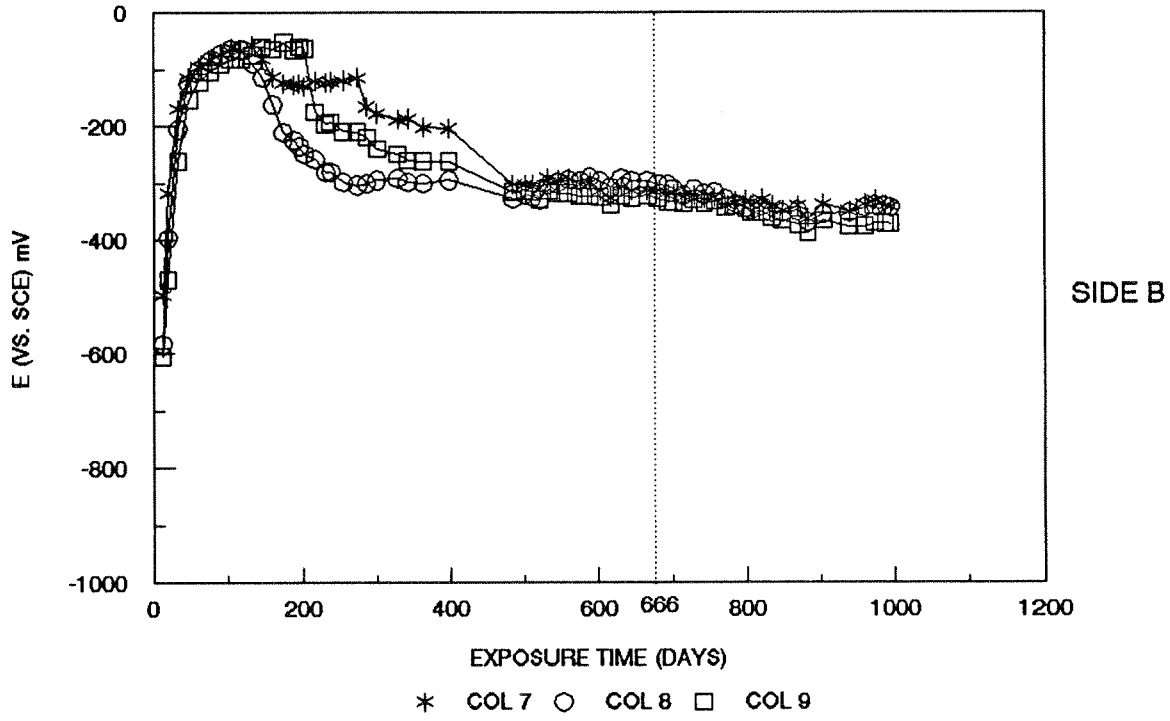

Figure I.18 Open Circuit Potential vs. Time at Level 4 in Group 3.

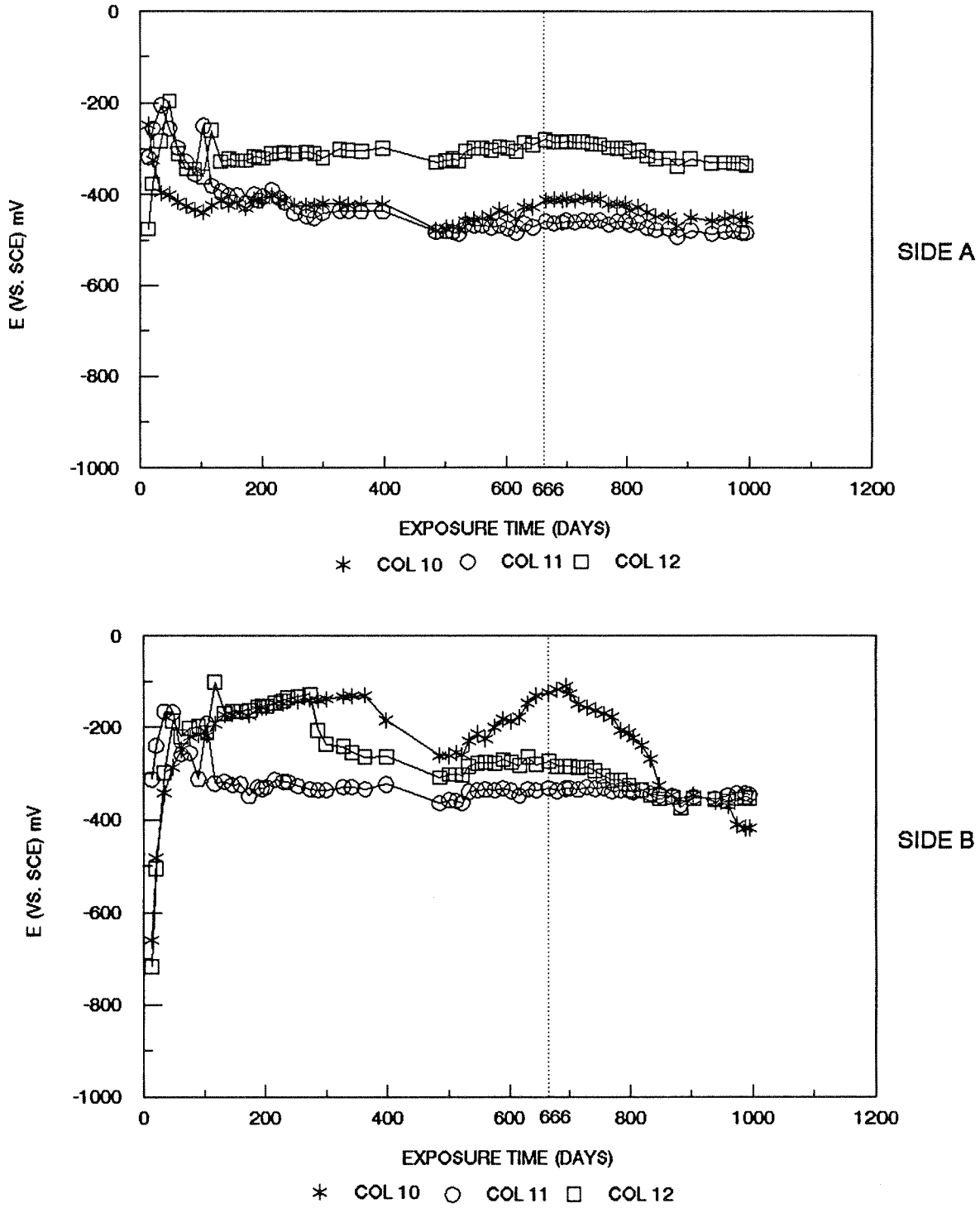

Figure I.19 Open Circuit Potential vs. Time at Level 4 in Group 4.

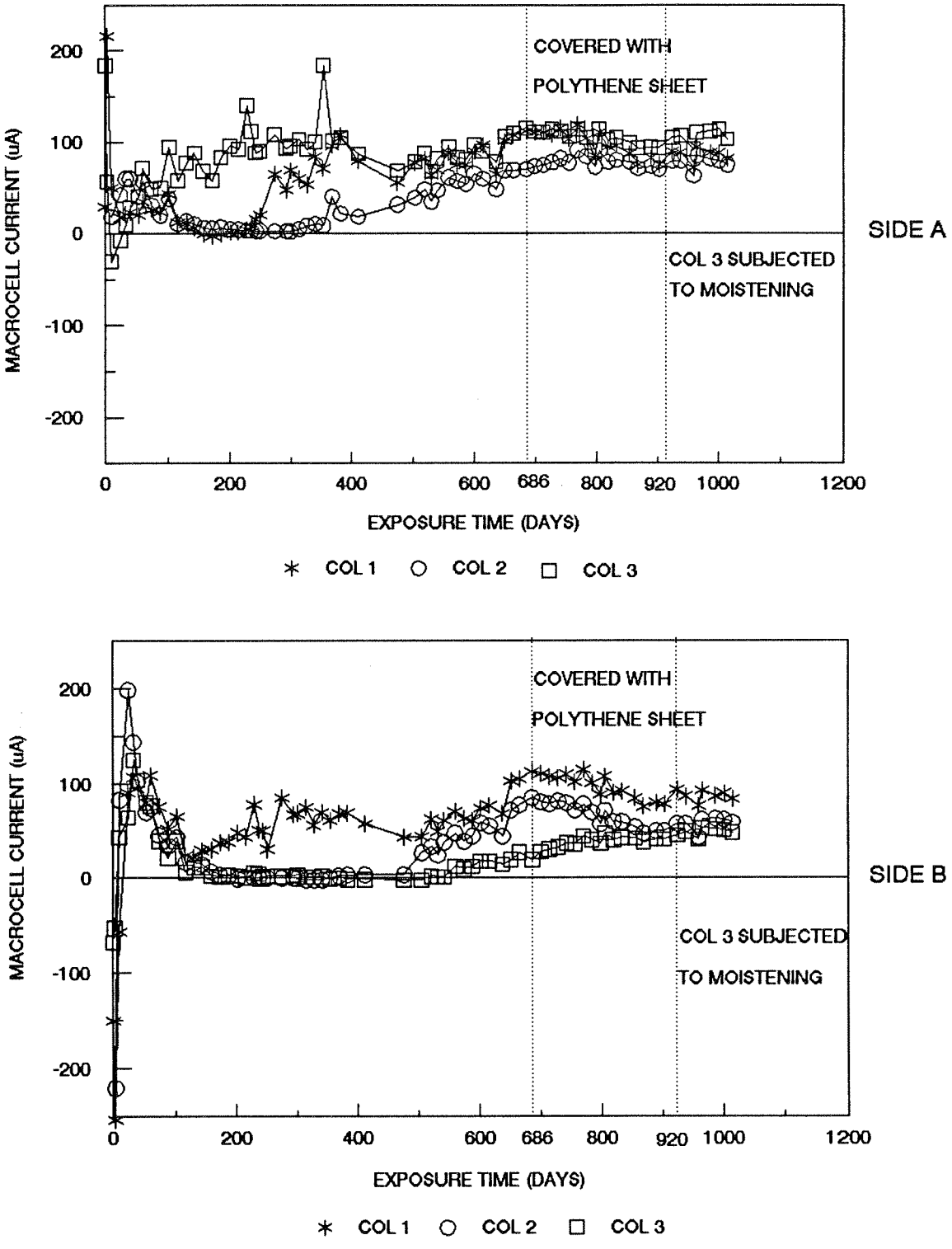

Figure I.20 Macrocell Current vs. Time at Switch 3 in Group 1.

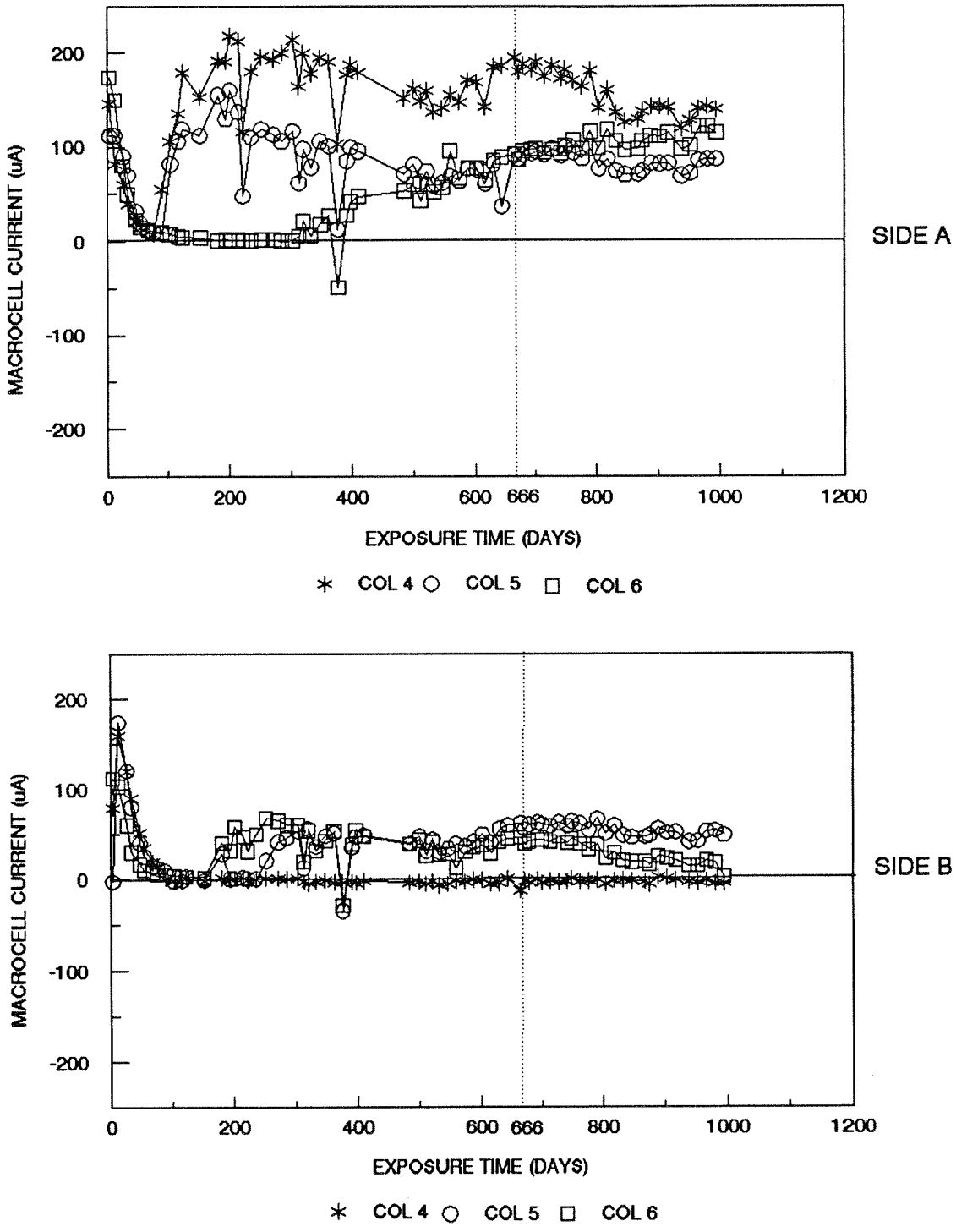

Figure I.21 Macrocell Current vs. Time at Switch 3 in Group 2.

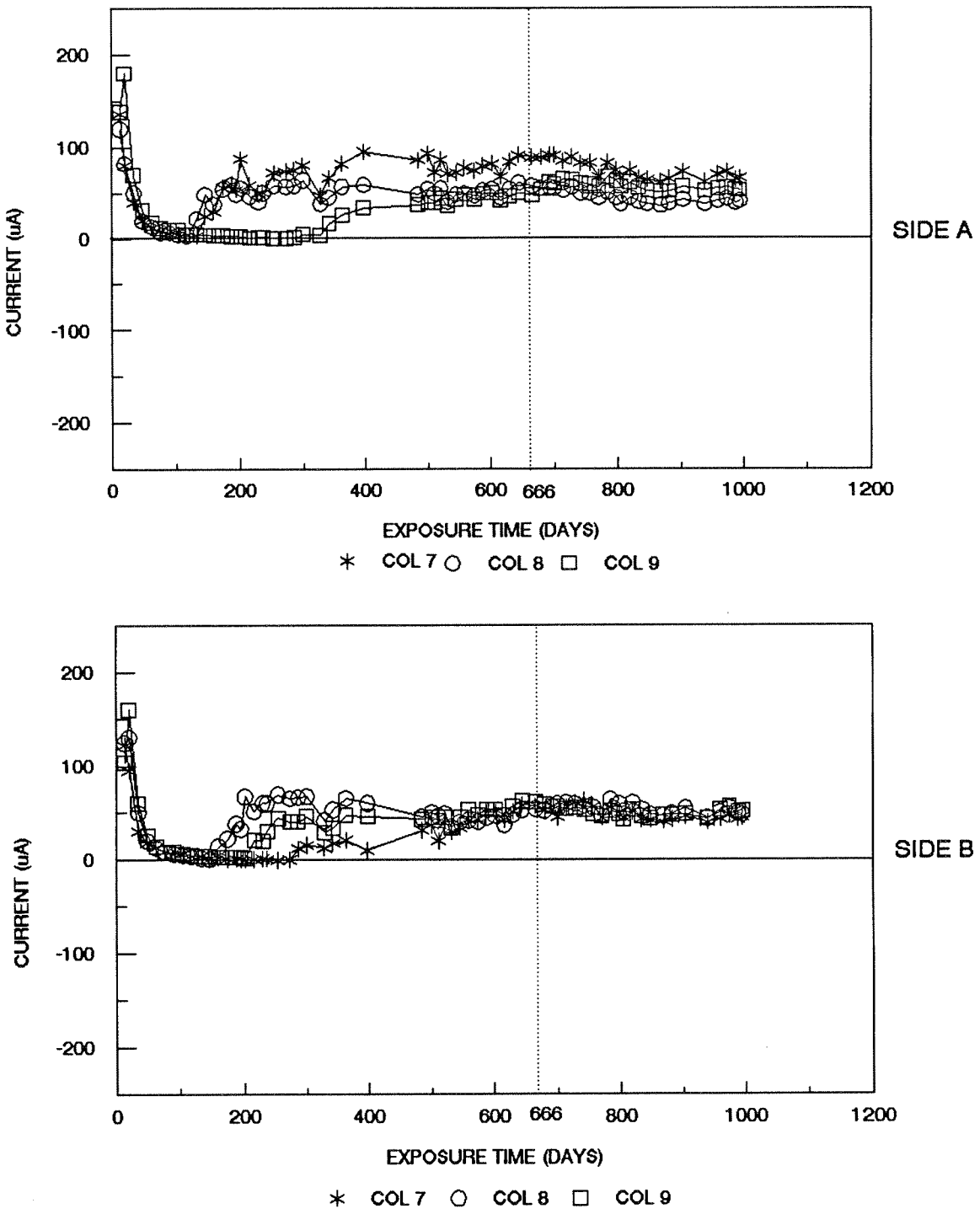

Figure I.22 Macrocell Current vs. Time at Switch 3 in Group 3.

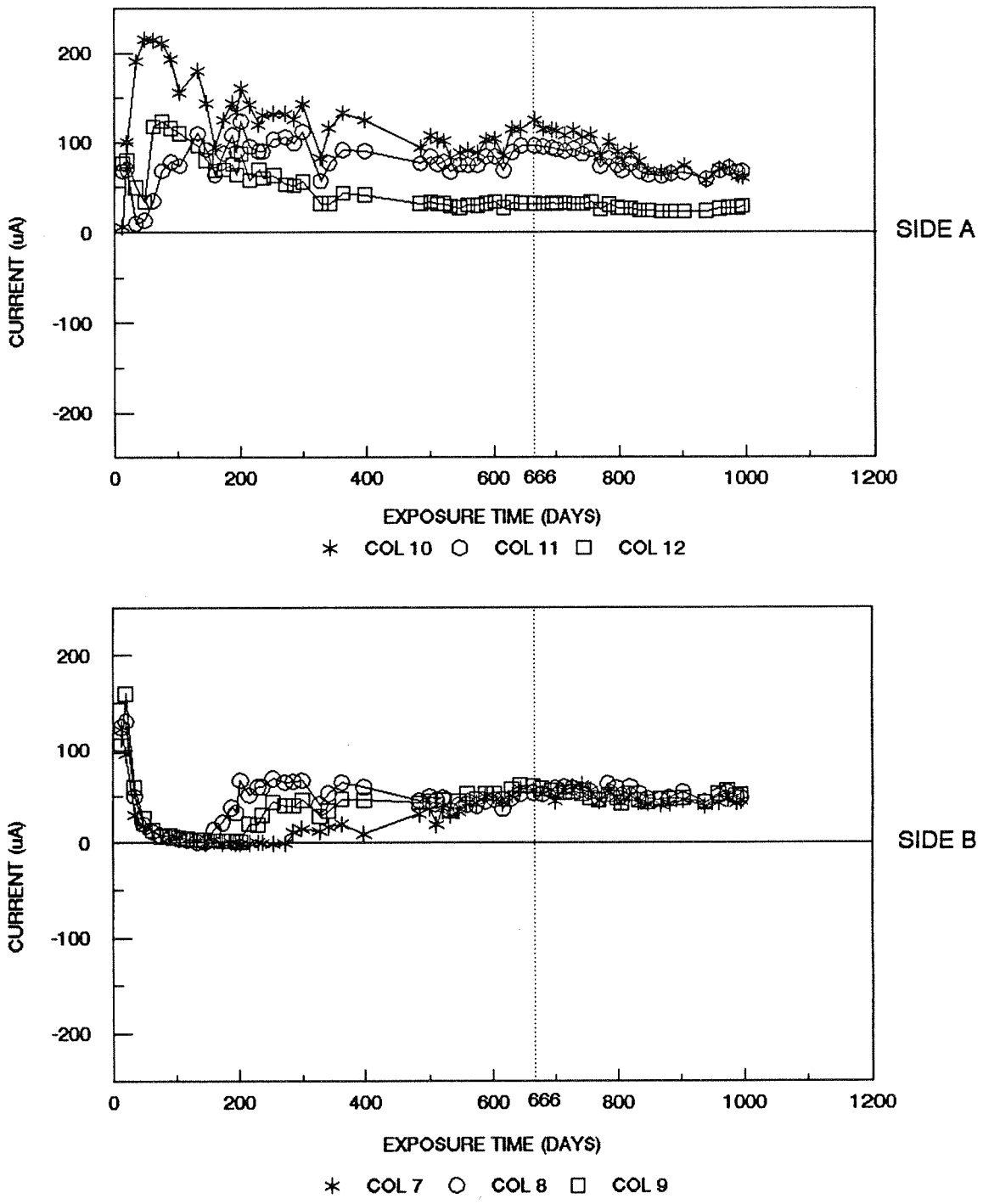

Figure I.23 Macrocell Current vs. Time at Switch 3 in Group 4.

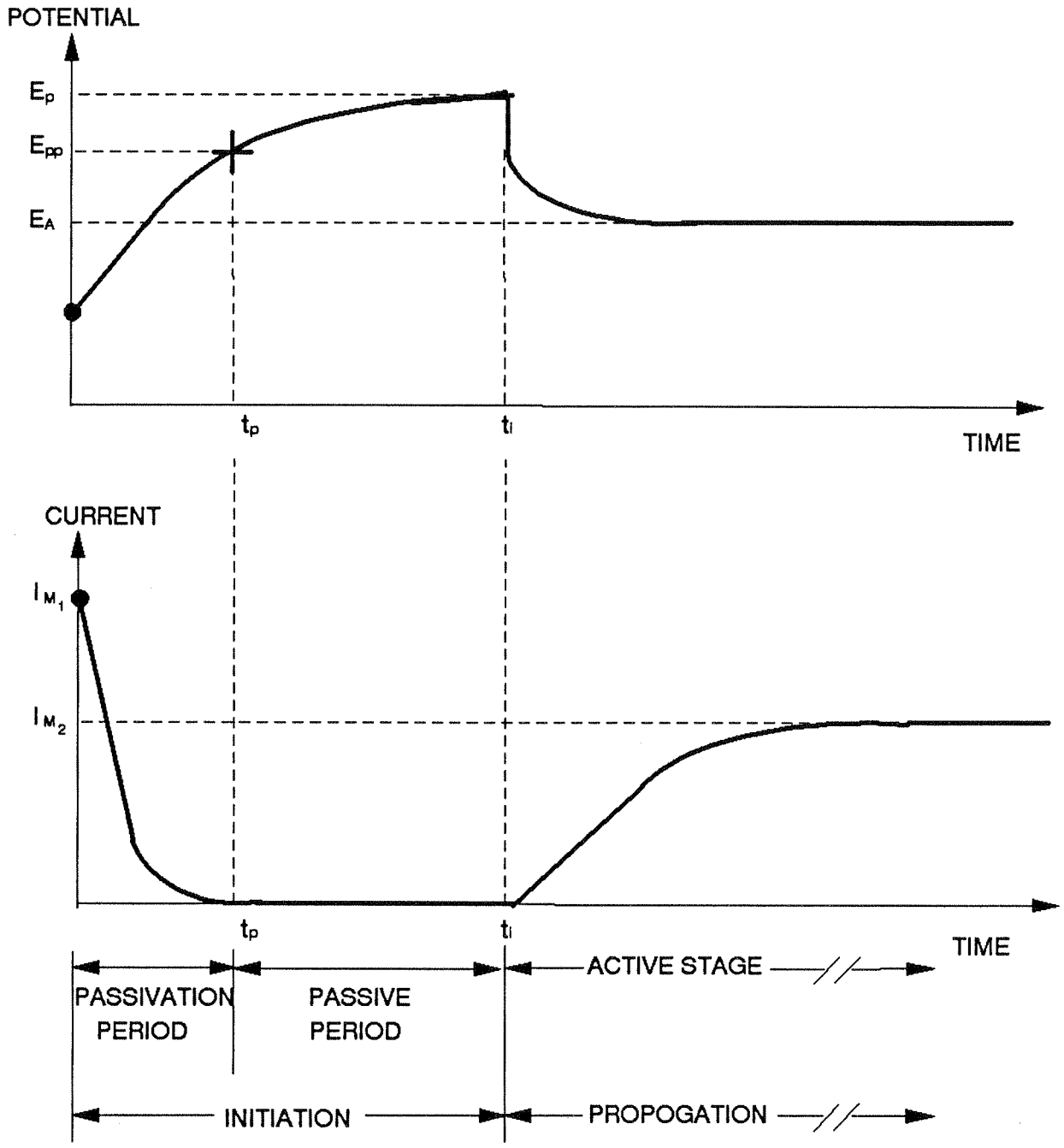

Figure I.24 Interpretation of Potential and Current Trends.

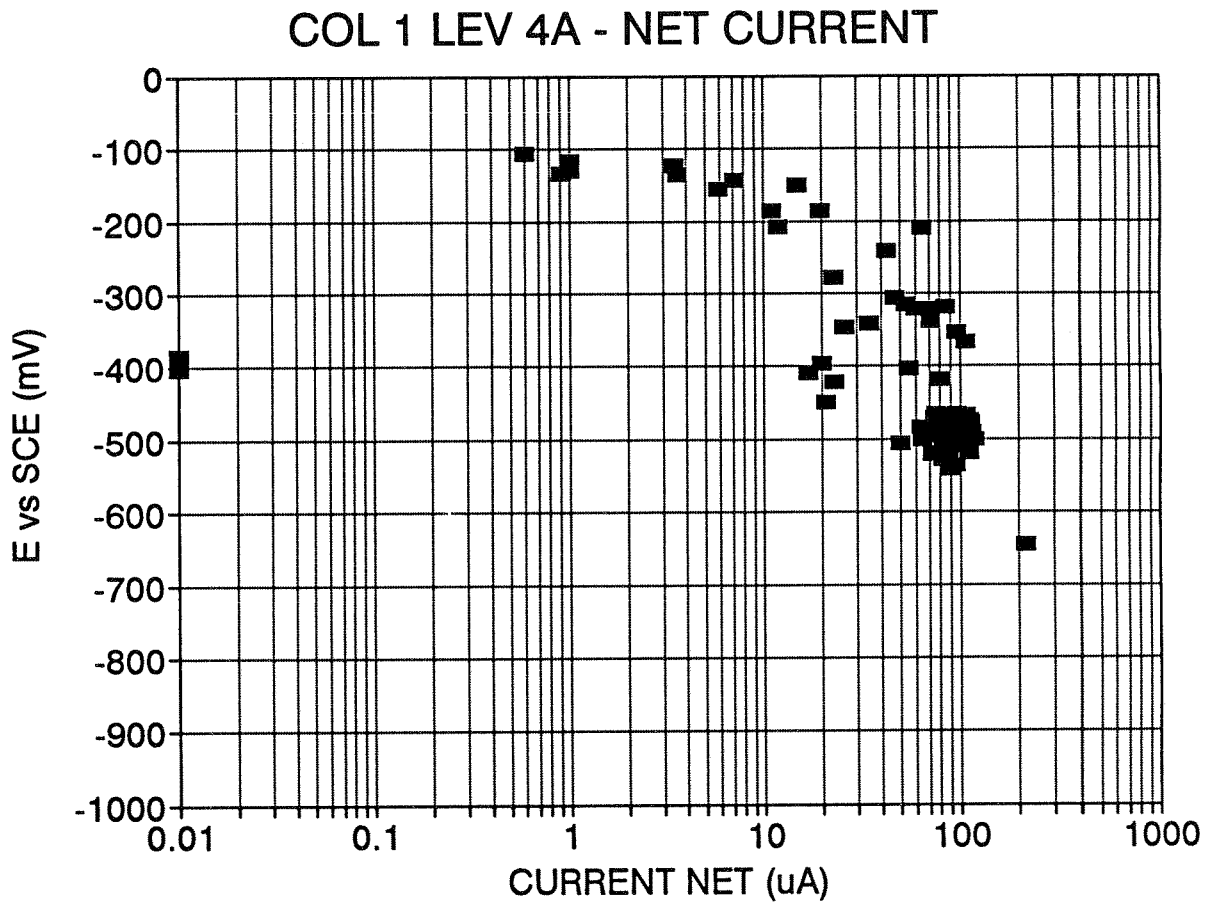

Figure I.25 Example of Potential-Net Current Composite Polarization Behavior for the Rebar Element Below the Waterline (Element No. 4, Side A, Column 1, S + F).

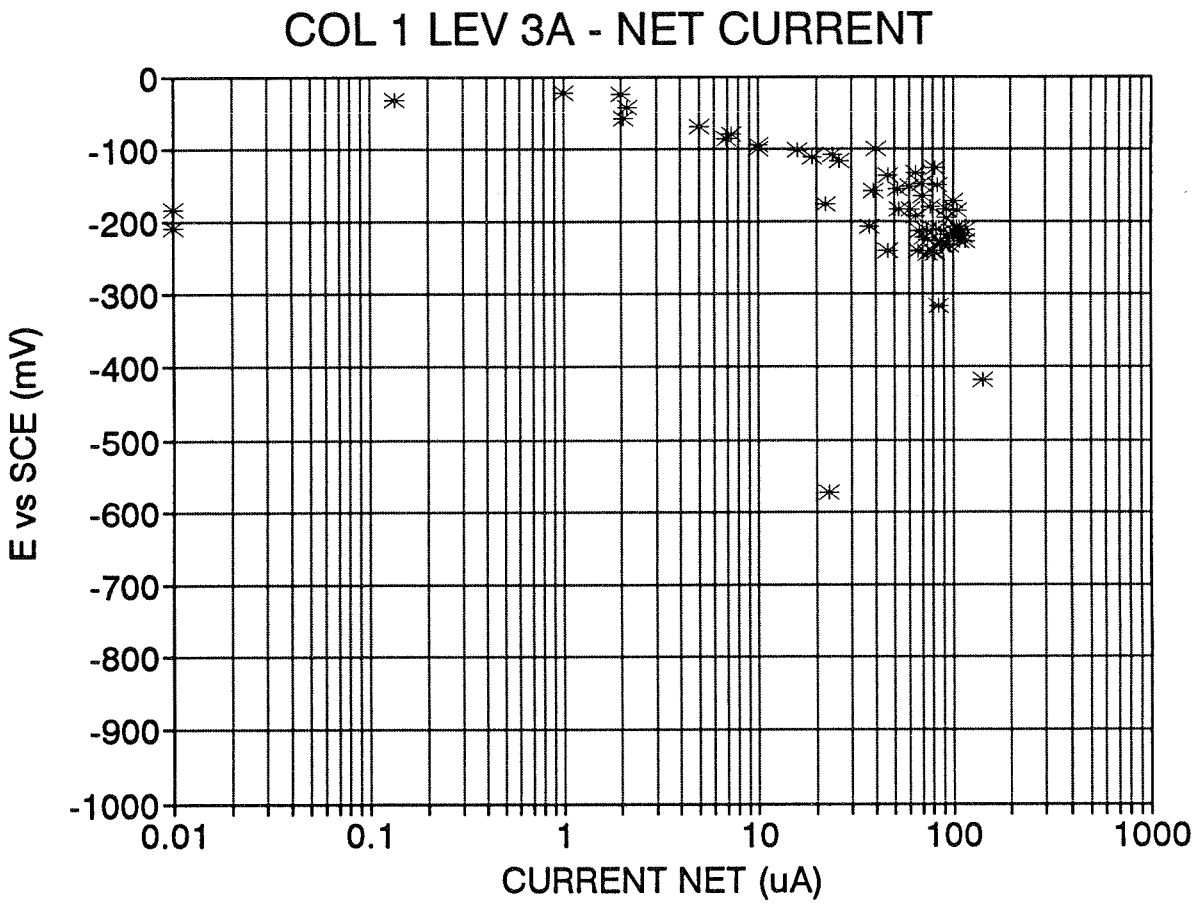

Figure I.26 Example of Potential-Net Current Composite Polarization Behavior for the Rebar Element Immediately Above the Waterline (Element No. 3, Side A, Column 1, S + F).

4. PART II: EFFECT OF CONCRETE MOISTURE.

4.1 PROCEDURE

4.1.1 Concrete Columns.

Instrumented reinforced concrete columns identical to those of a previous work [2.1] were used in this investigation. The columns were designed to simulate a slice from an actual pile, where the exterior portion is dryer than the interior portion. The columns were constructed with a base configuration of 12 by 4 by 46 in (30.5 by 10.2 by 122 cm) and with an inset of 0.5 in (1.3 cm) on one side. Eleven segments of #7 (2.2 cm nominal diameter) regular "black" rebars were placed horizontally at 4 in (10.2 cm) center-to-center spacing. The length of each rebar segment was 9 in (22.9 cm). The bars were placed slightly off-center facing the inset to allow for reduced concrete cover on one side. The intention was to simulate the cross-sectional moisture gradient that normally is encountered in a pile. The rebar segments were numbered from No.1 (at the top of the column) to No. 11 (at the bottom). Figure 2.1 depicts the main features of the test columns.

Each rebar had an activated titanium reference electrode placed about 0.5 in (1.3 cm) below the bottom. Electrical connections were made to all rebars and associated reference electrodes. All rebars were normally interconnected by toggle switches. The switches were numbered from No. 1 (below rebar element No.1) to No. 10 (below rebar element No. 10). The electrical connections to the bars were covered by metallographic epoxide compound to prevent unwanted galvanic action. The rebar segments were pre-rusted before concrete placement, in the same manner as the bars used for the laboratory columns in Part I. Other details on the column construction can be found in Refs [II.1-II.2].

4.1.2 Concrete.

The concrete mix design was the same for all columns. The mix design was based on a standard FDOT design using Type I Portland cement with a cement factor of 611 pcy (360 Kg/m^3), limestone coarse aggregate, and silica sand. A w/c ratio of 0.45 was used. Because a low concrete cover was used in the columns, the coarse aggregate size (3/8 in; 1 cm) was smaller than that normally used in bridges, on account of the low concrete cover used in the columns. To accelerate the test, the concrete mix for the lower 10 in (25.4 cm) of each column had an addition of 20 pcy (11.8 Kg/m^3) of chloride ion, obtained by using the appropriate amount of NaCl. Rebar elements No. 10 and No. 11 were in the high chloride zone. Rebar element No.11 was also just below the waterline (see the next paragraph).

4.1.3 Testing Environment.

A total of 4 columns , labeled A, B, C and D were prepared. The columns were moist-cured for 5 days after casting, and then exposed to the laboratory air for 6 additional days. All the columns were then put in an exposure tank so that the lower 5 in (12.7 cm) were immersed in water containing 5% NaCl solution. The rebar segments within each column were electrically interconnected shortly afterwards. Exposure time was counted from the nominal moment of rebar interconnection.

All testing was performed at ambient room temperature (typically 21°C±1°C) and ambient room relative humidity (typically 60%±10%). The upper portion of all the columns was allowed to dry in room temperature and humidity conditions for the first 343 days of exposure. Then the above-water surface of columns A and D was subjected to controlled applications of fresh water moisture. This was performed by covering the plain vertical face of each of the two columns with plastic sheets, and pouring fresh water from the top of the column inside the plastic cover three times a week. This resulted in permanent water saturation of that face of the column while the other face (with the inset) remained surface-dry. This condition of columns A and D will be referred from here on as the "partially wet" condition. Starting at day 681, the

wetting procedure was extended to both faces of columns A and D, resulting in water saturation of the entire column. This condition will be called the "fully wet" condition. Columns B and C, not wetted above the waterline, acted as controls and will be referred to as the "non-wetted" columns.

4.1.4 Corrosion Monitoring.

During the test exposure, periodic electrochemical measurements were made on each column. The following parameters were monitored: (1) Static potential measurements of each rebar segment with respect to the immediately surrounding concrete, (2) macrocell current flowing through the switches joining the rebar segments, and (3) resistivity of the concrete at elevations corresponding to the space between the rebar segments. The procedures for these measurements have been described in detail in Refs. [II.1-II.2].

4.2 RESULTS AND DISCUSSION

4.2.1 Concrete Resistivity.

Figures II.2 to II.5 show the evolution of the concrete resistivity at various elevations of each column during the 3-year exposure period. The non-wetted columns experienced a general increase in resistivity of the upper levels with time, with fluctuations reflecting variations in room relative humidity. The highest resistivity levels encountered are comparable with those of the non-wetted columns examined in Part I of this investigation, and with values usually reported for dry concrete of similar composition [II.3]. At the lowest levels, the resistivity was nearly constant, while at intermediate levels, the resistivity reached a maximum after about one year and then began to decline again. This latter behavior possibly reflects the increasing contamination with chloride ions shortly above the waterline, which resulted in a reduction in pore solution resistivity and a better retention of moisture.

The resistivity of the wetted columns clearly reflected the effect of wetting. One-side moistening was enough to create a dramatic reduction on the average resistivity of the upper column regions. Moistening the entire upper portion of the column resulted in resistivities throughout the column that were less than 5,000 Ω-cm, a value comparable with some of the most severe field conditions encountered in marine substructures in Florida [II.5]. The resistivity values of these conditions correspond to Coulomb test values of roughly 4,000 C in the Rapid Chloride Permeability test. This is consistent with the high w/c ratio and unblended cement concrete used in these experiments [II.6, II.7].

4.2.2 Steel Potential and Macrocell Currents.

Figures II.6 and II.7 show the steel potential measured at the two lowest column elevations (where chloride ion contamination was present from the start) as a function of exposure time and wetting condition. Unlike the case of the columns in Part I of this report, the steel even in the high chloride region showed potentials associated with passive behavior at the beginning of the test period. The potential decayed rapidly toward active values and experienced a further, slow decrease throughout the experiment. The potential in the high chloride portion of the columns being wetted (A and D) dropped to the lowest values by the end of the 3-year test period. Figure II.8 shows the steel potential as a function of elevation after the columns had acquired a mature corrosion pattern under the either non-wetted or partially wet conditions (day 681). The non-wetted columns (B,C) showed a range of potentials from very active near the bottom to clearly passive behavior at the top. The partiallly wet columns (A,D) showed also a distribution of potentials but with less of a difference between the upper and lower regions. Figure II.9 shows the result of the same type of measurements after the full-wetting regime had been developed for columns A and D. The potential profiles for the dry columns B and C remained similar to those in Figure II.8; the fully wet columns developed a potential regime that was more narrow than before.

Figures II.10 and II.11 show the corrosion macrocell current patterns after the systems matured in the dry, partially wet and fully wet regimes. The plots show the currents flowing through the switches that interconnected the rebar segments at the various elevations. The amount of macrocell current actually flowing from or sinking into a given rebar element is given by the difference between the current passing through the switches above and below the element. The values of the net currents were computed for each condition and the results are shown in Figures II.12 and II.13. The electronic macrocell currents were commonly flowing from the lowest to the highest elevations. This was expected because the chloride contamination around the lowest elements caused them to behave as anodes while the upper elements tended to behave as cathodes because of the absence of chloride (and easier oxygen availability except when very wet). The net current calculations confirmed the net anodic character of the lowest rebar element (No. 11), indicating that electron generation in that element significantly exceeded its consumption by cathodic reactions. While element 10 (and possibly 9 later in the exposure life) was also the site of anodic reactions, its net character was either cathodic or anodic depending on the relative electron demand on its surface and that of the upper elements for cathodic reactions. Elements above 9 were invariably net cathodes.

The rate of the cathodic reaction in the upper elements depended on the electron supply from the corroding elements at the lower levels. The electronic current was in turn determined by the polarization of the cathodic reaction (both by activation and concentration mechanisms), the potential of the anodic bars, and the resistive potential drop due to the intervening concrete between anodic and cathodic regions. The latter effect was responsible for the gradual drop in cathodic activity with increasing elevation. Application of moisture reduced the concrete resistivity and consequently the extent of ohmic potential drop. The effect is manifested in the increased macrocell current at the upper levels of columns A and D upon partial wetting and later full wetting (Figures II.10 to II.13). Net cathodic currents experienced dramatic relative increases (on a percent basis) as a result of wetting. To

better visualize those increases, the absolute values of the net sink or source currents at each element are shown in Figures II.14 to II.17. These plots illustrate the various stages in the life of the columns. Full wetting of the columns resulted in net cathodic current levels at the upper elements that were almost two orders of magnitude greater than for the unwetted columns.

Although surface wetting reduced the disparity between the amount of cathodic current among the rebar elements in chloride-free concrete, the effect on overall corrosion activity of the column was more complicated. Figure II.18 shows the total amount of net anodic current measured in the columns. The data for the early stages of evolution, before column wetting, shows that there is considerable variability from specimen to specimen. Application of partial wetting to columns A and D resulted in a significant increase in overall macrocell current in both columns. However, the increase was no larger than the column-to-column variability illustrated by the difference in behavior between the dry columns B and C. Application of full wetting caused the overall anodic currents of columns A and D to actually drop from the values experienced under partial wetting (columns B and C continued their previous behavior).

The varying effect of increasing amounts of moisture on the overall corrosion intensity can be further examined by plotting the potentials versus cathodic current of the segments in the chloride-free concrete, in the manner of an E-log i plot. Figure II.19 shows the composite behavior of all segments in the four columns near the end of the partial wetting period. The data delineate a polarization curve descriptive of the oxygen reduction reaction, approaching an activation Tafel slope between 100 mV to 200 mV per decade [II.1] in the low current portion of the curve. At high current densities there is a suggestion of the onset of concentration polarization. The data for the unwetted columns span a relatively wide range, showing how the polarization available at the upper column portions is quite small. The wetted columns achieved larger cathodic polarization at the upper regions as a result of the lower resistive drop in the moist concrete. The potential range of the cathodic elements in those columns was consequently smaller and approached the potential of the anodic regions.

The effect of full column wetting is manifested in Figure II.20. The polarization behavior in the unwetted columns remained as before. The potentials in the cathodic portions of the fully wetted columns became even lower than before. However, the cathodic currents became about the same for all elements and were limited to a smaller value than in the partially wetted case. The behavior is characteristic of diffusional limitation. The difference in behavior between the partially and fully wetted cases can be explained by the dependence of the speed of oxygen transport in concrete with its moisture content. In the partially wetted case, only one side of the concrete slab was wetted which reduced the resistivity of the concrete and consequently the ohmic drop across the macrocell. The opposite side of the slab remained partially dry, which created relatively little hindrance to oxygen transport across the concrete cover [II.8]. In the fully wetted case, both sides of the columnar slab were wetted which resulted in nearly water-saturated concrete. Under those conditions oxygen transport can become several orders of magnitude slower than in the partially wet case [II.8]. While the ohmic drop becomes still smaller under those circumstances, the oxygen supply is much smaller and diffusional limitation of the cathodic current results. This interpretation is in agreement with the observed drop in macrocell currents observed upon application of full wetting to columns A and D.

A rough estimate of the effective diffusion coefficient, **D**, for oxygen in concrete can be made for the fully wetted case by simplifying the system as an one-dimensional flow case, with a concrete cover **h** of 1 in (2.5 cm), and an approximate steel/concrete surface ratio of 1:1. Under those conditions the limiting current density i_l is given by

$$i_l = 4 F D Cs / h \qquad (II.1)$$

where **F** is the Faraday constant and **Cs** is the effective concentration of oxygen at the concrete surface. Since the rebar segments have a surface area approaching 100 cm^2 , then per Figure 26, $i_l \sim 0.3\ \mu A/cm^2$. Cs (when expressed in terms of concentration in the pore water) can be taken to be approximately equal to $3\ 10^{-7}$ mol/cm^3 if equilibrium between air and fresh water is assumed. Those parameters

yield $D \sim 6\ 10^{-6}$ cm^2 /sec . This value is consistent with measurements reported in the literature for water-saturated concrete (after appropriate accounting of the manner in which oxygen concentration is defined) [II.9-II.13] and supports the above interpretation of the polarization behavior observed.

The results of these experiments confirmed the general expectations of behavior in substructure conditions, and agreed with the predictions of earlier theoretical models of macrocell behavior [II.1] as well as with the calculations presented in Part III. A noteworthy finding of this part of the project was that intermediate amounts of moisture can increase macrocell action significantly by reducing the extent of resistive polarization. However, when the moisture additions cause water saturation, the effect of resistance reduction is offset by a decrease in the oxygen supply.

4.3 PART II REFERENCES

II.1 Sagüés, A., Perez-Duran, H. and Powers, R., Corrosion, Vol. 47, p. 884, 1991.

II.2. Al-Mansur, A.K.M., "Effect of Moisture Application on the Corrosion Behavior of Reinforcing Steel in Marine Bridge Substructures", M.S. Thesis, University of South Florida, Tampa, Florida, December, 1992.

II.3. Monfore, G., "The Electrical Resistivity of Concrete", Journal of the PCA Research and Development Laboratories, May 1968, p. 35.

II.4. Millard, S. G., Ghassemi, M., Bungey, J. and Jafar, M., "Assessing the Electrical Resistivity of Concrete Structures for Corrosion Durability Studies", in Corrosion of Reinforcement in Concrete, C. Page, K. Treadaway and P. Bamforth, Eds., p. 303, Elsevier Appl. Sci., London-New York, 1990.

II.5 Sagüés, A., "Corrosion of Epoxy-Coated Rebar in Florida Bridges", Final Report to Florida D.O.T., WPI No. 0510603, University of South Florida, Tampa, May, 1994.

II.6 Berke, N.S. and Hicks, M.C., "Estimating the Life Cycle of Reinforced Concrete Decks and Marine Piles Using Laboratory Diffusion and Corrosion Data", p. 207 in "Corrosion Forms and Control for Infrastructure", ASTM STP 1137, Victor Chacker, Ed., American Society for Testing and Materials, Philadelphia, 1992.

II.7 Feldman, R., Chan, G., Brousseau, R. and Tumidajski, P., ACI Materials Journal, Vol. 91, p. 246, 1994.

II.8. Tuutti, K., Corrosion of Steel in Concrete, Swedish Cement and Concrete Research Institute, Stockholm, 1982.

II.9 Page, C. and Lambert, P. J., Mat. Sci., Vol 22, p. 942, 1987.

II.10 Yu, S. and Page, L., Cement and Concrete Research., Vol. 21, p. 581, 1991.

II.11 O. Gjorv, O. Vennesland and A. El-Busaidy, Materials Performance, Vol. 25, No. 12, p. 39 (1986).

II.12 Kobayashi, K., Cement and Concrete Rsch., Vol. 21, p. 273, 1991.

II.13 Ohama, Y. and Demura, K., Cement and Concrete Research., Vol. 21, p. 309, 1991.

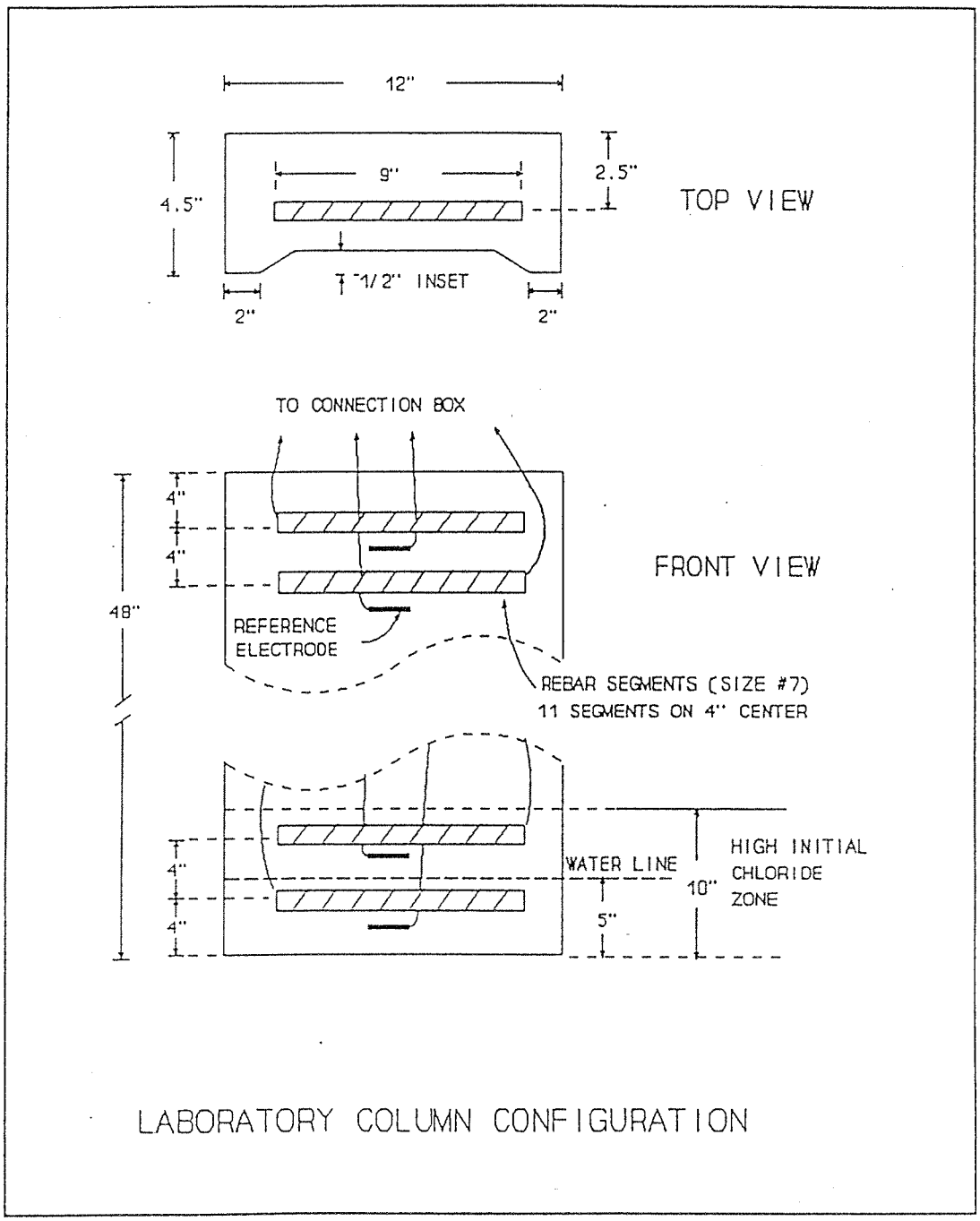

Figure II.1 Sketch of the Laboratory Column Configuration.

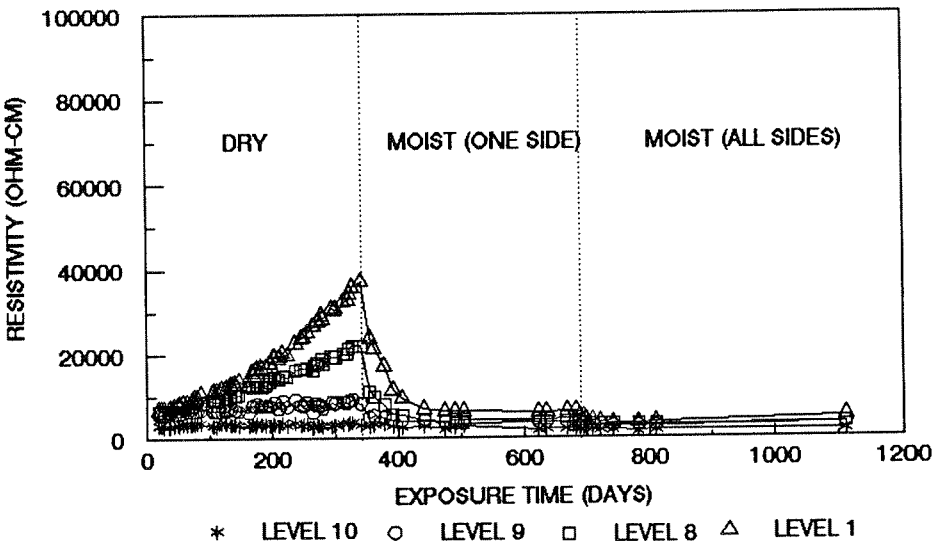

Figure II.2 Concrete resistivity (Column A).

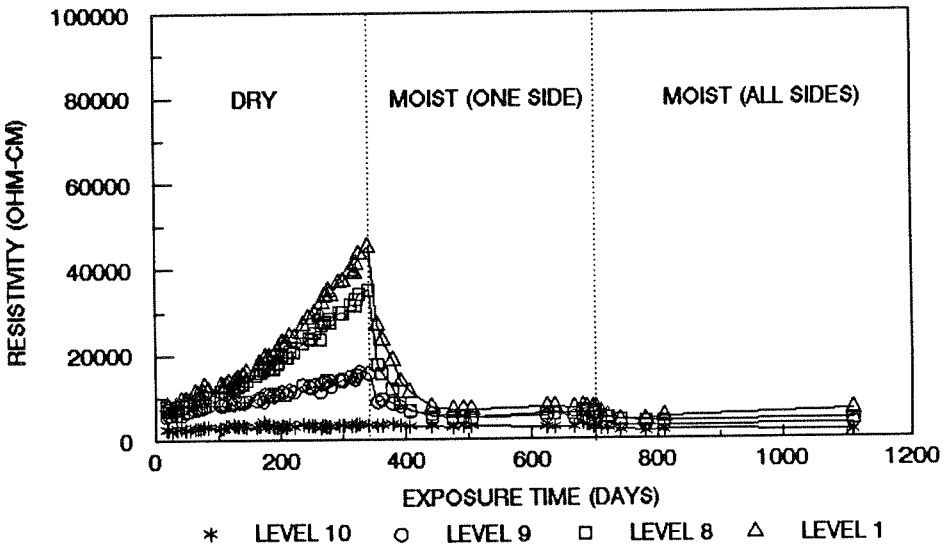

Figure II.3 Concrete resistivity (Column D).

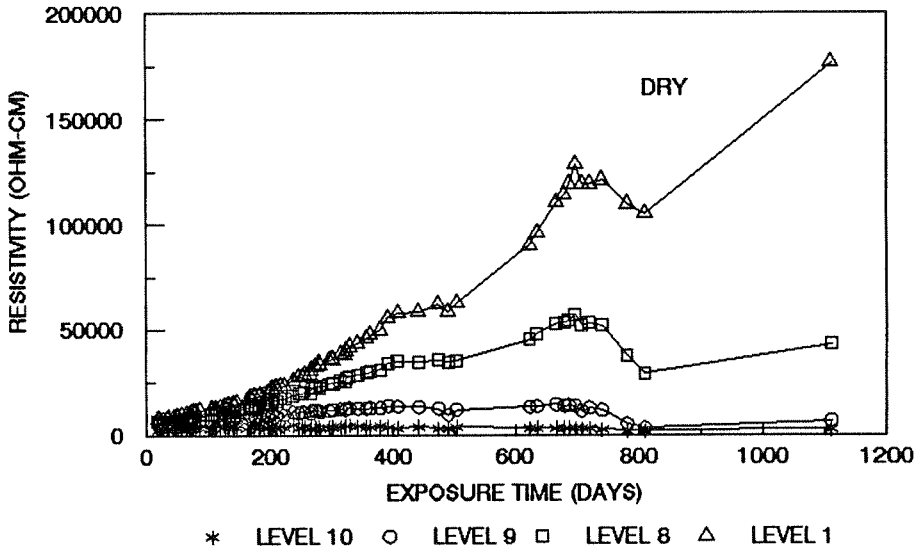

Figure II.4 Concrete resistivity (Column B).

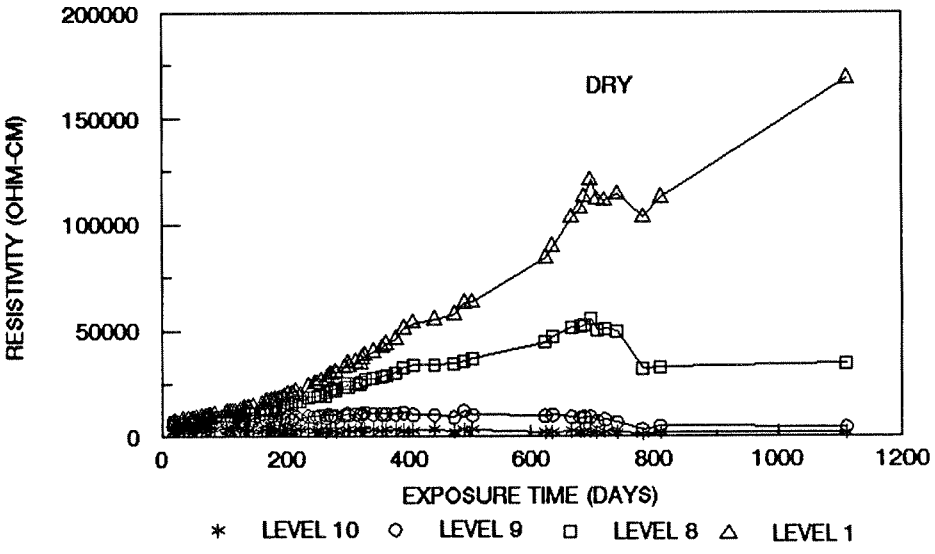

Figure II.5 Concrete resistivity (Column C).

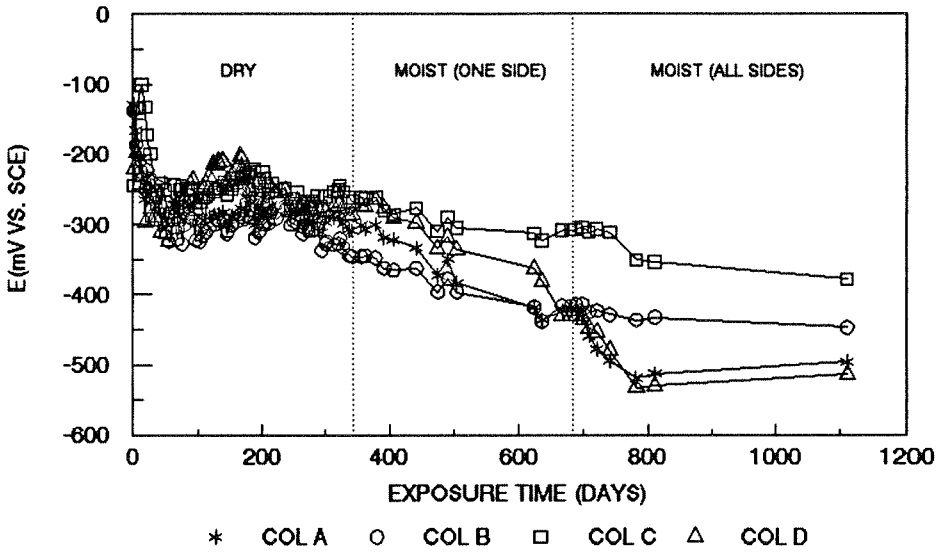

Figure II.6 Static Potential Measured at Level 10.

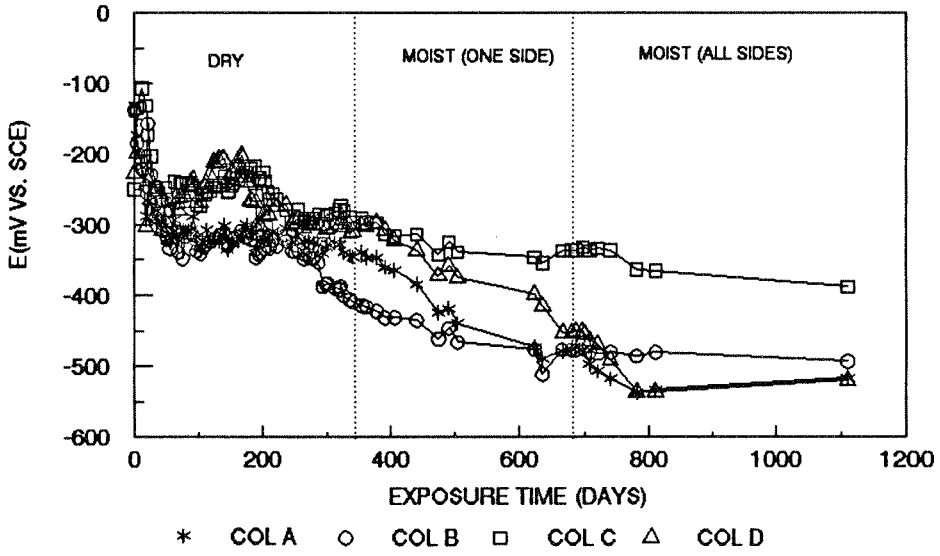

Figure II.7 Static Potential Measured at Level 11.

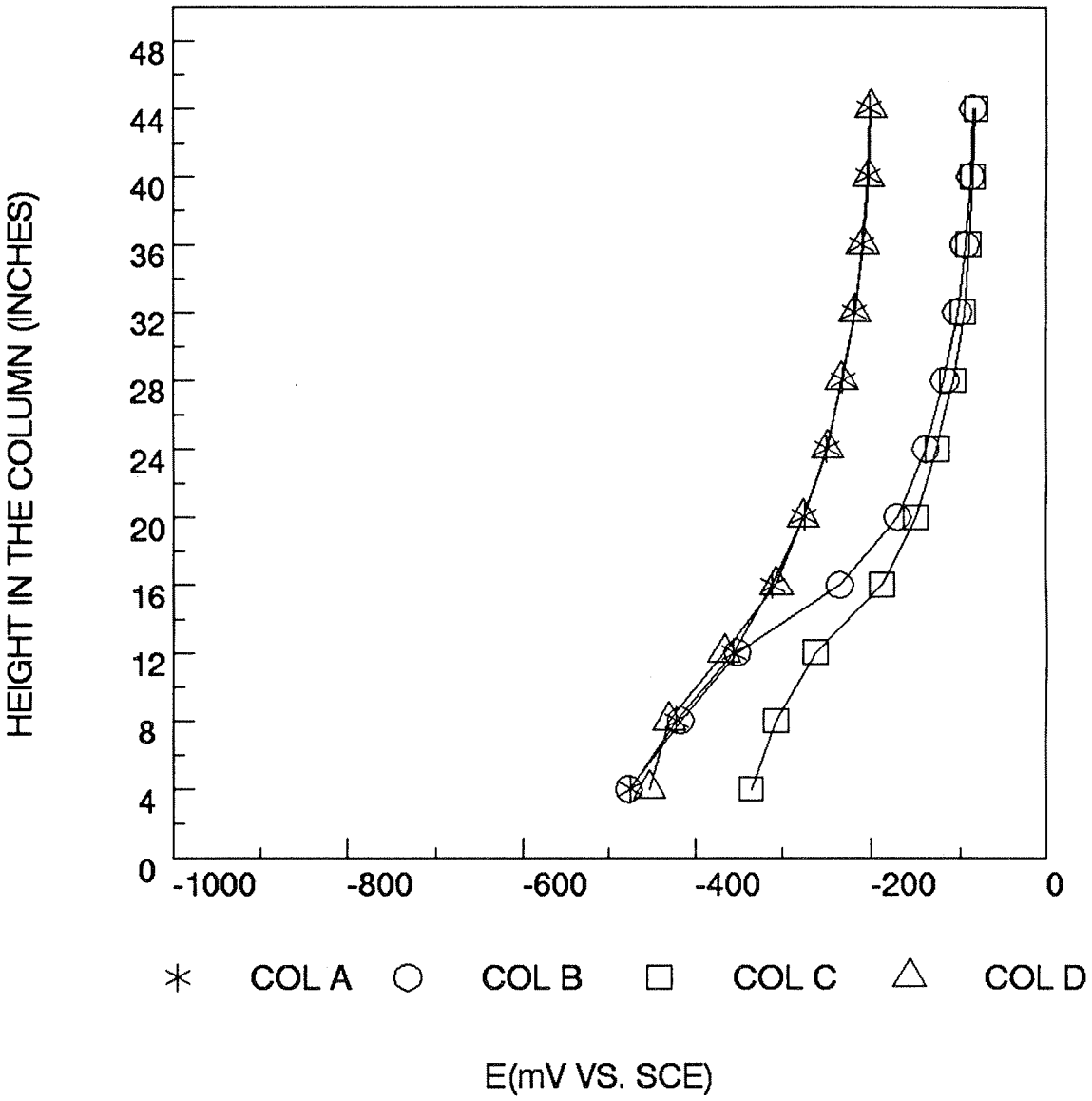

Figure II.8 Static Potential vs. Height (Day 681).

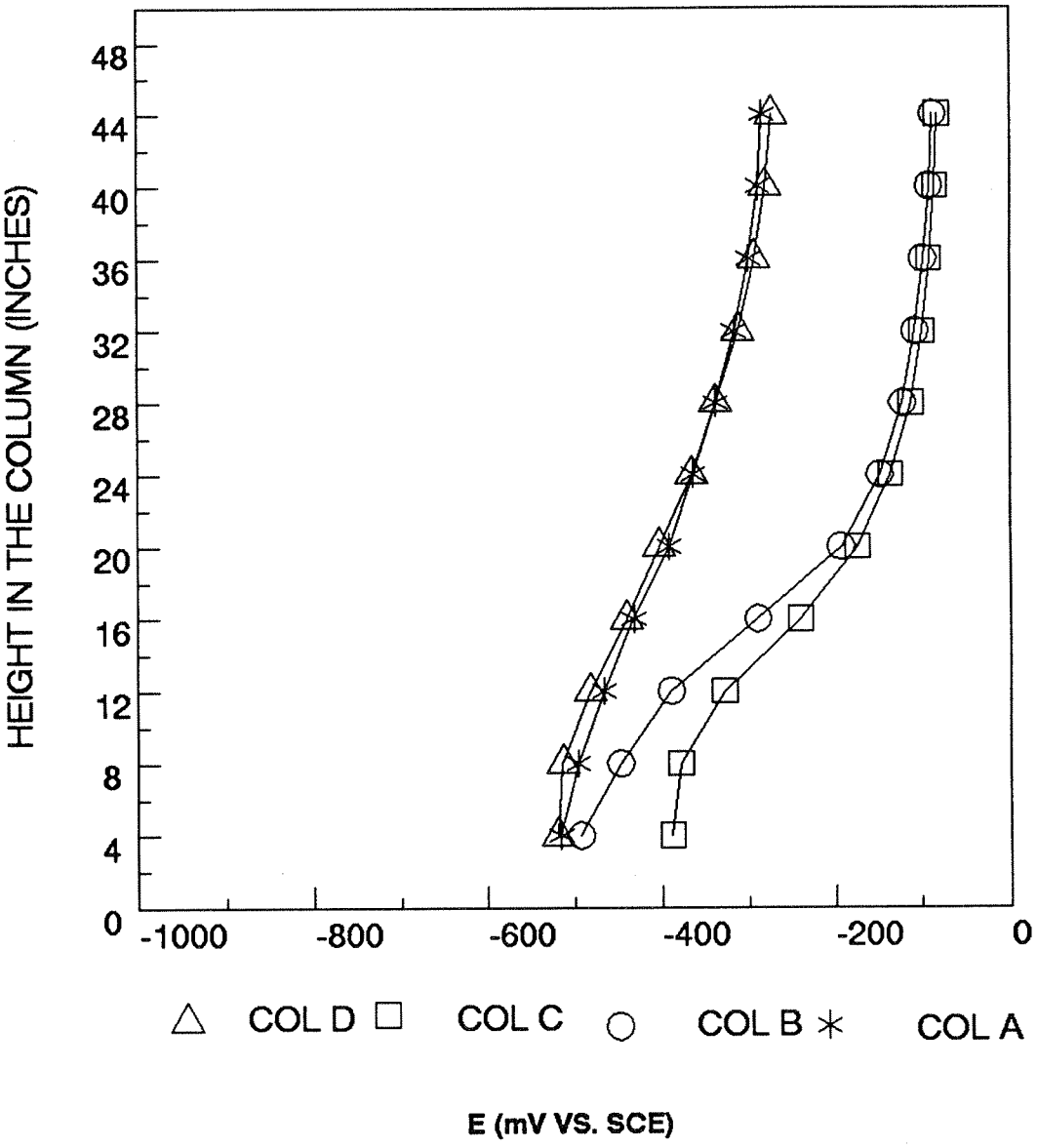

Figure II.9 Static Potential vs. Height (Day 1111).

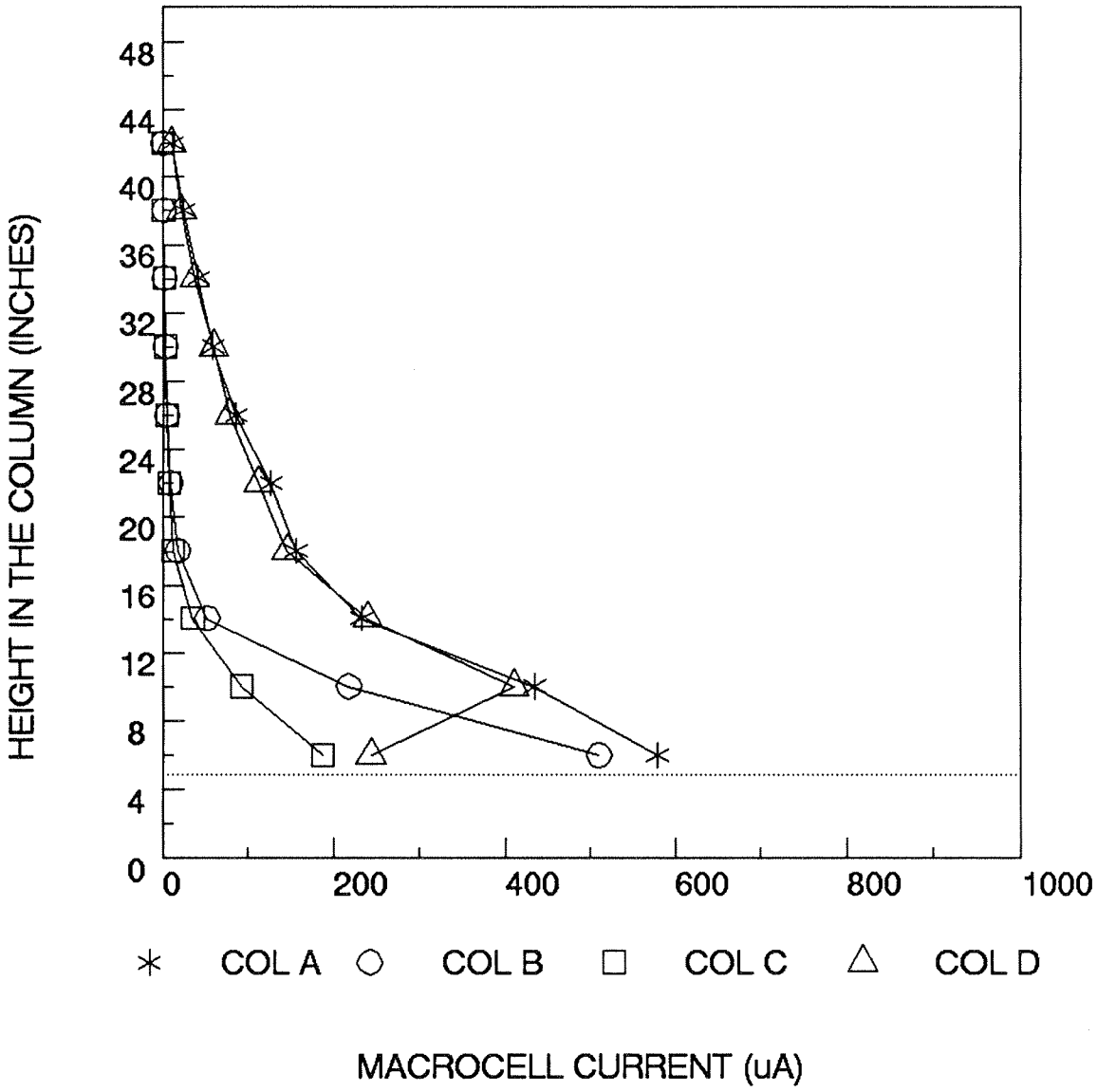

Figure II.10 Macrocell Current vs. Height (Day 681).

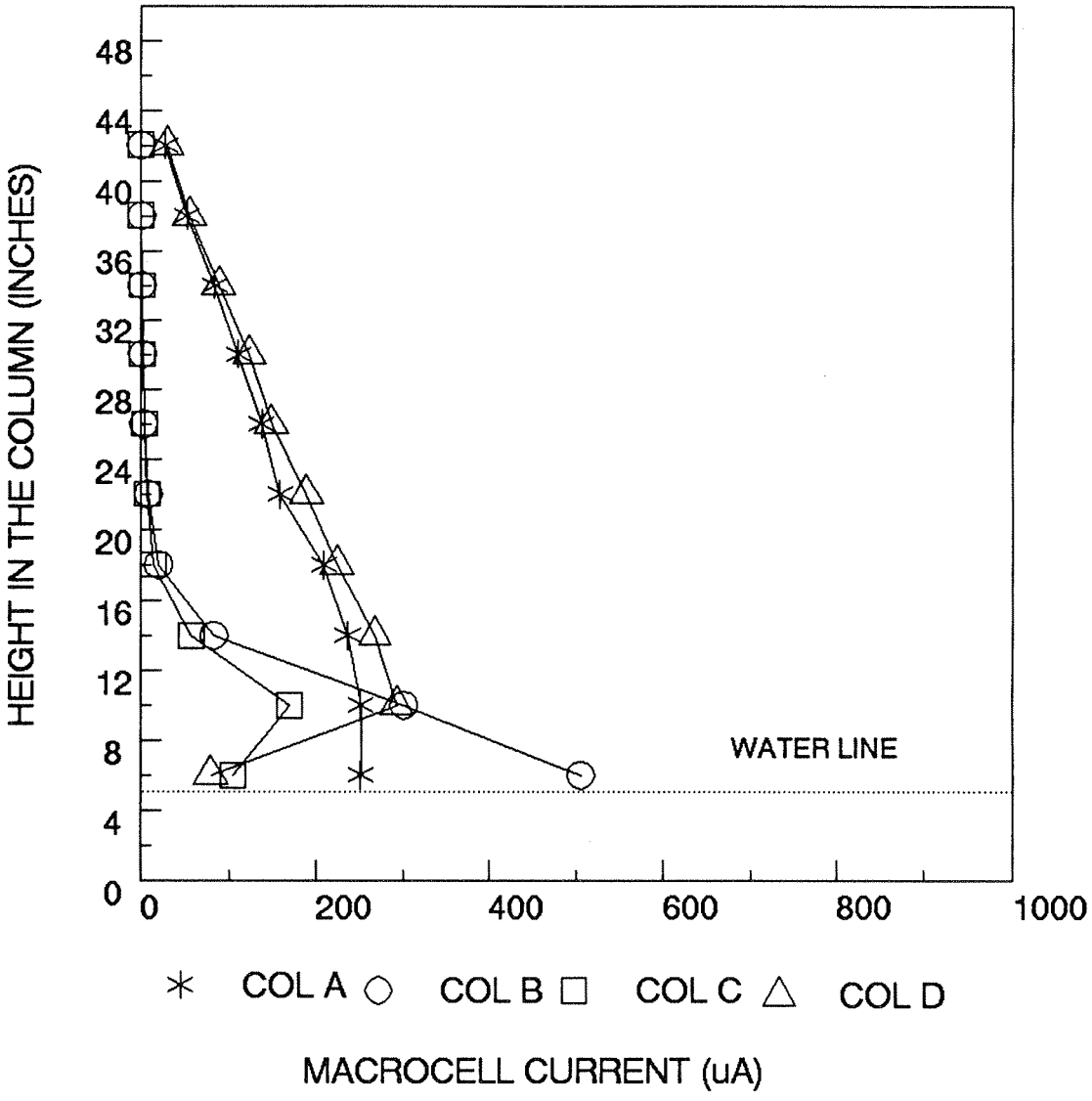

Figure II.11 Macrocell Current vs. Height (Day 1111).

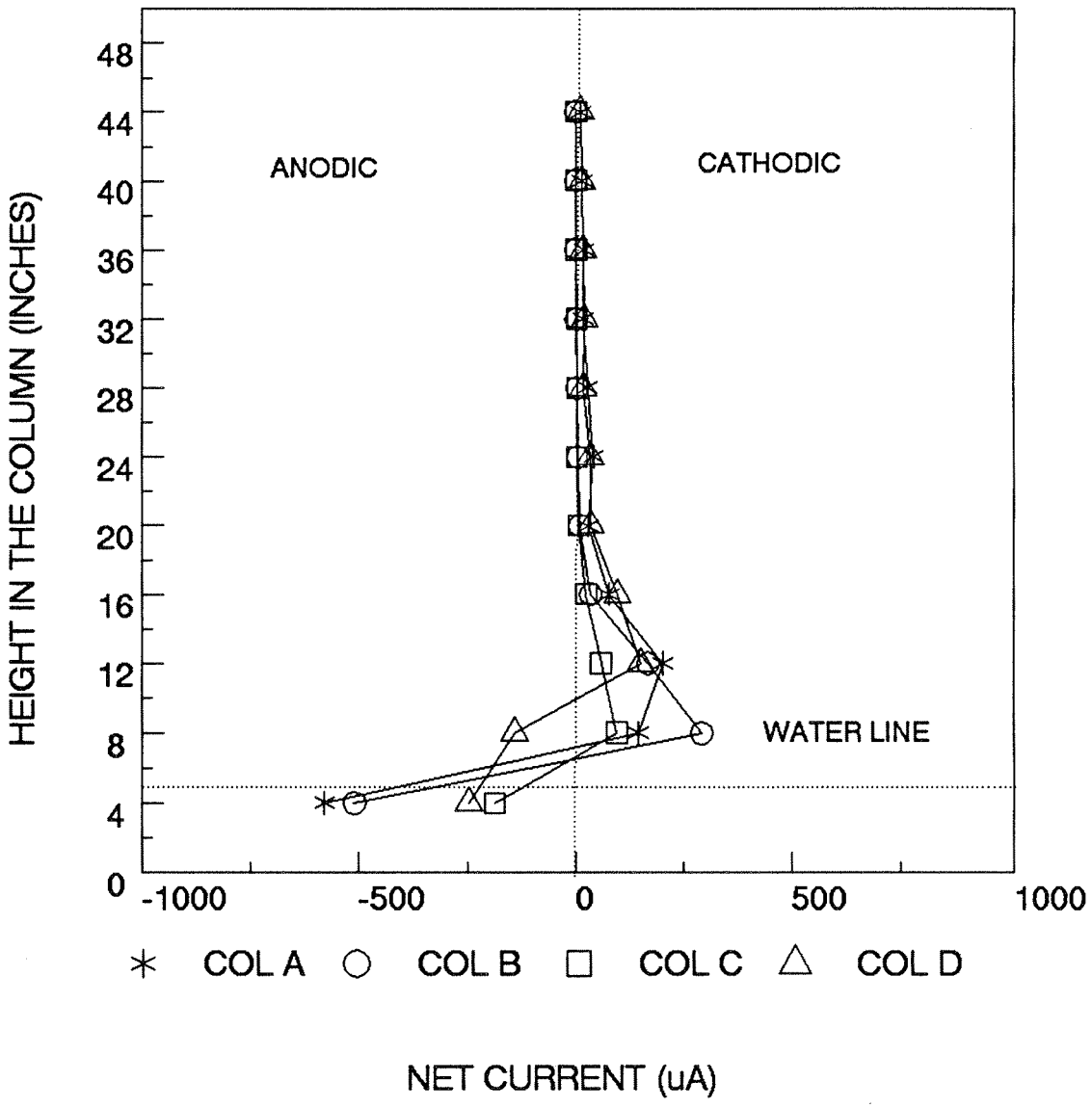

Figure II.12 Net Current vs. Column Height (Day 681).

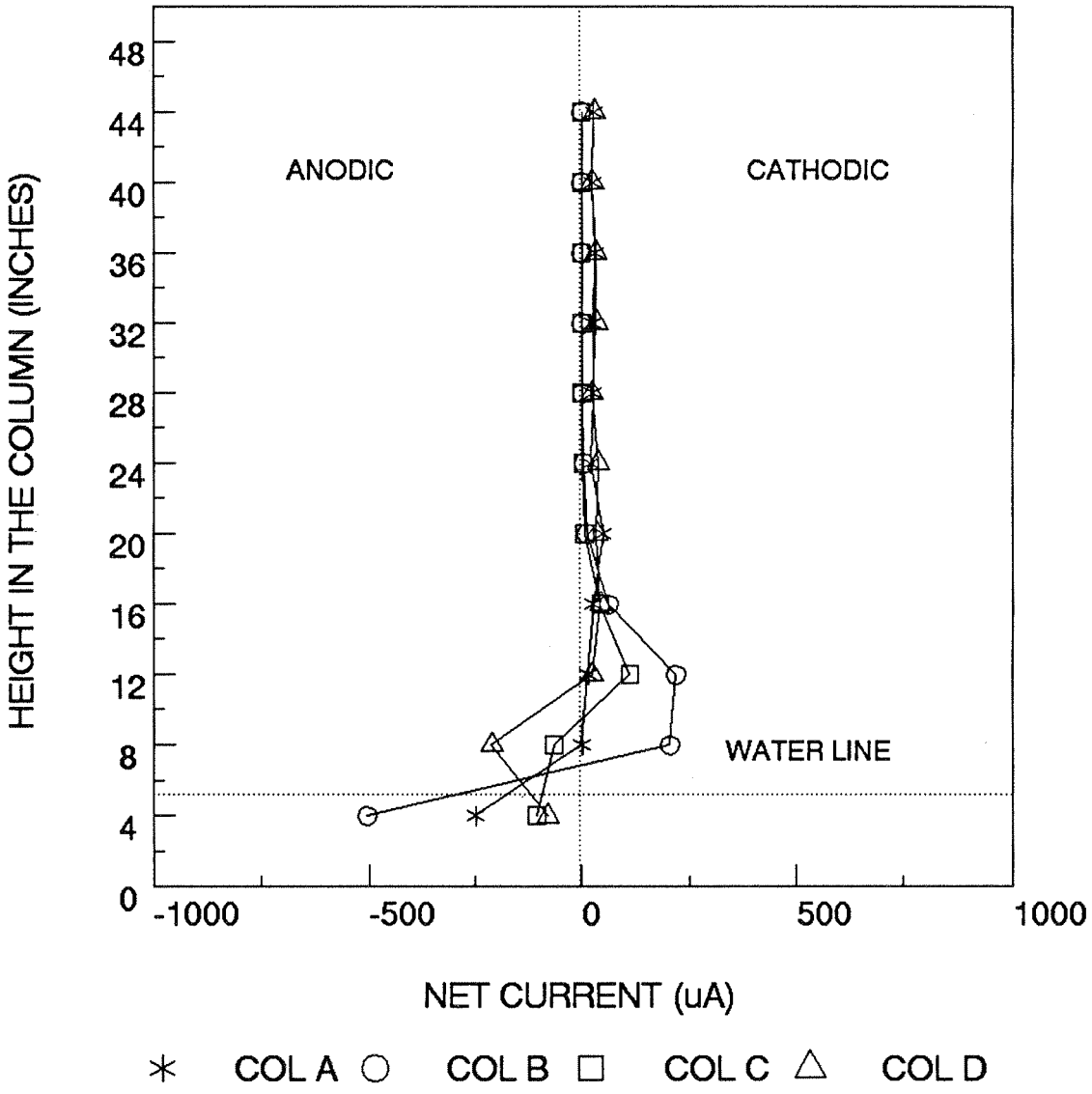

Figure II.13 Net Current vs. Column Height (Day 1111).

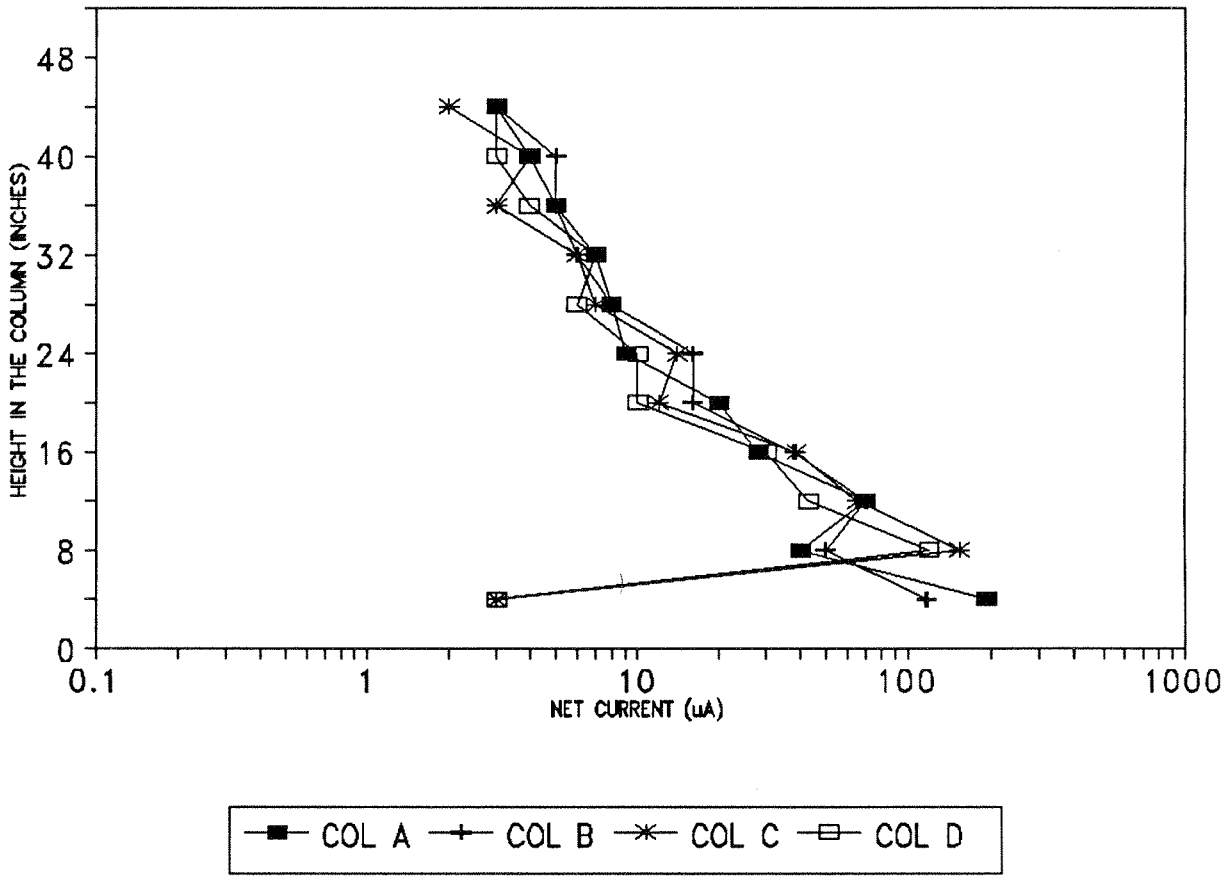

Figure II.14 Absolute Value of Net Current vs. Column Height (Day 90).

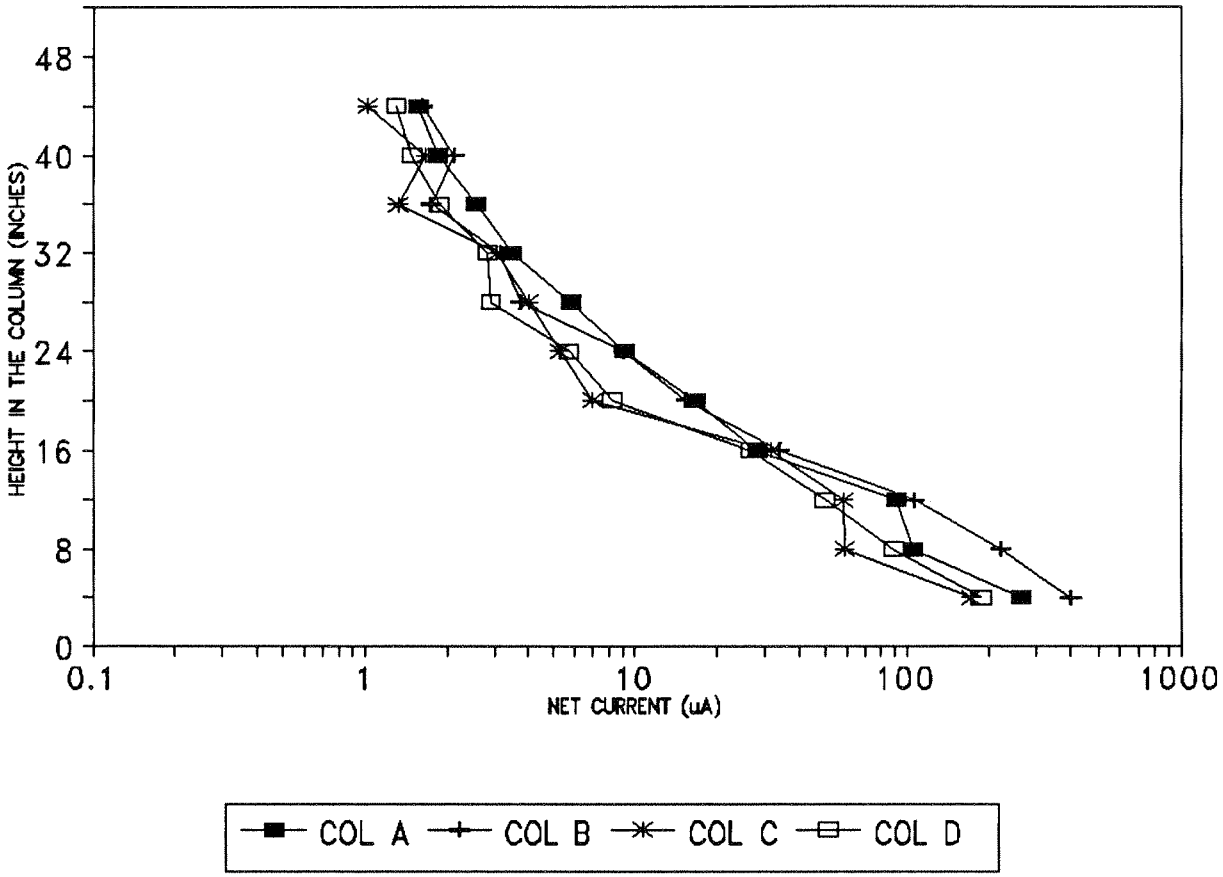

Figure II.15 Absolute Value of Net Current Associated With Rebar Segments vs. Column Height (Day 300).

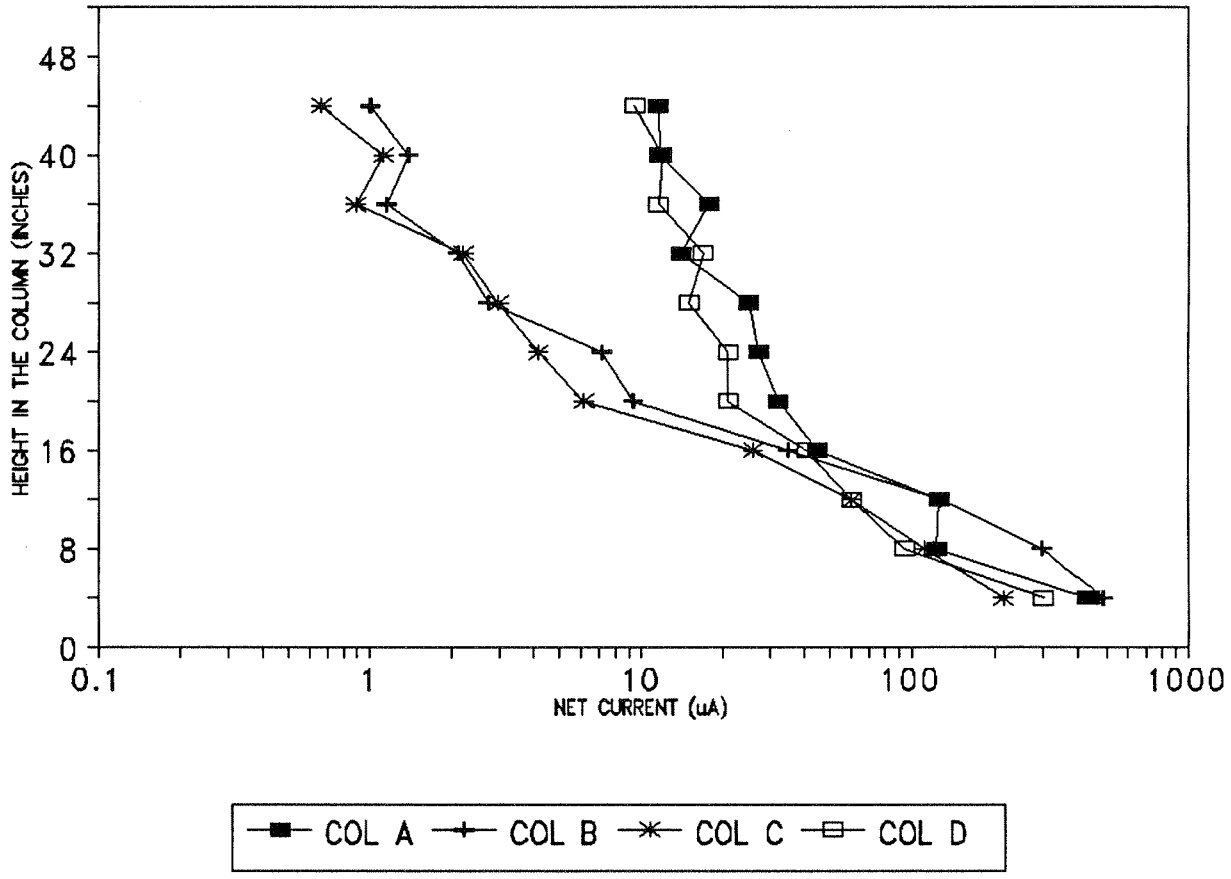

Figure II.16 Absolute Value of Net Current Associated with Rebar Segments vs. Column Height (Day 442).

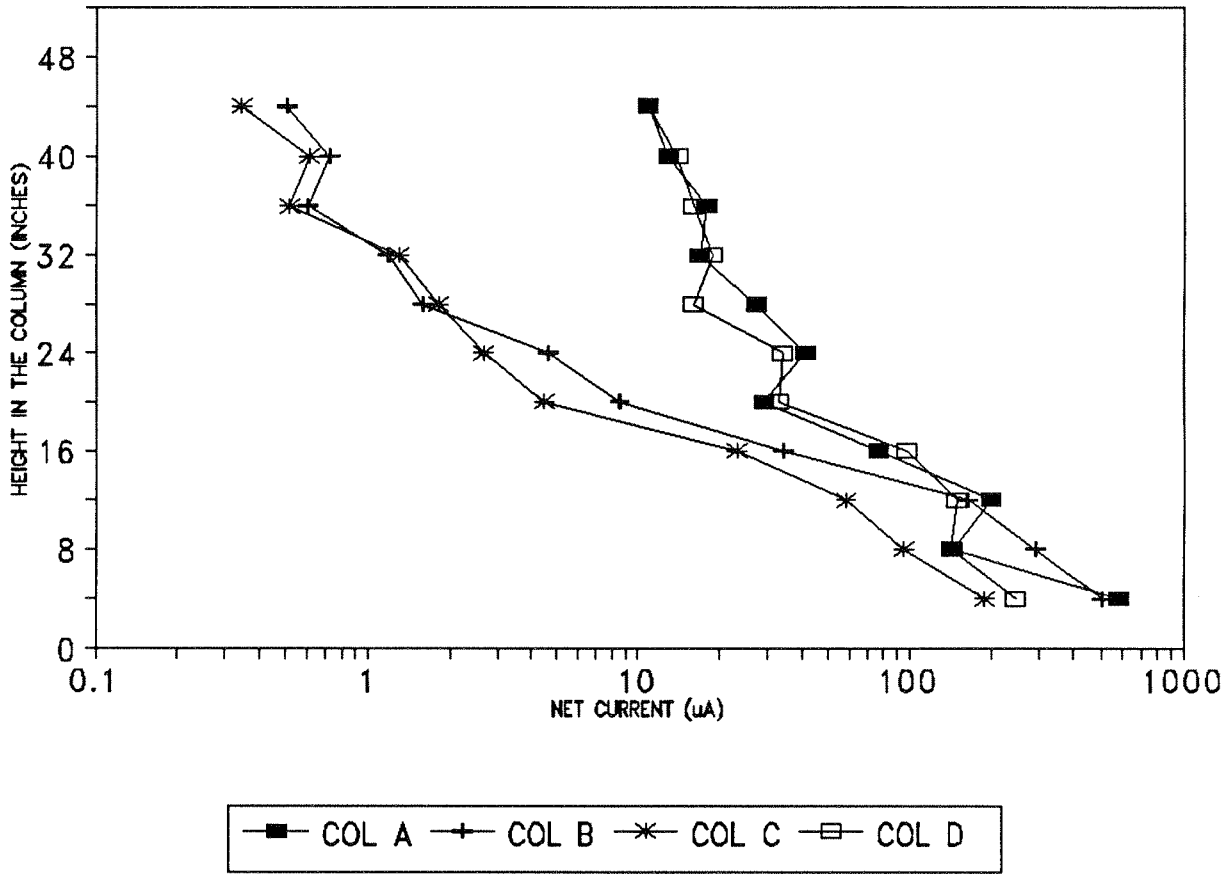

Figure II.17 Absolute Value of Net Current Associated with Rebar Segments vs. Column Height (Day 681).

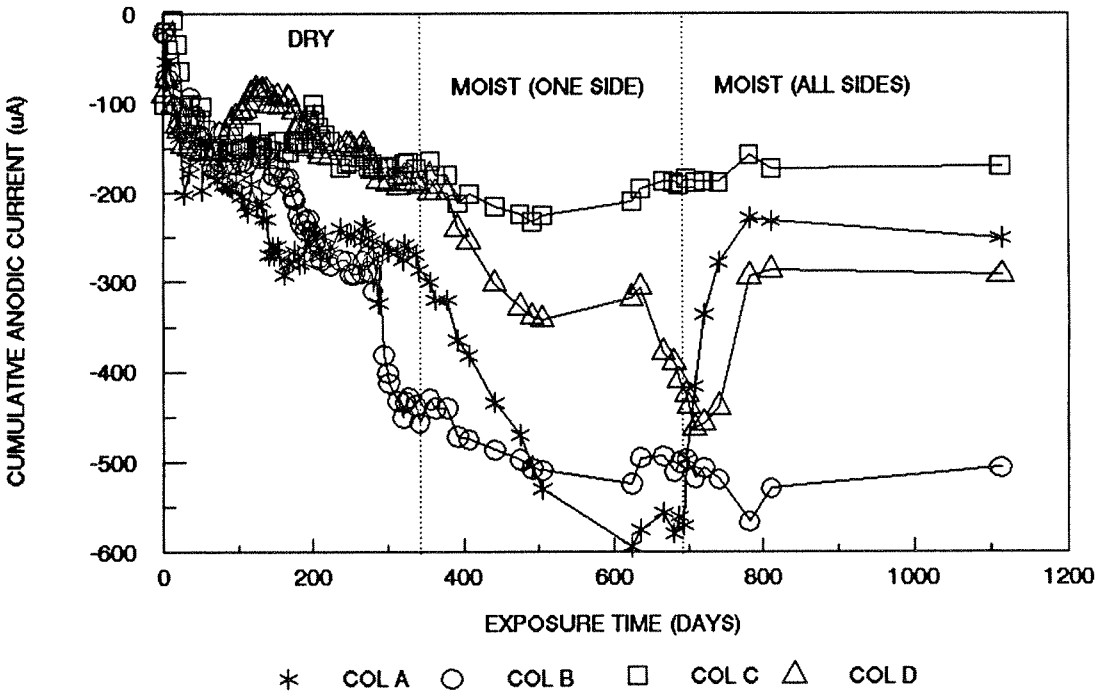

Figure II.18 Cumulative Anodic Current vs. Exposure Time.

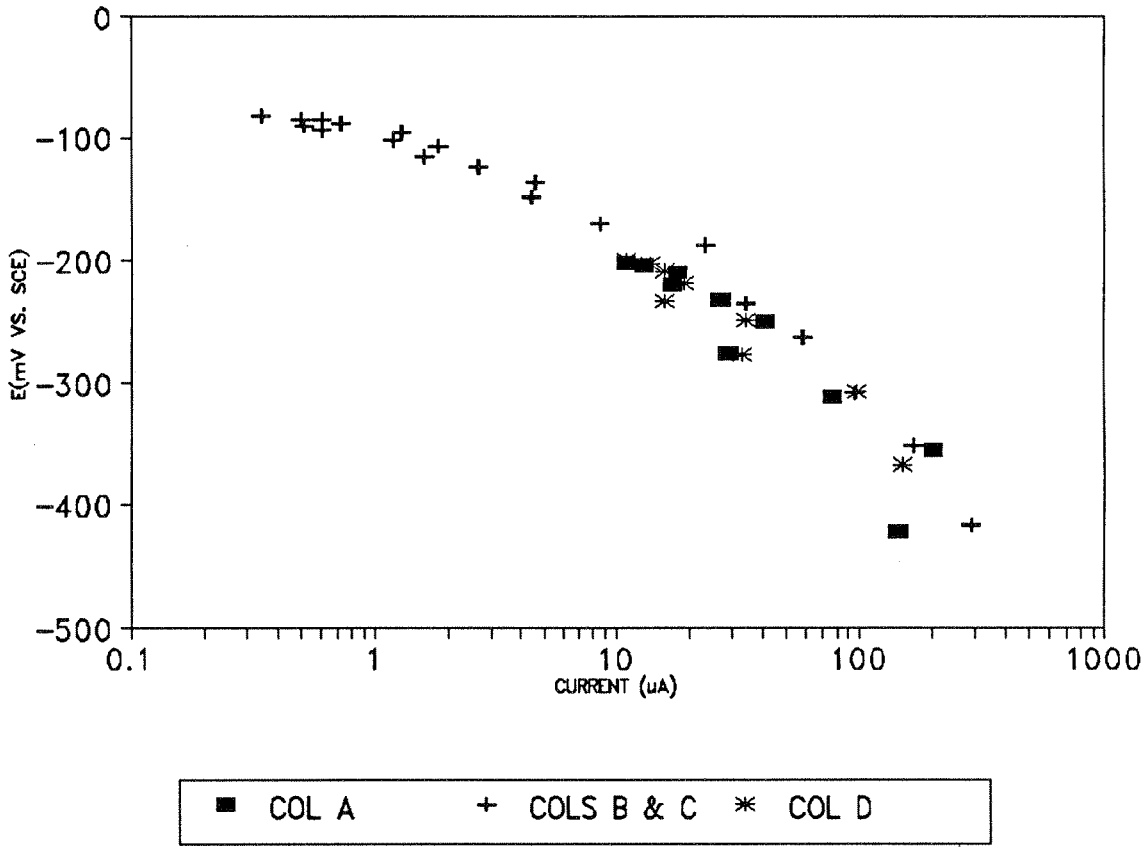

Figure II.19 Potential vs. Current (Day 681).

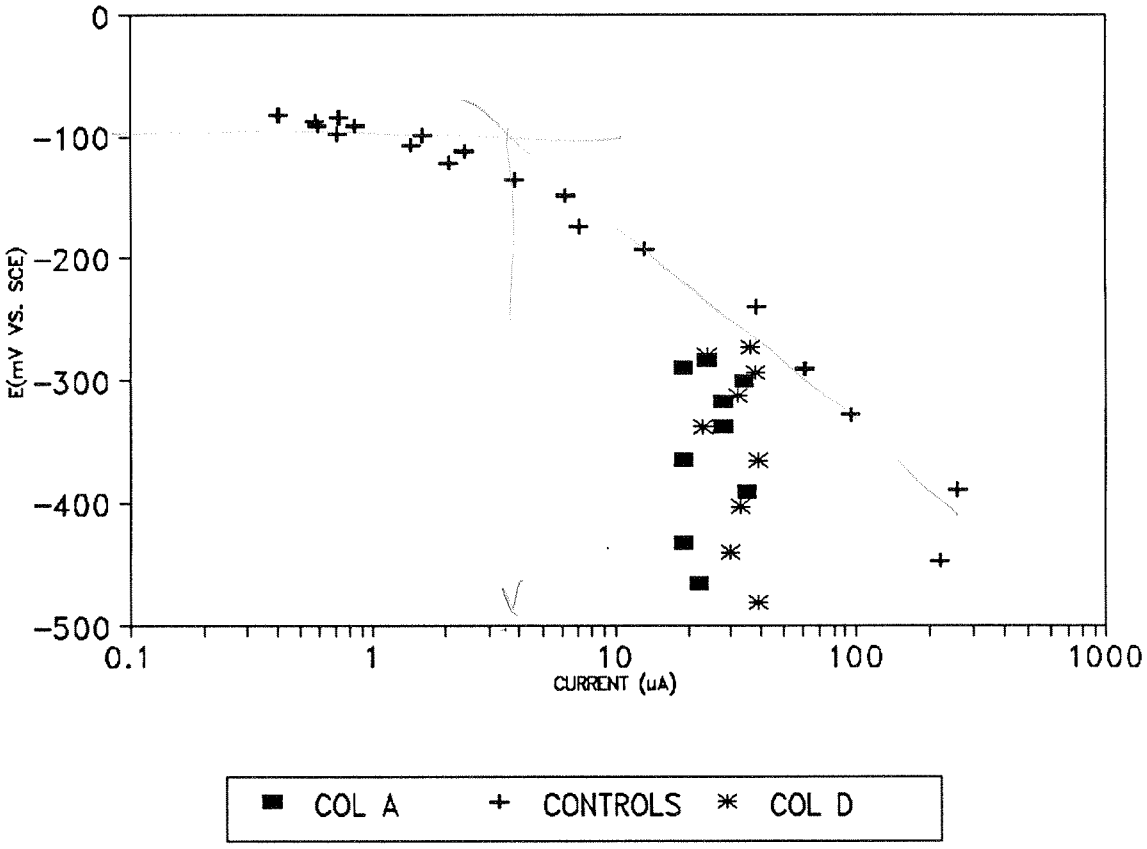

Figure II.20 Potential vs. Current (Day 1111).

5. PART III: CORROSION DISTRIBUTION MODELLING

5.1 BACKGROUND

Steel-reinforced concrete is frequently used to build substructure members in marine bridges. The lower substructure may include piles made of concrete containing prestressed steel strands, or drilled shafts of concrete reinforced with steel bars. A reinforced concrete footer is often placed on top of the lower elements, and reinforced concrete columns may be built on top of the footer. Horizontal reinforced concrete struts are sometimes used to join adjacent columns. The lower portion of the substructure is permanently submerged in seawater, and the region immediately above is subject to tidal variations in the local sea level. The substructure above the high tide line experiences wave splash, seawater mist and occasional wash due to the wakes of watercraft traffic. Depending on the local conditions, the latter action may result in seawater contact reaching as high as the lower portion of the bridge superstructure.

The water solution present in concrete pores is initially highly alkaline (pH near 13 [III.1]) and the steel embedded in the concrete becomes passivated as a result. However, passivity breakdown can take place if chloride ions from the external seawater penetrate through the concrete cover. Various investigations indicate that passivity loss occurs when the concentration of chloride ions in the pore solution is of the same order as the hydroxide ion concentration [III.1-III.3]. With typical concrete formulations and cover thicknesses, it is not uncommon to observe the onset of active corrosion in marine bridge substructures after only a few years of service. Steel depassivation is by no means limited to the portion of the structure that is always submerged. Indeed, chloride buildup is faster and more pronounced in the region directly above the high tide line. This is due to evaporation of the seawater between wetting events, leading to chloride enrichment of the solution remaining absorbed at the concrete surface and a consequent increase in the quantity of chloride ion diffused inward.

After depassivation of the steel, the distribution of corrosion in marine substructures tends to develop a maximum in a region typically 0.5m to 2m above the high tide mark [III.4]. Several factors are thought to act jointly in creating this situation. Early accumulation of chloride above high tide should allow for longer evolution times in the process of corrosion product accumulation and subsequent cracking that characterizes reinforcement corrosion damage [III.2, III.3]. Perhaps more important are the roles of the distribution of the cathodic reaction and of the electrolyte resistance along the substructure elements.

The main cathodic reaction responsible for reinforcement corrosion is considered to be oxygen reduction [III.5]. Oxygen is transported through the concrete cover to the surface of the reinforcing steel. Oxygen reduction can proceed readily even if the surface of the steel is passive, so the reaction is not limited to those areas of the steel in contact with chloride ions. While there is only limited experimental evidence available, it is generally thought that oxygen transport is much faster in dry than in water-saturated concrete. Measurements by Tuutti [III.6] indicate a three orders of magnitude difference in the effective diffusion coefficient of oxygen in concrete exposed to 100% relative humidity (R.H.) air versus concrete exposed to dry air. If the rate of the cathodic reaction were subject to simple transport limitation, the cathodic current density would then be expected to be greatest in the regions above water.

The anodic reaction would first take place in the area of chloride concentration above the waterline. Later, anodic dissolution would be possible also in the entire submerged portion of the column, where the chloride content will have reached the critical level for depassivation. A corrosion macrocell pattern may then develop, with the cathodic reaction predominant above water, and anodic processes taking place in all the regions where steel passivity was lost. However, as indicated above corrosion is usually less important in the permanently submerged portion of the substructure. The finite resistivity of concrete may provide an explanation for this behavior.

Hardened concrete is a highly inhomogeneous medium, composed of cement paste in which fine aggregate (typically sand) and coarse aggregate (stone, often with sizes in the 2 cm range) are mixed. Oven-dry concrete behaves much as an electrical insulator, but in the presence of common ambient air enough water is present in the cement paste and aggregate pores to result in significant conduction. Thus, resistivities on the order of 10 KΩ-cm to 1 MΩ-cm are often observed in ambient air for concrete specimens large enough to average out local inhomogeneities. Water-saturated concrete has space-averaged resistivities typically in the 1-10 KΩ-cm range [III.7, III.8]. The concrete resistivity results in finite resistance paths between the constituents of the corrosion macrocell. Since the cathodic reaction is expected to be taking place primarily above water, the effective circuit resistance is thought to be high enough so that the anodic reaction rate cannot be large much below the waterline. In the portion of the column above water similar IR drop effects may result in the cathodic reaction being of importance for only a limited distance above the active region of the reinforcement.

The factors determining corrosion current distribution in these systems can be understood qualitatively. However, the complexity of the geometric, physical and electrochemical factors involved prevents applying limited qualitative arguments to specific engineering questions. For example, it might be of interest to know how much will the total rate of corrosion be changed if the concrete resistivity is doubled. Likewise, it may be argued that the seawater surrounding the submerged region may, in some cases, provide enough parallel conductance to extend the macrocell action significantly below the waterline.

The purpose of this paper is to present a computational model of substructure conditions that can address quantitatively the main operating conditions of the system, and subject to numerical test the expectations of previous qualitative assessments. The computational approach used contains features of earlier models by the authors and others [III.9-III.12].

5.2 APPROACH

The calculations are based on a vertical, cylindrical reinforced concrete column, with its lower part immersed in seawater (Figure III.1). The entire system is axisymmetric. The column contains a single cylindrical reinforcing steel cage, with a radius equal to that of the column minus the thickness of the concrete cover. For the purpose of these calculations, the reinforcing steel cage will be treated as a screen with mesh spacing much smaller than the dimensions of the rest of the system. In effect, the rebar cage will be considered as a two-sided pervious sheet. This represents a simplification from the discrete bar lattice geometry (which has a typical characteristic spacing on the order of 1/4 of the column diameter). Nevertheless this simplification permits the evaluation of general corrosion distribution trends and the corrosion macrocell pattern of the column.

The concrete is treated as a radially homogeneous conducting electrolyte with variable conductivity along the column axis. The concrete is also treated as a medium where oxygen can be transported by diffusion. Oxygen diffusivity is considered constant in the radial direction but variable along the column axis. It is assumed that oxygen concentration in the column medium is constant along the entire external cylindrical surface, for both the upper and submerged portions of the column. For simplicity, oxygen flow across the upper and lower end surfaces of the column is considered to be zero.

The rebar cage surface is considered to be active in a region that includes the entire submerged portion and a length reaching from the waterline to a preset height. The latter region is representative of the rebar zone above water where chloride contamination has reached the threshold for active corrosion. The rest of the cage is treated as a passive surface, which is considered as the site of cathodic reaction (oxygen reduction: $O_2+2H_2O+4e \rightarrow 4OH^-$) only. Active surfaces support both the cathodic reaction and the anodic reaction. The anodic reaction considered is iron dissolution: $Fe \rightarrow Fe^{++}+2e$.

Reverse reactions (oxygen evolution and iron reduction) are considered to be negligible for the operating potential regime present in the column. The polarization behavior of the anodic and cathodic reactions will be assumed to be determined by a simplified adaptation of Butler-Volmer kinetics:

$$i_{Fe} = i_{o\,Fe} \exp[II.3(E_s - E_{o\,Fe})/b_a] \qquad (III.1)$$

$$i_{OR} = i_{o\,OR} (C_s/C_O) \exp[II.3(E_{o\,OR} - E_s)/b_c] \qquad (III.2)$$

(symbols are explained in the Nomenclature section.)

Eq.(III.1) assumes that the anodic reaction is subject only to simple activation polarization. Eq.(III.2) takes into consideration both activation and concentration polarization effects for the oxygen reduction reaction. Corrosion of steel in concrete may be viewed in its early stages as a form of pitting [III.13]. However, the cases examined here are intended to represent a more mature corrosion stage where iron dissoluiton proceeds in a delocalized fashion. As a result, a finite Tafel slope was chosen for the anodic reaction instead of the value $b_a = 0$ that might be used to approximate ideal pitting conditions [III.14, III.15, III.16]. The model presented here can nevertheless be adapted for computations using either approach [III.9]. Alternative representations of polarization behavior in localized corrosion are amply discussed in the literature [III.14-III.16].

The two-sided sheet approximation corresponds to a steel placement density of 2 m^2 of steel surface for every 1 m^2 of nominal mat area. Actual placement densities in structures are typically closer to 1 m^2:1 m^2. Examination of the system conditions shows that a 1:1 placement density can be simulated by using exchange current densities in Eqs. (III.1) and (III.2) that are one-half the value of those encountered on an actual steel surface. The same considerations show that for a 1:1 placement density the actual average current densities of the reactions on the steel surface can

be simulated by adding the computed current densities on both sides of the pervious sheet. To better represent an actual system, the 1:1 steel placement density will be simulated in the present calculations by means of the scaling procedure just described. Other placement density values can be simulated if desired by using the appropriate scaling factors.

For the purpose of evaluating the polarization conditions at every point of the rebar cage, the volume of the column is divided into axisymmetric regions defined by divisions along the radial and longitudinal directions (see Figure III.1). The radius is divided into 35 zones (36 radial nodes), and the column length into 240 zones (241 longitudinal nodes). The rebar cage is located at node 28, counting from the center (node 0).

The steady state current distribution within the concrete is calculated by solving the continuity equation:

$$\nabla \mathbf{i} = 0 \qquad \text{(III.3)}$$

since by Ohm's law:

$$\mathbf{i} = -\sigma \nabla E \qquad \text{(III.4)}$$

the continuity equation becomes:

$$\nabla (\sigma \nabla E) = 0 \qquad \text{(III.5)}$$

Note that Eq.(III.5) would reduce to the Laplace equation (commonly used in previous calculations of corrosion current distributions in concrete [III.9-III.12]) if σ were constant.

The boundary conditions for Eq.(III.5) at the rebar cage are provided by the polarization conditions, Eqs. (III.1) and (III.2). Each element of the rebar cage is considered as a two-sided surface. The electrolyte potential is a continuous function along a direction crossing the cage, so E is the same (E_s) on either side immediately next to the cage. On either side, the component of current density in the electrolyte normal to the surface will be given by

$$i'_n = i_{Fe} - i_{OR} \qquad \text{(III.6)}$$

and by application of Eq.(III.4)

$$\Sigma_{\text{both sides}}(-\sigma \nabla'_n E) = \Sigma_{\text{both sides}}(i_{Fe} - i_{OR}) \qquad \text{(III.7)}$$

At the two column ends current flow is assumed to be zero so that

$$\nabla'_z E = 0 \quad \text{(column end faces)} \qquad \text{(III.8)}$$

Likewise, current flow is taken as zero perpendicular to the external column surface above the waterline (air insulation) and perpendicular to the column axis along the axis itself (by symmetry):

$$\nabla'_r E = 0$$

(column exterior above water and r=0) (III.9)

The portion of the column below water is in contact with an electrolyte that is typically two orders of magnitude more conductive than the adjacent concrete. This permits using a convenient approximation to an otherwise difficult boundary condition, by treating the surface in contact with seawater as a constant potential region:

$$E = \text{constant}$$

(submerged column outer surface) (III.10)

The oxygen distribution problem was addressed by taking into consideration that steady-state conditions prevailed. Therefore, at every point of the concrete, the oxygen concentration satisfied a condition similar to that of Eq. (III.5):

$$\nabla(D \nabla C) = 0 \qquad \text{(III.11)}$$

The oxygen supply, in turn, needs to equal the amount consumed by the cathodic reaction at the metal surface. Assuming that 4 electrons are consumed for each oxygen molecule:

$$\Sigma_{\text{both sides}}(i_{OR}) = \Sigma_{\text{both sides}}(4 F \nabla i_n C) \qquad \text{(III.12)}$$

The remaining boundary conditions were provided by the absence of oxygen transport at the column ends, and constant oxygen concentration at the sides.

$$\nabla i_n C \,|_{\text{ends}} = 0 \qquad \text{(III.13)}$$

$$C|_{\text{sides}} = C_0 \qquad \text{(III.14)}$$

Concrete is heterogeneous, and oxygen transport is expected to proceed through pores that are partially filled with water to an extent depending on the moisture content. The assumption of Fickian diffusion is at best an approximation, and the diffusion coefficient should be viewed as an effective magnitude. Reported measurements of effective diffusion coefficients of oxygen in concrete are derived from concentration gradients variously based on the oxygen content of air or of water in contact with the external concrete surfaces [III.5, III.6]. For the purposes of these calculations, C is expressed in terms the concentration of oxygen present in the pore solution, which is in turn assumed to be in equilibrium with any surrounding gas. The seawater is assumed to be in equilibrium with atmospheric oxygen within the depth range considered here [III.17]. For simplicity, both seawater and the pore solution were assumed to have oxygen solubilities (and associated pressure dependencies) equal to those of pure water.

The conditions expressed in Equations (III.1-III.14) were formulated as difference equations based on nodes placed on a longitudinal section of the column, representing the concrete in the column. The difference equations were formulated to account for cylindrical symmetry along the main axis, thus obtaining full spatial simulation. Because of the complexity of the boundary conditions a dedicated computer program was constructed. The equations were solved by means of a Gauss-Seidel method, stopping the iteration process when a predetermined maximum error criterion was met. For each internal node of the system, and at each iteration step, the new value of C was obtained from the surrounding values of the previous iteration, by Equation (III.11). The same procedure was used for E, using Equation (III.5) in the same step. At the appropriate boundaries, Equations (III.15, III.16) were applied consecutively at each node during the same step to obtain the new node values. Similar procedures were used for Equations (III.6-III.10).

5.3 RESULTS AND DISCUSSION

5.3.1 Cases Examined.

Table III.1 shows the cases examined. The baseline case consisted of a column with a total length of 1200 centimeters, half of which was above the water line. The active zone extended to 202.5 centimeters above the water line. The diffusion coefficient of oxygen varied along the column from a value $D_L=10^{-5}$ cm^2/sec to a value $D_H=10^{-3}$ cm^2/sec. Keeping in mind the gas-liquid equilibrium assumptions made above, these values correspond roughly to the typical range of oxygen diffusivity reported in the literature [III.5, III.6]. Figure III.1 shows the assumed pattern of variation of D along the column. Above water, the log of D was taken to vary linearly with height, to represent the expected rapid variation of D with moisture content [III.6]. The concrete resistivity was taken to vary from 2 kΩ-cm to 10 kΩ-cm. These resistivity values are in the range commonly observed in actual substructure applications in humid environments. The variation was assumed to be linear with height above water, as a rough approximation to actual observed patterns [III.18]. The column diameter was 105 cm, whereas the concrete cover over the rebar was 10.5 cm. These values are representative of typical construction dimensions. The iron dissolution and oxygen reduction polarization parameters used in the calculations are also shown in Table III.1. These polarization parameters are equivalent to those used by the authors in previous computations [III.9-III.11], except that the exchange current densities are approximately halved to account for the two-sided sheet model as explained previously. In addition to the baseline, other cases investigated included variations in the height of the active zone above the water line, the height of the column above the water line, the diffusion coefficient limits and the concrete resistivity limits.

It is emphasized that the parameter ranges chosen for the calculations are intended only to obtain insight on the general patterns of corrosion behavior in the systems investigated. Specific dimensions and trends of parameter variation along the column could be very different from those assumed here, and detailed analysis of particular cases would require customized calculation with appropriate initial data.

The computations returned the value of the electrical potential and the oxygen concentration at every point in the concrete. From these values and by application of Equation (III.7), the distributions of the current along entering or leaving the rebar cage surface, and the amounts of oxygen consumed at various points of the system could be obtained. In addition, by application of Equation (III.1), the value of the corrosion current density could be obtained at any point where the surface of the rebar was active. Cathodic current densities will be treated as positive; anodic current densities will be treated as negative. The net current density flowing at any point from the rebar surface into the electrolyte will be denoted as the macrocell current density (which will be taken as positive). As indicated earlier, to account for the pervious sheet used to represent the rebar cage the results have been interpreted by taking at any point the sum of the process rates (current densities) of both sides of the mesh. The designation "sum of both sides" will be used as a reminder of this interpretation.

5.3.2 Potential and Oxygen Concentration Distributions.

Figure III.2 shows iso-electric potential and iso-oxygen concentration diagrams on longitudinal column cross-sections for the conditions of the baseline case A (note that in the convention used in the calculation the potentials are given with respect to the metal, so that less noble conditions correspond to higher potentials). The isopotential diagram shows that the potential increases as one moves from the air portion of the column to the submerged region. The increase reflects both the presence of the active region and the lower availability of oxygen in the wet portions of the column.

The isopotential lines indicate that there is a general flow of conventional current across the concrete from the lower to the upper parts of the column. This is because iron dissolution takes place only in the active, lower region while oxygen reduction is more predominant in the upper portion of the active zone and is the only reaction in the passive area. The resulting net ionic flow corresponds to the calculated conventional current direction.

The isoconcentration lines show predominant oxygen flow from the top to bottom in the upper part to the column, and from the exterior into the rebar cage in the lower regions. The oxygen concentration is very low inside the cage over the entire active steel portion; in that region there is no significant oxygen transport through the interior of the column. In examining the diagram it should be remembered that the oxygen diffusivity is not constant along the column. Thus, although the isoconcentration lines show roughly the same spacing at the bottom of the passive region than in the region below water, the oxygen flow normal to the lines in the latter region is much smaller than in the former.

5.3.3 Current Distribution.

The potential and concentration distributions discussed above, together with the conductivity and diffusivity distributions, define the extent of electrochemical reactions at the steel surface. The following discussion refers to current densities treated as the sum of both sides of the pervious sheet.

Figure III.3 (top) shows the macrocell current density at points along the rebar cage as a function of position for the baseline case (A) and for a higher resistivity condition (B). The magnitude of the macrocell current density reaches a maximum at the highest active point of the column. At that location, the macrocell current also changes sign when going from the active portion to the passive portion of the column.

Figure III.3 (center) shows the anodic current density (equal in magnitude but, by convention, opposite in sign to the corrosion current density) along the column. The corrosion current density reaches a maximum also at the highest active point in the column; the current density is zero (by assumption) at the passive region. The corrosion current density values obtained are typical of those encountered in reinforced concrete systems exposed to aggressive environments. The maximum corrosion current densities in Figure III.3 would be enough to result in the observation of external cracks after several years of service [III.19] in that area of the column, in agreement with field observations. Nevertheless, the simplifications used in these calculations need to be kept in mind when interpreting these results.

Figure III.3 (bottom) shows the cathodic current density (equal in magnitude and sign to the value of the oxygen consumption rate) at the rebar cage surface as a function of position along the column. The oxygen consumption is nearly constant for the entire submerged portion of the rebar cage, reflecting the assumption of constant oxygen diffusion coefficient in that region (where, as shown before, the oxygen supply is also under diffusion-limited conditions). The value computed by the model for the underwater oxygen consumption rate (0.12 $\mu A/cm^2$) is consistent with that obtained with an approximate calculation that would assume one-dimensional diffusion across the concrete cover: $i = 4\ F\ D\ C_o/c = 0.11\ \mu A/cm^2$. Oxygen consumption increases as elevations above the water line are reached, reflecting the increase in the diffusion coefficient as a function of height above the water line. However, the oxygen consumption begins to decay after a maximum at or near the highest point of the active zone. This behavior is a consequence of the electrical potential distribution on the rebar cage surface along the column. As indicated in Figure III.2, the potential at the zone above the highest active spot tends to decrease in magnitude with further height, therefore reducing the demand for oxygen to the cathodic reaction.

Figure III.3 also illustrates the effect of changing the value of the concrete electrical resistivity. As the electrical resistivity is increased by one order of magnitude (that is, going from case A to case B), the distribution of the corrosion macrocell is confined to a smaller distance range. This is as expected, since the potential attenuation from the highest electrochemical activity point will be greater at greater electric resistivities. The same effect applies to the corrosion current density distribution. In addition, the maximum magnitudes of the corrosion current and macrocell current densities are smaller when the concrete resistivity is higher.

The effect of varying concrete resistivity on the oxygen consumption is more complex (Figure III.3, bottom). Below the water line, the amount of oxygen demand does not change significantly upon increasing the resistivity, since that portion of the rebar cage behaves much as a uniform mixed-potential electrode. In that regime, oxygen transport is the limiting factor on the rate of corrosion, and resistivity has no significant effect. Above the water line, the increase in concrete resistivity results in a narrower transition region in the rate of oxygen consumption. The total rate of oxygen consumption is, as expected, lower for the high resistivity case. However, the peak value of the oxygen consumption rate tends to be actually slightly greater when the concrete resistivity is higher. This behavior is not surprising, since the peak rate results from a complex balance between the overall rate of the reactions and the size of the spacial region affected.

The model simplifications assumed that the rate of the electrochemical reactions depends only on the electrode potential, oxygen concentration and active/passive status of the surface. Significant variations in the predicted behavior could result if the extent of contact between metal and the surrounding electrolyte were a function of position. It has been suggested [III.20] that the fraction of the steel surface in actual contact with liquid may be strongly reduced as the moisture content of the concrete decreases. In that case, it is possible that the maximum corrosion density spike might be replaced by a maximum taking place at a lower elevation point

closer to the waterline. While that type of case has not been considered here, the model could be used to examine this effect including a position-dependent preexponential factor in Eqns. (III.1) and (III.2).

5.3.3 Corrosion Behavior Trends.

Table II summarizes information that can be extracted from the results of all the cases computed. All magnitudes and rates correspond to the sum over both sides of the pervious sheet. The total macrocell current is equal to the absolute value of the integral of the macrocell current density over either the entire net anodic or the entire net cathodic portion of the column. The total corrosion current is equal to the absolute value of the integral of the corrosion current density over the entire active portion of the rebar cage surface. The maximum corrosion current density corresponds to the absolute value of the anodic current density at the highest point of the active zone. The oxygen consumption below water is the integral of the oxygen consumption rate over the portion of the rebar surface which lays below the water line. Finally, the iron solution rate below water results from integrating the corrosion current density over the portion of the rebar cage surface below the water line.

In order to better understand the influence of concrete resistivity on corrosion behavior, the results from cases A, B, L, and M were examined graphically as shown in Figure III.4. The values of the total I_{corr} and I_{macro}, as well as maximum i_{corr} are plotted as a function of ρ_L for each case (ρ_H is always equal to $5\rho_L$) using a log-log representation. The corrosion severity decreases as the resistivity increases. The absolute average slope of the trend lines (akin to the exponent n in a power law relationship) is a rough indicator of the sensitivity of each corrosion magnitude to variations in the concrete resistivity. Thus, within the parameter ranges examined the total macrocell current shows the greatest sensitivity to resistivity changes ($|n|\sim 1/2$), followed by the maximum corrosion current density ($|n|\sim 1/4$) and the total corrosion current ($|n|<1/4$).

In a similar fashion, Figure III.5 shows dependence of corrosion severity on the diffusivity of oxygen. A series of cases (A,F,G) with low resistivity (ρ_L=2 kΩ-cm, solid lines) are compared to a series (B,J,K) with high resistivity (ρ_L=20 kΩ-cm, dashed lines). In both series, the corrosion severity increases as the overall diffusivity increases (D_H/D_L is always kept equal to 100). The sensitivities of total corrosion current and maximum corrosion current density to changes in oxygen diffusivity ($|n|$~2/3) tend to be greater than those observed in Figure III.4 for changes in resistivity. In contrast the total macrocell current shows only moderate sensitivity ($|n|$~1/4) to diffusivity changes, less than that encountered for resistivity variations. In general, with the exception of the total macrocell current, a relative change in oxygen diffusivity has a greater effect than a similar change in concrete resistivity.

Figure III.6 shows the effect of changing the height of the active zone above water on the corrosion severity. The total corrosion current increases with the height of the active zone, as expected since more active material is available for corrosion, in a region where oxygen supply is less restricted than below water. The same happens for the maximum corrosion current density. Interestingly, the total macrocell current changes little with the height of the active zone above water. The corrosion current density distribution associated with this behavior is seen in Figure III.7. As the active zone above water becomes shorter, the corrosion current density in the submerged zone becomes greater. In the presence of a sizable active steel zone above water, the oxygen consumed there served to increase the local iron dissolution rate. Without a large active zone above water, the effect of oxygen consumption there is to increase the corrosion rate below water (which was otherwise restricted by the slow local delivery of oxygen through water-saturated concrete). The combination of the system dimensions and the diffusivity and resistivity distributions used here creates an effective limiting current phenomenon, with the resulting observed stability of the total macrocell current. It should be noticed also that the calculated increase in corrosion rate below water is uniform over that region. This results form the assumption of an equipotential concrete surface in the submerged area. Some deviation from this behavior would result if a finite resistivity for seawater were assumed.

5.3.4 Polarization of the Oxygen Reduction Reaction.

Further insight on the corrosion process in these systems can be gained by examination of the potential-current relationship of the oxygen reduction reaction. Figure III.8 shows a composite E-log i (sum of both rebar cage sides) curve for the entire column, for the baseline case (A). The more noble potentials correspond to the passive region above water, where diffusional transport is not limiting. As a result, the curve approaches ideal Tafel behavior, with a slope close to the assumed value of 0.16 V per decade. As more active potentials are reached, a diffusional limitation is encountered. However, because the system is three-dimensional and the diffusion coefficient is variable, the curve does not approach a simple limiting current density. The kink in the curve corresponds to the transition into the active portion of the rebar cage. The current density actually decreases dramatically as the potential becomes less noble. Finally, the curve portion representing most of the submerged portion of the column is compressed near the end point (which corresponds to the flat portion of the plots in Figure III.3, bottom.) The composite polarization curve illustrates the complexity of the phenomena encountered in large, heterogeneous systems. It should be noted that this curve does not represent the polarization behavior of an individual surface element on the rebar cage; the behavior of each element varies with position along the column length. Rather, the complex nature of the system examined here prevents the use of a master cathodic polarization curve, as is sometimes assumed in the computer modeling of extended structures [III.12, III.21].

It should also be noted that the steel in the portion of the column below water, which has the less noble potentials, does not have the highest corrosion rate. This observation is in line with the behavior observed in similar systems [III.22], and emphasizes the importance of not equating high corrosion rates with extreme potential readings, as it would result from an uncritical application of specialized corrosion criteria (such as ASTM C-876).

5.3.5 Modeling Considerations.

The interpretation of the peak current density magnitudes reported (Figures III.3-III.7) must be qualified by keeping in mind that discretization errors are unavoidable. The peak current densities present at the active-passive transition line would be finite even if a continuous model were used (as required by Eqs. (III.1) and (III.2)). However, the computational grid used here prevents obtaining the actual values of the peak current densities at the transition itself, and only values at points half a grid space away can be estimated. The actual value at the transition will differ from the reported value by an amount depending on the effective polarization slope acting at that point, and on the rate of potential variation across the transition. Since the potential tends to vary rapidly across the region of interest, the peak current density results reported here are to be considered as an approximation, useful to evaluate the relative effects of the corrosion parameters of the system. It should also be understood that in a real system a sharply defined spacial active-passive transition is not likely to be present, and that the simulation of a rebar cage by means of a fine mesh has already involved numerous simplifications.

5.3.6 Implications on Marine Substructure Conditions:

The calculations provide quantitative support to the long-held view that the corrosion rate in the underwater portion of the structure is small as a result of limited oxygen access. The calculations indicate however that corrosion underwater could be enhanced as a result of corrosion macrocell coupling with the portion above water, if the anodic activity there is lessened. This finding merits consideration if corrosion abatement methods for the splash zone (such as the use of concrete surface treatments) become successful. The possibility of enhanced corrosion underwater in those cases should be examined in more detail.

The calculations showed that limitation of the oxygen reduction reaction below water need not be due, as sometimes thought, to low availability of oxygen in the seawater itself; oxygen concentrations comparable to those present near the sea

surface can be encountered even at great depths [III.17]. In the computed cases the severe limitation observed results from the oxygen diffusion process through the concrete cover. Additional limitation could result of course, if other sources of oxygen depletion such as biologically active layers were present at the submerged concrete surface. The calculations also suggest that oxygen supply from above through the core of the column is not likely to be important to the corrosion behavior underwater.

The quantitative results agreed also with the common observation of severe corrosion in the splash-evaporation zone of marine substructures. Depending on the choice of parameters assumed, macrocell currents ranged from about 10% to 90% of the total corrosion current of the system. In general, total macrocell currents were a larger fraction of the total corrosion current when the concrete resistivity or the oxygen diffusivity covered a low range of values. The high calculated corrosion current densities near the top of the active zone resulted from a combination of increasing oxygen diffusivity with height (which allowed for greater local cell action), and coupling with the oxygen reduction at the nearby portion of the passive zone. The "throwing power" of the macrocell effect into the passive zone can be estimated from Figure III.3 (bottom) to be on the order of 0.1 m to 1 m for the conditions investigated. As indicated earlier, the macrocell effect distances could be much larger into the less resistive submerged zone. Other characteristics of the system (such as steel placement density and effective exchange current densities) will be expected to play a role in determining the extent to which the macrocell action contributes to the overall development of corrosion in the column.

Regardless of the relative importance of local versus extended cell action, the results underscored the importance of increasing concrete resistivity and reducing the effective oxygen diffusivity to lower the overall corrosion rate. The present trend toward using denser concretes in marine construction is therefore expected to be beneficial not only in delaying the onset of active corrosion (by retarding chloride ion ingress), but also because of the reduced gas transport and higher resistivities of those materials [III.23].

5.3.7 Model Extension and Enhancement.

The results presented here covered only some of the most important variables in the problem. The present model is suitable also to evaluate the effect of concrete cover thickness, alternative oxygen diffusivity and concrete resistivity profiles, alternative steel placement density and polarization variables, truncated column geometries and a number of service-related situations. Those conditions should be examined in detail for possible implications on structural design for improved corrosion resistance. The model could also be modified to evaluate the performance of various cathodic protection options; work along those lines is in progress and will be presented elsewhere.

Numerous factors of importance remain unaddressed because of the assumptions of the present model; the following is only a partial account of possible improvements leading to a more realistic simulation.

A desirable enhancement would be the implementation of a more realistic rebar geometry simulation. It is expected that typical three-dimensional cage assembly geometries give rise to current and oxygen flow concentration effects that may significantly alter the local corrosion distribution from the more uniform conditions examined here. A detailed three dimensional model might also be used to investigate pitting conditions, by modelling the chloride-contaminated areas with multiple small active regions (with effectively zero Tafel slope) spaced by an appropriate characteristic distance.

The polarization characteristics assumed here make no allowance for back reactions, which might be important in the submerged zone. The anodic reaction can be very complex and involve several intermediate states not considered here. In addition, the simple active-passive behavior assumed here is a strong simplification of the actual material behavior. The cathodic reaction rate may be strongly sensitive on the surface condition of the steel, and it may also involve other reactions (such as

ferric to ferrous ion conversions) not considered here. The effect of corrosion product accumulation on both the locus and the rate of anodic and cathodic reacitons should be investigated. As indicated earlier, the model could be also used to examine the effect of variations in the effective electrolyte contact area of the steel as resulting, for example, from changes in the moisture content of the concrete with height within the column. Reliable data on oxygen diffusivity in concrete are scarce; in view of the importance of that parameter suggested by the results more extensive information may be highly beneficial in that area.

5.4 NOMENCLATURE

L	Column length.
w	Column diameter.
c	Concrete cover.
h_A	Height of active zone above water.
i_{Fe}	Current density of the iron oxidation reaction.
i_{OR}	Current density of the oxygen reduction reaction.
$i_{o\ Fe}$	Exchange current density for the $Fe/Fe^{++}+2e$ system.
$i_{o\ OR}$	Exchange current density for the OH^-/O_2+2H_2O+4e system.
i_{CORR}	Corrosion current density.
I_{CORR}	Corrosion current.
I_{MACRO}	Macrocell current.
$\mathbf{i}$	Current density vector.
E	Potential at a point of the electrolyte (through an idealized reference electrode) with respect to the body of the metal. Note that this convention, used throughout this paper, is the opposite of the common usage of referring potentials with respect to a reference electrode placed in the electrolyte.
E_s	Potential at the electrolyte immediately next to the metal surface.
$E_{o\ Fe}$	Redox potential for the $Fe/Fe^{++}+2e$ system.
$E_{o\ OR}$	Redox potential for the OH^-/O_2+2H_2O+4e system.
b_a	Activation Tafel slope for the anodic reaction.
b_c	Activation Tafel slope for the cathodic reaction.
ρ	Concrete resistivity.

ρ_H, ρ_L	Highest and lowest values of ρ.
σ	Concrete conductivity ($\sigma = 1/\rho$)
$\nabla i_p A$	Component along the direction p of the gradient of scalar magnitude A.
n	Direction normal to a surface, pointing away from the surface.
z	Axial column direction.
r	Radial column direction.
C	Oxygen concentration.
C_s	Oxygen concentration at the steel surface.
C_O	Oxygen concentration at the external concrete surface.
D	Oxygen diffusion coefficient.
D_H. D_L	Highest and lowest values of D.

5.5 PART III REFERENCES

III.1 Macias, A., and Andrade, C. , Corrosion Sci., Vol. 30, p. 393, 1990.

II.2 "Corrosion of Metals in Concrete", ACI Journal Committee Report by ACI Committe 222, Journal of the American Concrete Institute, p. 3, Proceedings Vol. 82, 1985.

III.3 Slater, J., "Corrosion of Metals in Association with Concrete", ASTM STP 818, ASTM, Philadelphia, 1983.

III.4 Sagüés, A. , Perez-Duran, H. and Powers, R., Corrosion, Vol. 47, p. 884, 199I.

III.5 Gjorv, O., Vennesland, O. and El-Busaidy, A., Materials Performance, Vol. 25, No. 12, p. 39 (1986).

III.6 Tuutti, K., Corrosion of Steel in Concrete, Swedish Cement and Concrete Research Institute, 1982.

III.7 Strattful, R., Materials Protection, p. 29, March 1968.

III.8 Millard, S. G., Ghassemi, M., Bungey, J. and Jafar, M., "Assessing the Electrical Resistivity of Concrete Structures for Corrosion Durability Studies", in Corrosion of Reinforcement in Concrete, C. Page, K. Treadway and P. Bamforth, Eds., p. 303, Elsevier Appl. Sci., London-New York, 1990.

III.9 Kranc, S.C. and Sagüés, A.A., "Computation of Corrosion Macrocell Current Distribution and Electrochemical Impedance of Reinforcing Steel in Concrete", in Computer Modeling in Corrosion, ASTM STP 1154, R.S. Munn, Ed., American Society for Testing and Materials, Philadelphia, p. 95, 1992.

III.10 Kranc, S.C. and Sagüés, A.A., "Calculation of Extended Counter Electrode Polarization Effects on the Electrochemical Impedance Response of Steel in Concrete", in Electrochemical Impedance: Interpretation and Analysis, ASTM STP 1188, D.C. Silverman, J.R. Scully and M.W. Kendig, Eds., American Society for Testing and Materials, Philadelphia, 1993.

III.11 Sagüés, A. and Kranc, S.C., Corrosion, Vol. 48, p. 624, 1992.

III.12 Naish, C., Harker, A. and Carney, R., "Concrete Inspection: Interpretation of Potential and Resistivity Measurements", in Corrosion of Reinforcement in Concrete, C. Page, K. Treadway and P. Bamforth, Eds., p. 314, Elsevier Appl. Sci., London-New York, 1990.

III.13 Kaesche, H., "Metallic Corrosion", NACE, Houston, 1985.

III.14 Smyrl, W.H., "Electrochemistry and Corrosion on Homogeneous and Heterogeneous Metal Surfaces ", p. 97, in Comprehensive Treatise of Electrochemistry, Vol. 4, Bockris, J.O'M., et al, Eds., Plenum Press, New York, 1981.

III.15 Wagner, C., J. Electrochem. Soc., Vol. 98, p.116, 195I.

III.16 Smyrl, W. and Newman, J. J., Electrochem. Soc., Vol. 123, p. 1423, 1976.

III.17 Shreir, L., Editor, Corrosion, Volume 2, Corrosion Control, p. 21:56, Newnes-Butterworths, London, 1976.

III.18 Sagüés, A., "Mechanism of Corrosion of Epoxy-Coated Reinforcing Steel in Concrete", Final Report No. FL/DOT/RMC/0543-3296, National Technical Information Service, Springfield, VA 22161, April 1991.

III.19 Clear, K., Measuring Rate of Corrosion of Steel in Field Concrete Structures, Transportation Research Board 68th Annual Meeting, January 22-26, 1989, Paper Preprint No. 88-0324.

III.20 Feliu, S., Gonzalez, J.A., Feliu, Jr., S., and Andrade, C., British Corrosion Journal, Vol. 24, p.195, 1989.

III.21 Munn, R.S., Editor, "Computer Modeling in Corrosion", ASTM STP 1154, American Society for Testing and Materials, Philadelphia, 1992.

III.22 Browne, R., "Mechanisms of Corrosion of Steel in Concrete in Relation to Design, Inspection and Repair of Offshore and Coastal Structures", in Performance of Concrete in Marine Environment, Publication SP-65, American Concrete Institute, Detroit, 1980.

III.23 Millard, S.G., Durability Performance of Slender Reinforced Coastal Defense Units, in Concrete in Marine Environment, p. 339, V. Malhotra, Ed., ACI SP-109, American Concrete Institute, Detroit, 1988.

TABLE III.1

CASES INVESTIGATED

CASES	h_A (cm)	D_L (cm^2/s)	D_H (cm^2/s)	ρ_L (kΩ-cm)	ρ_H (kΩ-cm)
A BASELINE	202.5	10^{-5}	10^{-3}	2	10
B	202.5	10^{-5}	10^{-3}	20	100
C	102.5	10^{-5}	10^{-3}	2	10
D	2.5	10^{-5}	10^{-3}	2	10
E	302.5	10^{-5}	10^{-3}	2	10
F	202.5	10^{-6}	10^{-4}	2	10
G	202.5	10^{-7}	10^{-5}	2	10
J	202.5	10^{-6}	10^{-4}	20	100
K	202.5	10^{-7}	10^{-5}	20	100
L	202.5	10^{-5}	10^{-3}	6	30
M	202.5	10^{-5}	10^{-3}	1	5

For all cases:

L = 1200 cm
w = 105 cm
c = 10.5 cm
$i_{o\,Fe}$ = 1.875 10^{-8} A/cm^2
$i_{o\,OR}$ = 6.25 10^{-10} A/cm^2
$E_{o\,Fe}$ = 780 mV*
$E_{o\,OR}$ = -160 mV*
b_a = 60 mV
b_c = 100 mV
C_O = 3 10^{-7} Mol/cm^3

* SCE scale, signs per convention in Nomenclature section.

TABLE III.2

SELECTED CALCULATED MAGNITUDES

CASE	TOTAL MACROCELL CURRENT (mA)	TOTAL i_{corr} (mA)	MAXIMUM i_{corr} ($\mu A/CM^2$)	OXYGEN CONSUMED BELOW WATER (mA)	IRON DISSOLVED BELOW WATER (mA)
A BASELINE	14.2	49.7	4.5	19.6	20.2
B	21.89	39.8	2.2	19.6	20.0
C	121.7	38.4	21.3	19.6	21.8
D	14.2	34.1	0.57	19.6	34.1
E	14.3	721.5	6.5	19.6	18.9
F	5.8	9.3	1.4	0.91	1.51
G	2.48	2.7	0.35	0.196	0.44
J	2.05	5.64	0.6	1.96	2.25
K	0.76	1.11	0.17	0.196	0.236
L	8.05	421.5	21.2	19.6	20.1
M	20.5	57	5.52	19.6	20.7

(rates correspond to the sum of both sides)

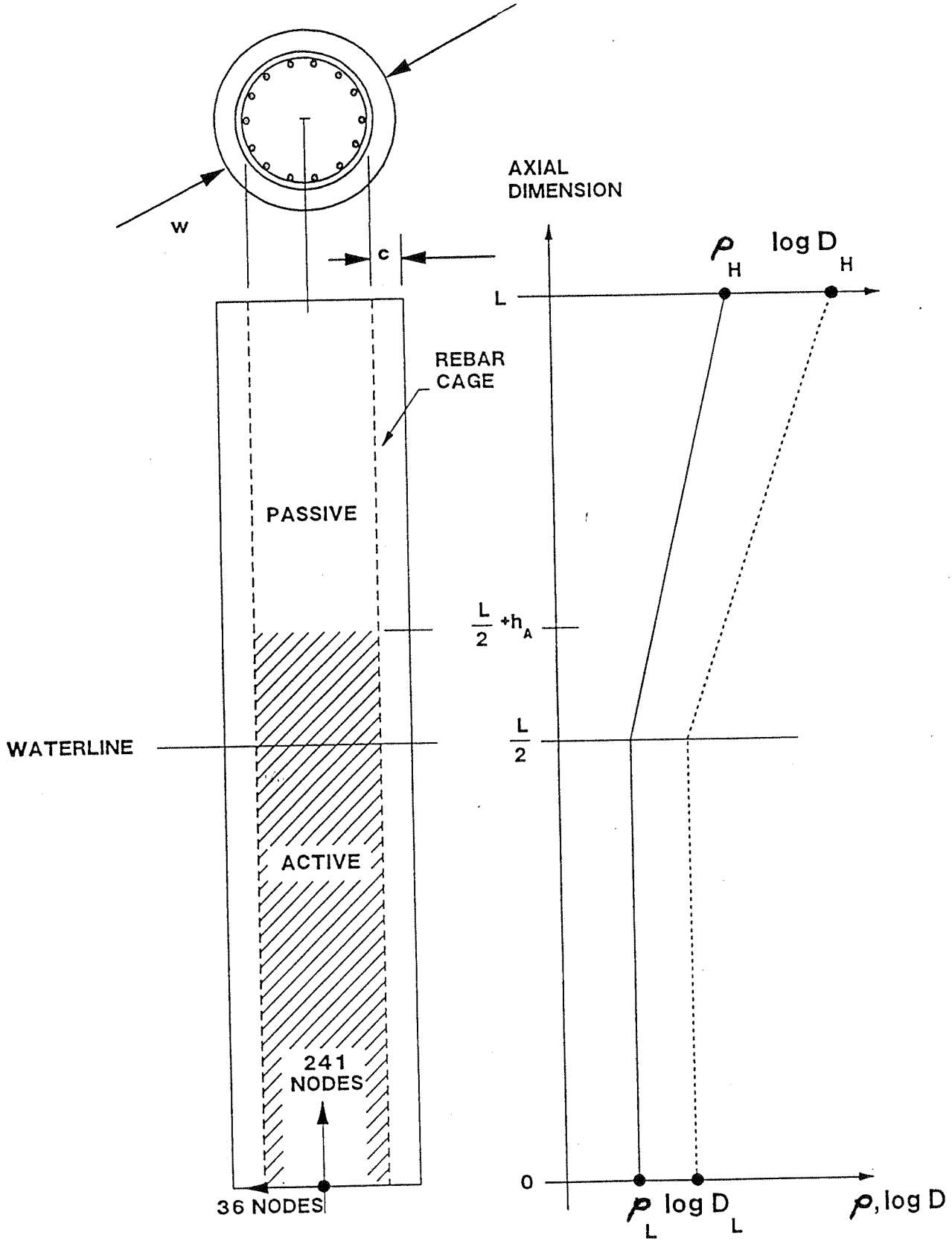

Figure III.1 Idealized Half- Submerged Reinforced Concrete Column Model.

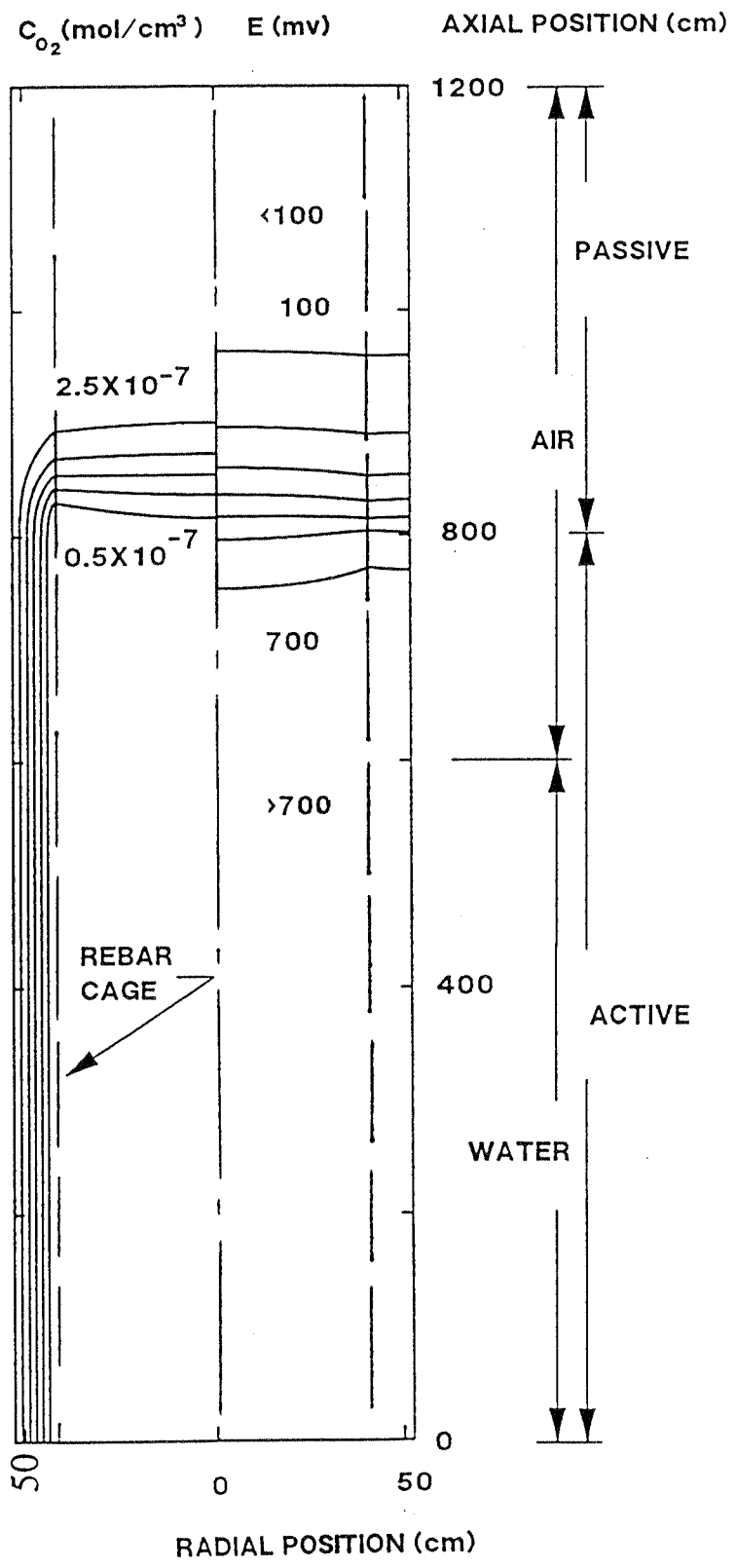

Figure III.2 Isopotential and Isoconcentration Lines Showing the Results of the Model Calculations for the Baseline Case A. The Equipotential Lines Are Separated at Equal Intervals of 100 mV Each. The Isoconcentration Lines Are 0.5 10^{-7} Mol/cm³ Apart.

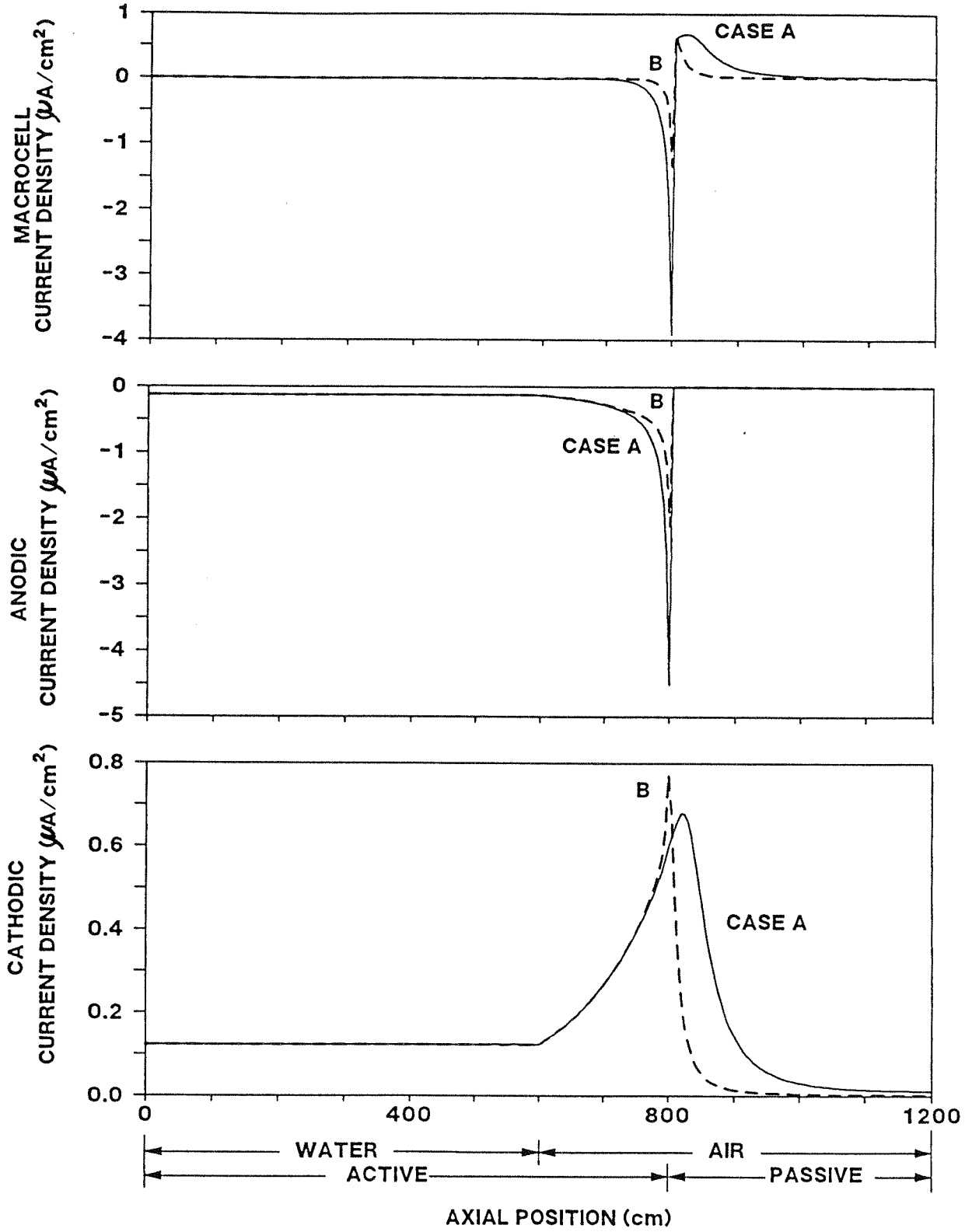

Figure III.3 Current Density (Sum of Both Sides) Distributions Along the Rebar Cage for the Baseline Case A and for Case B (Higher Concrete Resistivity). The Macrocell Current Density (Top) is Equal to the Algebraic Sum of the Anodic (Center) and Cathodic (Bottom) Current Densities. The Absolute Values of the Corrosion Current Densities and the Oxygen Consumption Current Densities are Equal to Those of the Anodic and Cathodic Current Densities Respectively.

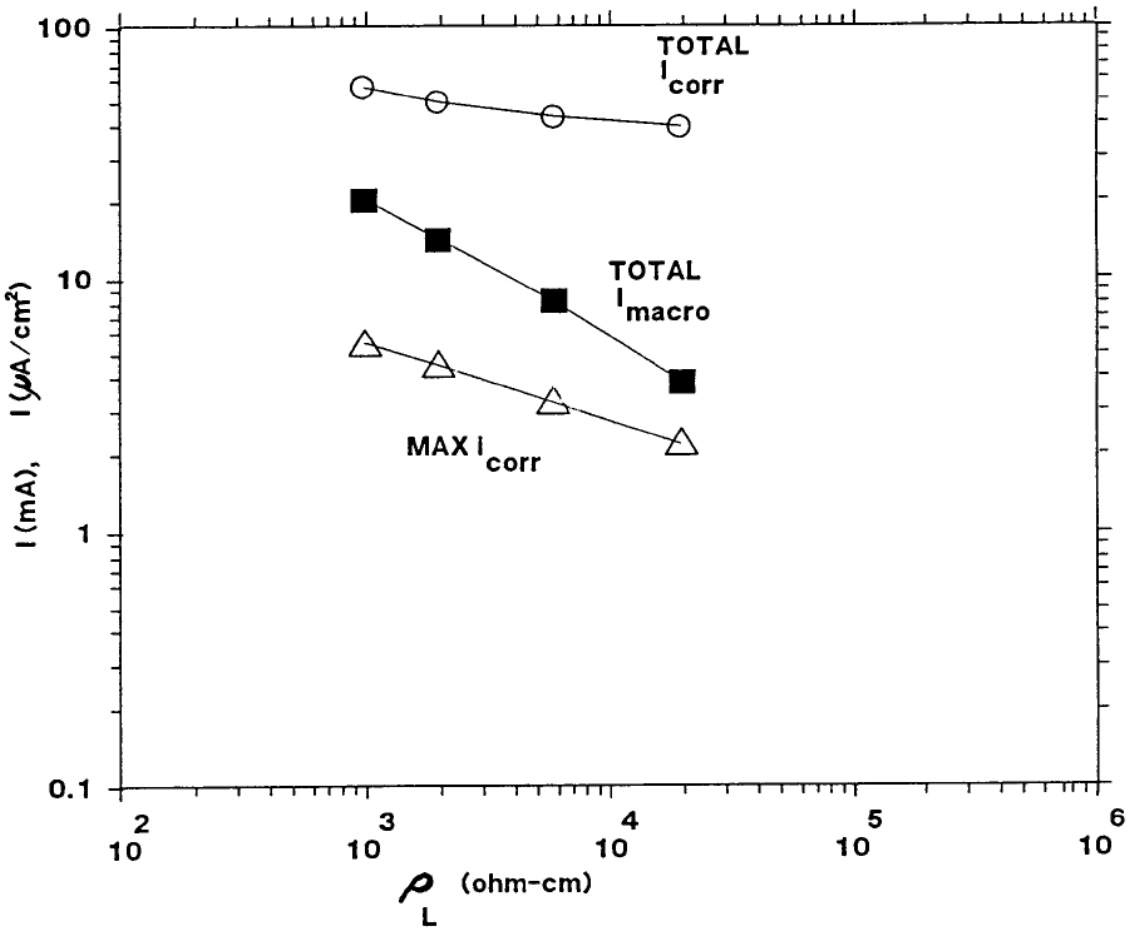

Figure III.4 Total Corrosion and Macrocell Currents, and Maximum Corrosion Current Density (Sums of Both Sides) As a Function of Lowest Concrete Resistivity While Keeping the Other Parameters Constant (Results from Cases A,B,L and M).

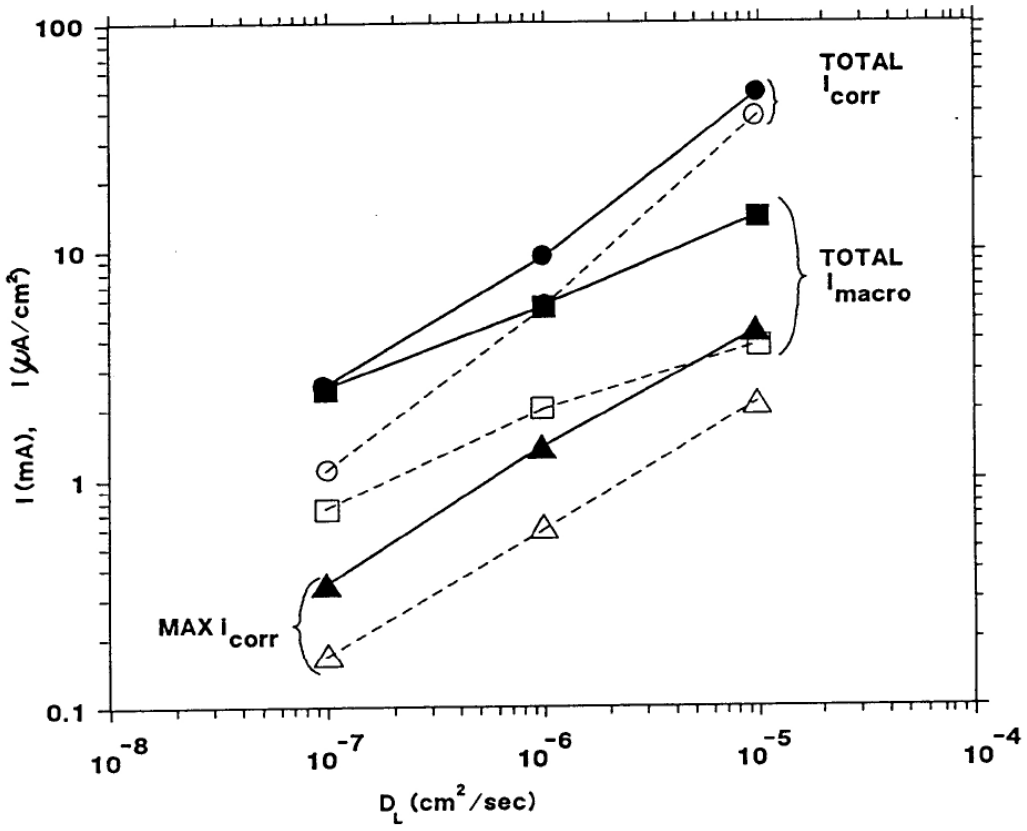

Figure III.5 Total Corrosion and Macrocell Currents, and Maximum Corrosion Current Density (Sums of Both Sides) As a Function of Lowest Concrete Diffusivity While Keeping the Size of the Active and Passive Regions Constant. The Solid Lines Correspond to the Cases With the Resistivity Range 2-10 KΩ-cm (A,F,G). The Dashed Lines Correspond to the Cases With the Resistivity Range 20-100 KΩ-cm (B,J and K).

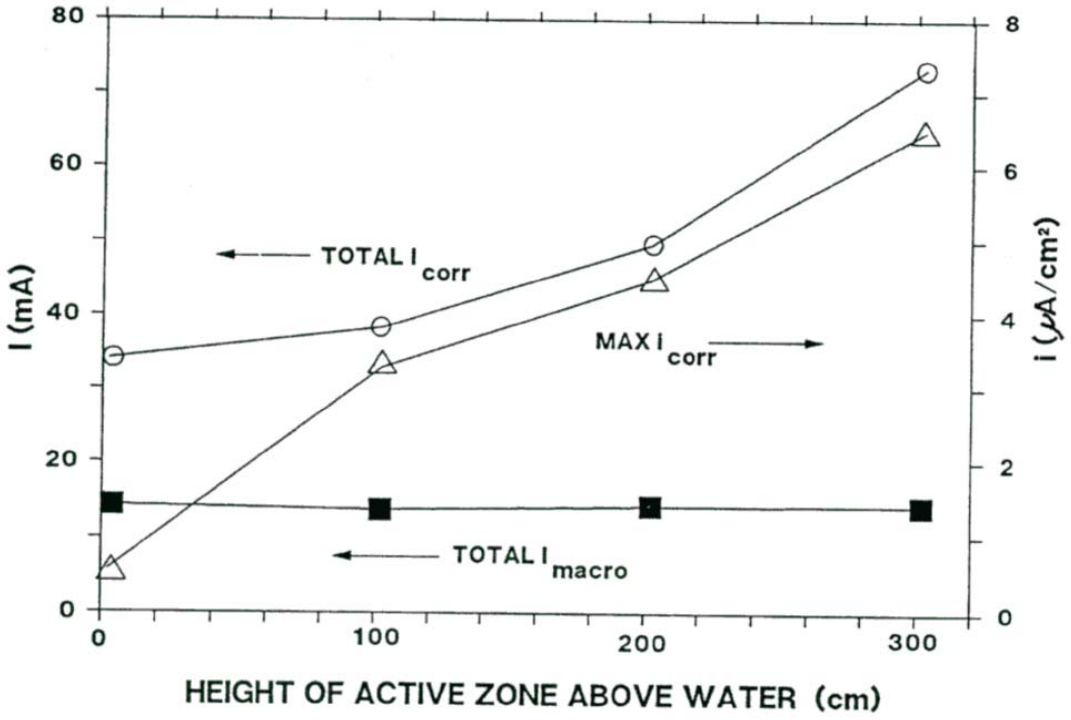

Figure III.6 Total Corrosion and Macrocell Currents, and Maximum Corrosion Current Density (Sums of Both Sides), As a Function of Height of the Active Zone Above Water While Keeping the Other Magnitudes Constant (Cases A,C,D and E).

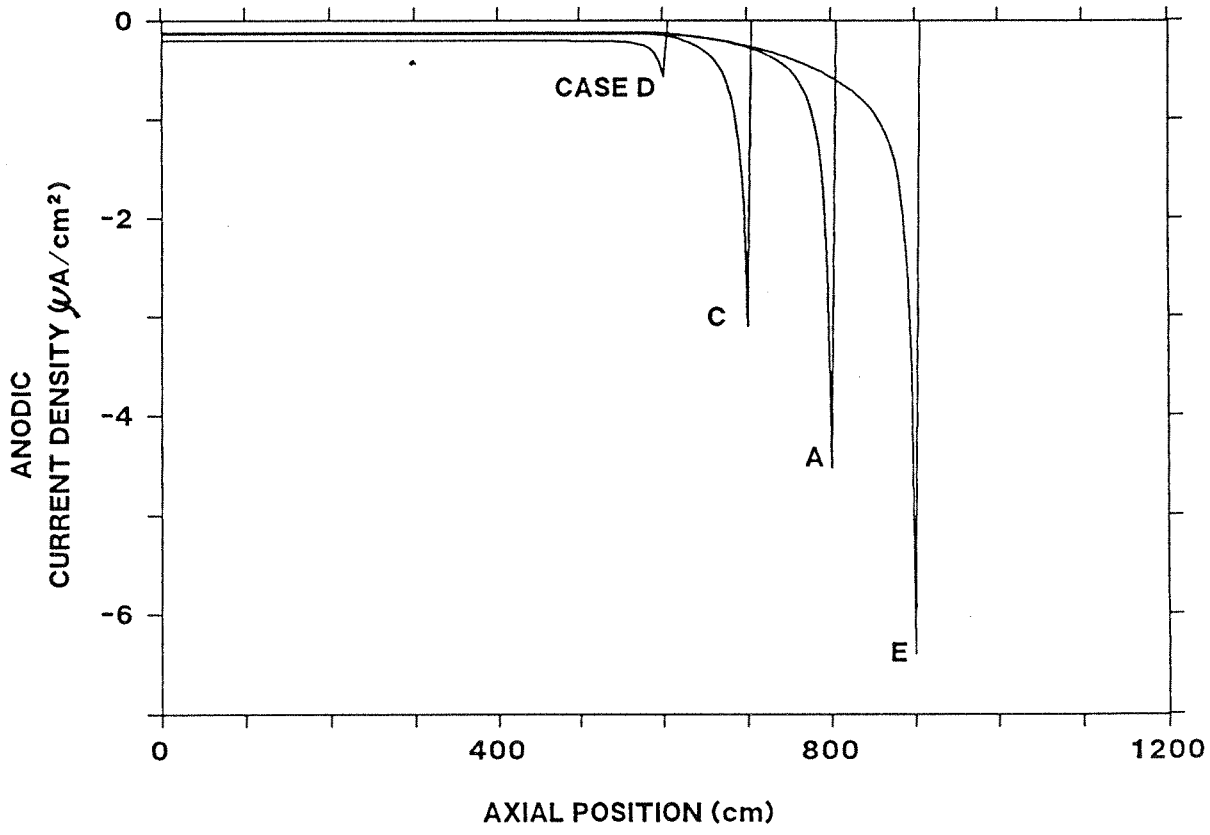

Figure III.7 Distribution of the Corrosion Current Density (Sums of Both Sides) for the Cases Indicated in Figure III.6.

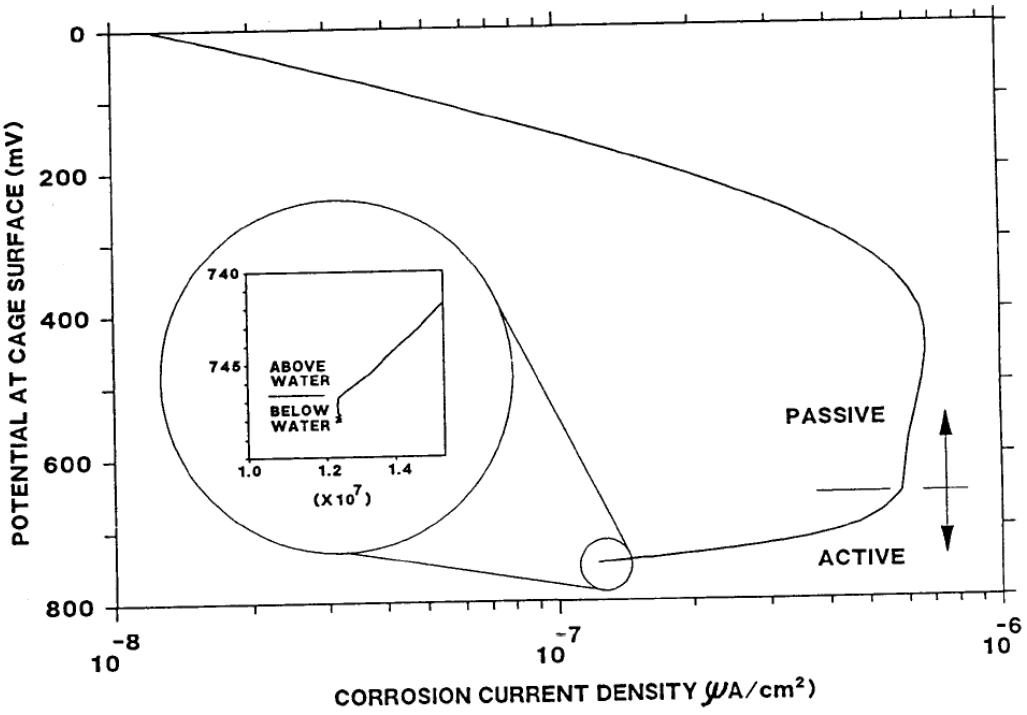

ıre III.8 Composite Polarization Diagram Showing the Locus of Potential at the Cage Surface and Oxygen Consumption Current Density (Sum of Both Sides) As It Varies Along the Rebar Cage (Baseline Case A). The Portions of the Diagram Corresponding to Different Column Regions Are Indicated in the Main Plot and in the Detailed Inset.

6. GENERAL DISCUSSION

The findings of each Part of the project have been individually discussed in each of the corresponding sections. This discussion addresses the mutual implications of the findings and their general significance.

All Parts of the investigation have identified, by separate means, the presence of significant macrocell action in marine substructure conditions. Substantial amounts of cathodic reaction took place both at regions where the steel is passive and also in portions of the chloride-contaminated concrete.

The findings of Part III suggest that much of the anodic reaction takes place above water, peaking at a region just below the beginning of the passive-steel zone. That prediction is also supported by the observation in the field of cracking and rusting almost exclusively in the splash-evaporation zone. The laboratory columns in Part I showed corrosion predominantly below water, and the columns used in Part II showed most of the net anodic activity also below the waterline. That behavior does not contradict the computer-model predictions because the laboratory columns were operated with a very small portion below water. The behavior in that case approaches an extension of Case D (Figure III.7), where the extent of anodic activity in the below-water portion is increased substantially by the relatively large amount of net cathodic action existing above water. In addition, the computer calculations assume that a mature active-passive pattern had developed in the column, which was not yet the case for the columns of the Part I study by the end of the test period.

The results in Part II provided an estimation of the effective value of the oxygen diffusion coefficient for water-saturated concrete ($3\ 10^{-6}$ cm^2 /sec). This supported the choice of D_L values used in the Part III computations. The relative importance of the diffusivity of oxygen (as opposed to only concrete resistivity) in establishing the overall extent of corrosion was emphasized by the findings of Part III. The laboratory

results in Part II provided experimental support for that prediction by showing that, because of a reduction in oxygen supply, corrosion activity did not increase after resistivity had decreased below a given amount.

For a given moisture condition, both oxygen transport, chloride transport and electric conduction through concrete are affected by the quality of the concrete. The interplay between concrete composition and transport parameters was illustrated by the results in Part I. The concrete with the microsilica addition showed improved behavior during relatively early ages. However, the advantage with respect to the concrete with fly ash as the only pozzolanic component became less important as both concretes aged. The model predictions from Part III suggest that the small resistivity differences (between both concrete mixtures) that may exist after 2 or 3 years of operation, would only marginally affect the relative distribution of corrosion. The results in Part I, showing essentially the same amount of macrocell current for both concretes at the end of the test period, suggest that the oxygen transport in both concretes are comparable. Longer-term monitoring of these columns will be necessary to reveal possible differences in behavior.

7. CONCLUSIONS

7.1 PART I CONCLUSIONS

7.1.1 All laboratory test columns developed concrete resistivity patterns consistent with concrete drying in the upper portions. The resistivity of the upper portions of the control condition (fly ash concrete, no surface treatment) was significantly reduced by periodic surface moisture application. The resistivity of the columns in the silane and siloxane surface treatment groups was not affected by periodic surface moisture application. The results indicated that in the upper regions the surface treatments prevented water ingress but did not cause water to be retained.

7.1.2 The resistivity of concrete in the submerged portions of the columns reflected the curing process and the type of concrete. The fly ash + microsilica (F+S) concrete cured quickly compared with the fly ash-only (F) material. The initial values of resistivity of the concrete mixtures corresponded to estimated rapid chloride permeability Coulomb values of 800 C and 3,000 C for the F+S and F type materials. After about two years of testing, both concretes had reached to similar levels of resistivity in the submerged portions of the columns, corresponding to Coulomb values of about 300 C. The resistivity of the concrete above water near the end of the 3-year test period was much higher than below water, but similar for both concrete types.

7.1.3 The steel below water in all test columns was initially in the active condition, but it passivated over a period of about 150 days for the F+S concrete, and about 100 days for the F concrete. The longer passivation time for the F+S concrete may be due to lower pore water pH in that material.

7.1.4 Activation of the steel below water took place after times of about 300 days for the F+S concrete and 150 days for the F concrete. The difference may reflect primarily the early differences in curing behavior of both concretes. The-time-to corrosion values agree with approximate calculations based on estimated diffusivity from the resistivity measurements.

7.1.5 Corrosion macrocell patterns developed on most columns with electronic macrocell currents generating in the element below water and being consumed by the element just above water. The amount of macrocell current was roughly the same for both types of concrete, suggesting that the behavior is similar following the early curing period.

7.1.6 Only 3 out of 12 columns had developed recognizable corrosion above water after 3 years of testing. It is proposed that the element above water was being partially cathodically protected by the submerged element, at least up the stage of corrosion pattern evolution examined during the test duration.

7.2 PART II CONCLUSIONS

7.2.1 The test columns developed a corrosion pattern with a cathodic upper portion (zone above water) and anodic regions in the chloride-rich areas.

7.2.2 The cathodic current in the upper column segments was strongly affected by partial moisture application on the column zone above water. Cathodic currents experienced dramatic proportional increases. The increase was due to the reduction of ohmic potential drops in the corrosion macrocell system as a result of moisture application.

7.2.3 Moisture saturation of the zones above water resulted in lesser ohmic potential drops in the concrete and an increase of cathodic reduction currents in the upper portions of the system. However, the cathodic currents (overall) experienced limitation to a value consistent with concentration polarization of the oxygen reduction reaction.

7.2.4 The value of the limiting current density for oxygen reduction corresponded to an effective diffusion coefficient for oxygen in water-saturated concrete ($D \sim 6\ 10^{-6}$ cm^2 /sec) which is in agreement with values reported in the literature.

7.3 PART III CONCLUSIONS

7.3.1 In a simulated reinforced concrete marine substructure column, the potential of the reinforcing steel varied continuously from the noble values in the zone above water to very active values in the submerged zone.

7.3.2 The concentration of oxygen inside the column varied from a value near equilibrium with the exterior at the top, to almost zero below water. Oxygen transport to the steel below water was almost exclusively through the concrete cover and not downward through the center of the column.

7.3.3 The corrosion current density was greatest at the top of the active zone of the column. Corrosion below water proceeded at a smaller rate even though the steel potential was significantly less noble than in the region of highest corrosion.

7.3.4 The local oxygen consumption rate was greatest near the top of the active steel zone. This resulted from a combination of the oxygen diffusivity pattern assumed in the calculations, and of the proximity of the active steel zone.

7.3.5 The total corrosion current varied from being almost equal to the total macrocell current, to being several times greater, depending on the values of concrete resistivity and oxygen diffusivity ranges assumed.

7.3.6 Corrosion below water was not enhanced by oxygen consumption in the air zone unless corrosion activity in the latter was greatly reduced.

7.3.7 The overall level of corrosion increased with increasing oxygen diffusivity and reduced concrete resistivity.

7.3.8 Relative changes in oxygen diffusivity had a greater impact on corrosion activity than comparable relative changes in concrete resistivity.

7.3.9 The three-dimensional, heterogenous nature of the system leads to polarization behaviors that cannot be described by a simple monotonic polarization curve.

7.4 GENERAL CONCLUSIONS

G1. Preponderance of corrosion below water in laboratory experiments is caused by the relative size of the submerged and free portions.

G2. The different approaches in the investigation provided results that confirmed the importance of corrosion macrocells in the development of corrosion in substructure columns.

G3. The overall results also indicated the importance of oxygen transport in establishing the severity of corrosion in substructure conditions.

G4. Oxygen diffusivity (or another appropriate measure of oxygen transport) should be considered as an important performance parameter for selection of concrete for future design for corrosion control.

G5. Design that promotes moist concrete condition (as in submerged footers) is recommended as a corrosion prevention/control approach.

8. STATEMENT OF BENEFITS

While this investigation addressed principally the propagation stage of corrosion, the present emphasis on long term durability (design service lives of 75 years or more) underscores the importance of extending the initiation stage of corrosion. Maintaining a thick concrete cover between the rebar and the external environment is still the first item of concern in successful design for corrosion control of marine substructure. A minimum cover of 4 in (10 cm) enforced by inspection is recommended whenever structurally feasible, to extend the length of the initiation period of corrosion [III.1].

The findings from Part I are by themselves not sufficient to decide the issue of whether microsilica addition is an economically desirable means of extending the length of the initiation period of corrosion in marine substructure. The results underscore the limitations of short term laboratory testing for evaluation of long term concrete behavior, revealing the relatively slow reaction of fly ash as it affects corrosion development. It is recommended that structures in the field be subject to monitoring of chloride penetration profiles, paying special attention to the effect of age on chloride ion transport.

All three parts of the project revealed the importance of oxygen transport through the concrete in determining the extent of corrosion reactions. It is recommended that measurements of oxygen diffusivity (or another suitable oxygen transport parameter) under both a water-saturated and an intermediate-moisture condition be made part of the testing used in the selection of future FDOT candidate mix designs for improved corrosion control. Concrete resistivity measurements, which can be easily performed instantaneously and non-destructively, should be performed routinely both to obtain a quality descriptor of wet concrete and for field investigations.

The findings also support structural design that promotes concrete moisture, such as partially submerged footers as a opposed to exposed piling below footers, to retard oxygen transport whenever possible. This type of design has the advantage of facilitating future cathodic protection of the structure and permitting the use of a thicker concrete cover than would be feasible in driven piles.